DOE/ET/25105--T1

SODIUM-SULFUR BATTERY DEVELOPMENT

PHASE VB FINAL REPORT

FOR THE PERIOD

OCTOBER 1, 1981 THROUGH FEBRUARY 28, 1985

DOE CONTRACT NO. DE-AM04-79CH10012

DE-AT04-79ET25105

APRIL 1985

DRAFT

DISTRIBUTION OF THIS DOCUMENT IS UNLIMITED

MASTER

Ford Aerospace & Communications Corporation
Aeronutronic Division
Newport Beach, California 92660

ARD-8181

DISCLAIMER

SODIUM-SULFUR BATTERY DEVELOPMENT

PHASE VB FINAL REPORT

FOR THE PERIOD

OCTOBER 1, 1981 THROUGH FEBRUARY 28, 1985

DOE CONTRACT NO. DE-AM04-79CH10012

APRIL 1985

DRAFT

Ford Aerospace &
Communications Corporation
Aeronutronic Division
Newport Beach, California 92660

CONTENTS

CONTENTS (continued)

ILLUSTRATIONS

ILLUSTRATIONS (continued

TABLES

SECTION 1

INTRODUCTION

This report describes the technical progress made under Contract No. DE-AM04-79CH10012 between the U.S. Department of Energy, Ford Aerospace & Communications Corporation and Ford Motor Company, for the period 1 October 1981 through 28 February 1985, which is designated as Phase VB of the Sodium-Sulfur Battery Development Program. During this period, Ford Aerospace held prime technical responsibility and Ford Motor Company carried out supporting research. Ceramatec, Inc., was a major subcontractor to Ford Aerospace for electrolyte development and production.

This program was initiated in 1975 between the Energy Research and Development Administration (ERDA) and Ford Motor Co. Previously, Ford had invented the basic sodium-sulfur battery concepts and had been actively engaged in their development since the early 1960s under in-house funding. The program had two primary goals: 1) development of batteries for electric vehicle applications; and 2) development of batteries for stationary energy storage (SES), emphasizing electric utility load leveling. The major emphasis during the first years of the program was research, design, engineering and testing to develop cells with good performance, long life, low cost and high producibility. Excellent progress was made in these areas, and in Phase VB battery systems development received increased emphasis, being conducted in parallel with cell development.

A major program goal was met in Phase VB through the design, development, fabrication, and testing of the Electric Vehicle Engineering Model-1 (EVEM-1) cell and battery. Data from the fabrication and testing of this battery defined additional requirements for a second generation cell which also was developed during Phase VB. This cell will be incorporated in a battery for testing in the DOE/Ford Motor Company Experimental Transaxle (ETX) Program under separate funding.

In addition to the successful development of two generations of electric vehicle cells, generic technology advanced in many areas, as described in this report. Of significance is the operation of a load-leveling cell for more than 2300 cycles in 4.5 years in a test still ongoing at the end of the program. Post-test analysis of similar cells removed from a 100-kWh battery after 32 months of testing substantiated the good corrosion protection offered by chromium plate. Also of note is the identification of silicon carbide/aluminum composites as materials of interest for future low-cost, corrosion-resistant cathode containers or liners. Encouraging data were obtained on electrolytes made by slurry-solution spray drying, a process that has potential for reducing electrolyte cost. Load-leveling cells being tested to evaluate these electrolytes had completed ∿670 cycles in 1.5 years by the end of the program, and electric vehicle cells had completed ∿1330 cycles in 1.2 years. These and other accomplishments are described in the following sections of this report which is organized as follows:

Section 2	--	Summary
Section 3	--	Program Description
Section 4	--	Cell Development
Section 5	--	Electrolyte Development and Production
Section 6	--	Battery Development
Appendix A	--	Materials for the Sulfur Electrode Current Collector

SECTION 2

SUMMARY

Research efforts in the early 1960s at Ford Motor Company resulted in the invention of the family of sodium-ion conducting materials known as beta aluminas, and the demonstration of the use of beta-double-prime-alumina (β"-alumina) as the solid electrolyte in sodium-sulfur (Na/S) cells. Research has continued under Corporate funding since that time, and has been augmented by Government funding since 1973 through programs sponsored by the National Science Foundation, the Department of Energy (DOE), and the Department of Defense.

This report covers the R&D effort sponsored by the Department of Energy during the period from October 1, 1981 through February 28, 1985, which is known as Phase VB of the Sodium-Sulfur Battery Development Program.

2.1 PROGRAM DESCRIPTION

The program addressed the development of Na/S batteries for stationary energy storage (SES) and electric vehicle (EV) applications, although during Phase VB the EV application was emphasized. The program was implemented through a tripartite contract between DOE, Ford Motor Company and Ford Aerospace & Communications Corporation, wherein Ford Aerospace held prime technical responsibility and Ford Motor Company carried out supporting research activities. Ceramatec, Inc., developed and supplied electrolyte assemblies under subcontract to Ford Aerospace. The technical effort was monitored by Sandia National Laboratories.

2.2 MAJOR ACCOMPLISHMENTS

Phase VB technical achievements are summarized below as follows.

2.2.1 Cell Development
2.2.2 Electrolyte Development and Production
2.2.3 Battery Development

2.2.1 CELL DEVELOPMENT

Cell development objectives were defined in terms of improved performance, durability, reliability, safety and cost. These objectives were addressed through the development of new EV cells based on battery specifications provided by Ford Motor Company and new high-energy cells for SES applications involving weekly duty cycles.

First and second generation EV cells were developed using a systems approach that included design and analysis at the battery level as well as cell component development. The first cell developed was for the Electric Vehicle Engineering Model-1 (EVEM-1) battery. The cell was designed to operate horizontally, permitting dense packing and low-resistance interconnection of cells into modules. An EV battery was constructed from 480 of these cells and eval-

uated in a bench test (described in Section 2.2.3). The EVEM-1 cells demonstrated: 1) excellent performance; 2) fail-safe characteristics (following intentional fracture of the ceramic separator); and 3) ruggedness to withstand acceleration and vibration well beyond levels foreseen for normal passenger vehicle operation. However, despite these excellent characteristics, the EVEM-1 module and battery tests concluded late in 1983 identified some shortcomings of the cell which helped to define two major 1984 cell development goals: 1) improved reliability (fewer early failures and improved freeze-thaw capability); and 2) lower post-failure resistance.

Additional goals for the next generation EV cell were set by the requirements for the battery to be built and tested in the DOE/Ford Experimental Transaxle (ETX) Program. The ETX cell was designed for a 33 percent larger capacity (than EVEM-1 cells) and for vertical operation with both anode and cathode connections located at the top of the cell for ease of maintenance. Preliminary test data on preproduction cells indicated that they: 1) provided very high specific energy and power density; 2) were safe; and 3) were able to withstand repetitive freeze-thaw cycles when charged.

Load-leveling cell development included continuation of Mark-II cell durability tests, both as single cells and in 25-kWh modules of the 100-kWh battery constructed in 1981. By the end of Phase VB, one cell had operated for more than 2300 cycles in approximately 4.5 years. After 675 cycles (32 months) of three 25-kWh modules, 295 of 384 cells were operable. Seventy-eight had failed, and eleven were rendered inoperable by blown fuses due to a control system malfunction. Cells were selected from the original modules for incorporation into modules of an alternative interconnection strategy where as many as 200 additional cycles were accumulated by the end of Phase VB. In experiments utilizing cells from the original battery modules, cells withstood more than 50 freeze-thaw cycles. In post-test analyses, chromium plate was found to provide good corrosion protection for the E-Brite stainless steel containers.

High-energy cells advantageous for utility applications using weekend charging and for use with renewable energy sources were designed, fabricated and tested. These cells utilized low-cost electrode materials and demonstrated excellent performance in cell sizes ranging in size from 440-Ah (for 20-h discharge) to 1250-Ah (for 40-h discharge).

Exploratory cells were built to test additional corrosion-resistant coatings (chemically vapor deposited molybdenum, a proprietary conductive glass, and improved chromium plates) as well as electrode materials of lower cost than the traditionally used WDF graphite felt. Cells were also fabricated and tested to evaluate electrolytes made by slurry-solution spray drying, a process with potential for lower cost. Based on results to date, all of these materials and components continue to hold promise for reducing cost while maintaining good performance.

Ford Motor Company carried out supporting research activities related to corrosion-resistant container materials. The work defined the acceptable operating conditions for chromium plate, and led to an improved plating process now under evaluation in cells at Ford Aerospace. The work also indicated

the possibility of using the proprietary conductive-glass coatings developed under Ford Aerospace funding. Also, several single and mixed ceramic oxides were found to be corrosion stable in environment of the operating sulfur electrode; however use of these materials will require development of thin coatings. Aluminum/silicon carbide (Al/SiC) composites were found to be suitable for container liners or coatings, although methods for lining or coating containers are yet to be developed.

2.2.2 ELECTROLYTE DEVELOPMENT AND PRODUCTION

Ceramatec, Inc., provided standard zeta-process electrolyte assemblies to Ford Aerospace for fabrication of cells and batteries, and worked to improve the reliability and reduce the cost of these assemblies.

Work related to improving electrolyte reliability included evaluation of residual stresses, static fatigue and wetting by sodium, as well as an extensive characterization study on zeta-process electrolytes and an evaluation of process sensitivities. A proof pressure test was also developed. It was observed that large defects related to processing were always responsible for electrolyte failures in burst testing. The intrinsic strength of β"-alumina electrolytes appeared to be high, indicating that processing improvements to reduce large defects should improve reliability. Residual stresses were found to be low and controllable and should not adversely affect reliability.

Characterization of the near-surface region of electrolytes by Dr. Walter Roth of the State University of New York at Albany under subcontract to Ceramatec showed the zeta-process electrolytes to be of uniform composition without surface concentration of impurities. Reactions that cause the formation of a sodium- and water-rich surface skin during normal handling were found to be reversible.

Cost-reduction activities centered on the development of the slurry-solution spray drying process. The process of seeding was found to have advantage over previous methods for enhancing the conversion to the β" phase and controlling the microstructure during seeding. Densities, resistivities and strengths equal to or better than those for zeta-process materials were obtained through incorporation of seeding into the slurry-solution spray drying process. Sodium life tests were initiated, but not concluded prior to the end of the program. A cost-reduction plan including incorporation of low-cost materials, continuous processes, and automated QC was developed.

During Phase VB, expiration of the lease necessitated a move of the pilot plant to another location. Upon reinstallation, each piece of equipment was operated and certified after production of acceptable quality product. The new pilot plant was fully qualified for production by the zeta process and by slurry-solution spray drying by the end of October 1983.

During Phase VB more than 1500 electrolyte assemblies were delivered to Ford Aerospace. Although production was accomplished by a labor-intensive batch process, powder efficiencies were good and improved throughout the course of the program. ETX electrolytes were produced with a powder yield of 68 percent (in 1984) compared to a 52 percent yield for the EVEM-1 assemblies pro-

duced earlier. In addition to the deliverables, 165 standard zeta-process electrolytes were produced for studies of hot isostatic pressing and proof-testing development.

2.2.3 BATTERY DEVELOPMENT

The main battery development activities included: 1) design, fabrication, and testing of the 36-kWh EVEM-1 battery and 2) continued evaluation of three 25-kWh modules of an experimental SES battery. Results from these battery development efforts guided subsequent cell and battery component development.

2.2.3.1 Electric Vehicle Battery Development. The Phase VB EV battery development activities included design, developmental testing, fabrication and testing of the EVEM-1 battery. The EVEM-1 battery design was based on eight modules of 60 cells each (four parallel strings, each of 15 cells in series). The horizontal cells were positioned head-to-toe (positive and negative ends adjacent) so that the aluminum cell-to-cell interconnects would be of minimum length and weight. Developmental testing of strings and a prototype module confirmed the expected performance, safety, and ability to withstand vibration.

During the bench test the modules were contained within a rectangular box fabricated from standard insulation. After assembly and checkout of the bench test battery, twelve electrical cycles were carried out. Approximately fifteen cells failed within the first two cycles, probably due to stresses associated with heatup. Seven additional cells failed during the 12 cycles of the bench test, possibly related to difficulties with test equipment for regenerative pulse testing. The failures were distributed within six of the eight modules. The combination of high post-failure resistance and unbalanced failure distributions among the strings in two of these modules limited the delivered capacity to about 75 percent of the rated value. For the last three cycles, these two modules were bypassed, allowing demonstration of full capacity by the remaining six modules. In this condition, the battery sustained the power and regenerative pulses typical of electric vehicle applications. Although the bench test was not entirely successful, results verified pretest predictions of performance in constant current and pulse discharges.

Following a review of the bench test results, the modules were refurbished and installed in a vacuum-insulated enclosure purchased from the Linde Division of Union Carbide with Corporate funds. The battery, renamed CARBAT-1, was installed in an LN7 vehicle and transported to Dearborn, Michigan for company-funded in-vehicle tests. After heatup at Dearborn, diagnostic tests indicated approximately 13 cell failures distributed among 11 of the 32 battery strings. At that point, the battery's power capability would have been acceptable, but rated capacity might not have been achieved. After a weekend idle period a severe electrical fault occurred within the battery, along with venting of smoke. The battery was cooled to ambient temperature and returned to Newport Beach, California for post-test analysis.

Battery disassembly and post-test analysis, carried out with the participation of Dr. James E. Battles of Argonne National Laboratory, confirmed that the incident was the result of shorting of two externally parallel thermocouples to their respective bus bars. The short circuit led to discharge of the two modules, accompanied by burning off of the insulation and damage to adjacent lead wires. The initial cell failures were not involved in the incident.

Since more than 340 cells remained operable, a reconfigured six-module battery (CARBAT-1A) was assembled and tested. Each CARBAT-1A module contained 60 series-connected cells. Approximately eight cells failed during the heat-up of CARBAT-1A, and half of the modules had high and erratic resistance as a result of cell failures. The other three modules were discharged in parallel to as much as 74 percent of rated capacity. Both hot and cold maintenance operations were performed on the three remaining modules to bypass failed and blocking cells and to replace failed cells with spares. These efforts were successful to the extent that these modules could be cycled individually for 75 percent of rated capacity in a repeatable manner. However, attempts to operate the three modules in parallel were thwarted by the failure and blocking of additional cells, and the test was discontinued.

Based on the results of the EVEM-1 and CARBAT-1A battery tests it was concluded that development of an external bypass is necessary. Also, improved maintainability and freeze-thaw capability were shown to be requirements for future EV batteries.

2.2.3.2 Stationary Energy Storage Battery Development. Testing of three 25-kWh modules of the 100-kWh battery continued during the first part of Phase VB until approximately 675 cycles had been accomplished in 32 months. Battery energy efficiency decreased over this time because some of the fuse links did not blow following electrolyte fracture, but continued to draw current. A Weibull probability plot for cell failures due to electrolyte fracture indicated a characteristic life of 860 cycles based on failures occurring during the first 300 cycles. For failures occurring after 300 cycles, a characteristic life of 2700 cycles was determined.

After 675 cycles, cells from the three modules were used to construct two modules utilizing an alternative interconnection strategy. The alternative method was selected because it effectively blocks leakage current from failed cells, eliminating the major problem found in the original 100-kWh battery. By the end of the program the first reconfigured module had operated for more than 200 cycles and was still exhibiting 100 percent coulombic efficiency and 75 percent energy efficiency.

SECTION 3

PROGRAM DESCRIPTION

Sodium-sulfur battery technology has been under continuous development since the invention of sodium ion-conducting β-type aluminas at the Ford Motor Company more than 20 years ago. Since 1975, the Government has accelerated the development of the technology through several sources of funding as described in Section 3.1. The objectives for Phase VB of the DOE-funded program are highlighted in Section 3.2 which also summarizes the status at the beginning of Phase VB.

3.1 PROGRAM BACKGROUND

The program is an outgrowth of effort initiated by Ford Motor Company in the early 1960s, which resulted in the concept and proof of principle of the sodium-sulfur battery. Research continued at Ford under in-house funding until 1973 when efforts were expanded as a result of added support from the National Science Foundation. The National Science Foundation support was augmented in 1975 by Phase I of a program funded by the Energy Research and Development Administration (ERDA). The long-range objective of the program (funded subsequently by the Department of Energy (DOE) was development of sodium-sulfur batteries for both stationary energy storage and mobile applications as a means of reducing the nation's dependence upon petroleum products.

The first three phases of the effort, covering the period 1975 through February 1979, were under the prime responsibility of the Ford Research Staff in Dearborn, Michigan. Efforts during this period primarily concentrated on developing suitable cell materials for predicted 10-year life, generating cell design concepts, and developing fabrication techniques for high performance and reproducibility. During the first three phases, Ford Aerospace functioned as a subcontractor in the areas of materials development, cell fabrication and testing. A second subcontractor, the University of Utah Research Institute (and later Ceramatec, Inc.), was responsible for scaling up development of the β"-alumina solid electrolyte which is the key component of the sodium-sulfur cell. By the end of 1978, cell concepts and designs were refined to the point where larger numbers could be produced and tested to generate meaningful data for prediction of battery performance. During 1978, fabrication facilities and testing and data acquisition capabilities were expanded at Ford Aerospace to facilitate testing of groups of cells (sub-batteries and batteries).

Phase IV began in March of 1979, under a new tripartite contract between DOE, Ford Motor Company and Ford Aerospace, wherein Ford Aerospace held prime responsibility for the technical effort. During the early stages of Phase IV, the primary efforts centered on fabrication and testing of the baseline Mark-I cell design established in 1978. This cell was of such a size and design to enhance investigation of various materials and design modifications while allowing performance correlation with prior data. As reproducibility of cell performance improved with refinements in manufacturing operations and materials selection, development of stationary energy storage and electric-vehicle systems designs was initiated. Concurrently, the Mark-II cell evolved during 1979. Rapid progress during Phase IV led to the fabrication and initial testing of

a 100-kWh stationary energy storage battery comprising 512 Mark-II cells and developmental control systems. Three of the four modules of the 100-kWh battery operated for more than 675 cycles in 33 months in tests that were concluded in 1983 for reconfiguration of the cells into modules representing an alternate cell interconnection strategy. Phase IV also included the fabrication and initial testing of a battery to power a utility vehicle which subsequently operated for 38 months of in-plant usage.

Beginning with Phase VA in 1981, the electric vehicle application was emphasized, although development of cells for stationary energy storage continued. Major achievements of Phase VA, which ended on 30 September 1981, included demonstration of high-rate discharge of laboratory-type electric vehicle cells as well as full recharge of rated capacity in 30 minutes.

Cell and battery development continued in Phase VB with the design, development, fabrication and testing of an EV battery representing a major accomplishment. Phase VB activities are described in Section 3.2.

During Phase VB, additional efforts directed toward EV battery development began at Ford Aerospace under contracts with Ford Motor Company/Aerospace Corporation and Sandia National Laboratories, both under DOE funding. The objective of these Ford Aerospace efforts is to develop an advanced battery for demonstration in an electric vehicle in 1986.

Also, since 1982, the U.S. Air Force has funded development of sodium-sulfur cells for satellite applications. Cells delivered by Ford Aerospace have been under test since 1983. The program emphasis is presently on fabrication and evaluation of advanced cells.

3.2 PHASE VB OBJECTIVES

The primary Phase VB cell and battery development objectives related to electric vehicle (EV) applications, although work also continued to address stationary energy storage (SES) through continued durability testing as well as investigations of alternate cell interconnection strategies and weekly duty cycles. Sections 3.2.1 through 3.2.5 provide an overview of the technical status at the beginning of Phase VB and the specific objectives for various development topics.

3.2.1 CELL RESEARCH (TASK 1)

At the beginning of Phase VB, a durability test of 19 Mark-II (load-leveling) cells had reached 775 cycles. Seven cells were still meeting all performance criteria. In addition Mark-II cells were being tested in three 25-kWh battery modules which had operated for more than 200 cycles. Laboratory EV cells, both horizontal and vertical, had demonstrated excellent high-rate capability under both steady and pulsed loads. The Mark-II and EV laboratory cell designs both were based on the use of chromium-plated cathode containers, zeta-process β"-alumina electrolytes, and Union Carbide WDF felt electrode material.

Cell research and development activities were guided by broad overall objectives of improved performance, durability, reliability, safety and cost. These objectives were to be addressed through the design and development of new EV cells based on battery specifications provided by Ford Motor Company and new high-energy SES cells for weekly duty cycles.

Specific objectives addressed in Phase VB included: 1) more corrosion-resistant cathode containers; 2) lower cost electrodes; 3) improved freeze-thaw capability; and 4) improved failed-cell resistance.

3.2.2 ELECTRIC VEHICLE (EV) BATTERY DEVELOPMENT (TASK 2)

Previously, fifty-two Mark-II load-leveling cells had been configured into a 14.4-kWh battery which was used to power a small Taylor-Dunn industrial vehicle. The use of conventional insulation and cells not optimized for the application resulted in a battery weight of 450 lb (compared to 250 lb for the lead-acid batteries supplied with the vehicle). Vehicle tests showed the range to be 73 miles (10.1 hours driving time) with the sodium-sulfur battery, compared to a range with the lead-acid batteries of 13.7 miles (2.0 hours driving time). At the beginning of Phase VB, the sodium-sulfur battery-powered vehicle was being used as a utility (errand) vehicle within the battery program.

Prior to Phase VB, computer projections of electric vehicle performance had been made by Ford for the Fiesta, Escort, E-150 Econoline van, a concept small car, small truck, and small van. The projections indicated that the Escort would be a good choice for a test bed for a first generation sodium-sulfur battery. A 600-lb sodium-sulfur battery was compared to a 600-lb nickel-zinc and a 1000-lb lead-acid battery (all at 80 percent depth of discharge) under the Federal Urban Driving Schedule (FUDS), using a DC drivetrain. The accelerations for all batteries were approximately equivalent, but the sodium-sulfur battery showed twice the range.

Ford Aerospace developed a provisional battery design for the Escort vehicle. The design was based on six 60-cell modules connected in series to provide a nominal 120-V, 36-kWh system. Each module comprised six parallel strings of 10 cells in series. This configuration also allowed for reconnection into a 240-V system. Iterations of cell and battery design and vehicle projections, coupled with refined packaging constraints were in progress at the beginning of Phase VB.

Major Phase VB objectives included the design, development, fabrication and evaluation of an EV battery designated as the Electric Vehicle Engineering Model-1 (EVEM-1) battery. Following the bench-test evaluation of the EVEM-1 battery, the battery modules were refurbished and installed in a superinsulating container purchased from the Linde Division of Union Carbide Corporation for Company-funded integration into an Escort-sized (LN7) vehicle and in-vehicle (CARBAT-1) tests at Dearborn, Michigan. Following conclusion of the Company-funded effort the battery was returned to Ford Aerospace. Additional

contract objectives were established for the post-test analysis of the CARBAT-1 battery and reconfiguration and testing of the battery modules to evaluate the performance characteristics of long series strings.

Other EV battery objectives included: 1) preliminary evaluation of the effects of battery circuit design and electrical control strategy on battery reliability; and 2) continued operation and maintenance of the sodium-sulfur battery-powered utility vehicle.

3.2.3 STATIONARY ENERGY STORAGE (SES) BATTERY DEVELOPMENT (TASK 3)

Earlier development efforts resulted in the design, construction and testing of a 100-kWh battery based on 512 Mark-II cells and utilizing experimental control systems. The battery comprised four 128-cell modules connected in series. Each module comprised two series-connected submodules of 64 parallel-connected cells, each. The battery met its goal under the conditions for which it was rated (1500-A discharge, 1070-A charge), delivering 102 kWh at 74.6 percent efficiency. The battery provided validation of thermal-control and charge equalization concepts, and demonstrated that modules can be cooled, repaired and reheated. Phase VB objectives included: 1) continued evaluation of a 100-kWh experimental battery; 2) applications analysis of weekly storage cycles; 3) development of improved system components; and 4) investigation of alternate cell interconnection strategies through reconfiguring and testing modules of the 100-kWh battery.

3.2.4 ELECTROLYTE DEVELOPMENT (TASK 4)

Since 1979, Ceramatec, Inc., worked as a subcontractor to Ford Aerospace to produce β"-electrolyte assemblies and to develop improved electrolytes. By Phase VB, the zeta process for electrolyte fabrication was well in hand, and research and development activities were directed at a process with potential for lower cost (slurry-solution spray drying of a lower cost powder). Preliminary tests showed that electrolytes with low resistivity (<5 ohm cm) and good endurance (2000 Ah/cm^2) can be prepared using this process. Efforts were also in progress to develop a proof-pressure test apparatus.

Ceramatec's Phase VB objectives included production of high-quality β"-alumina assemblies as well as R&D goals related to: 1) improved reliability; 2) reduced cost; and 3) an improved technique for nondestructive evaluation (NDE).

The reliability objective was approached through the evaluation of NDE methods and process sensitivites, as well as through fundamental studies to evaluate: 1) residual stresses in sealed assemblies; 2) static fatigue; 3) wetting of β"-alumina by liquid sodium; 4) hot isostatic pressing to decrease internal porosity; and 5) fracture-initiating flaws.

Cost-reduction objectives were related to slurry-solution spray drying development and included: 1) optimization of slurries with high solids content; 2) development of a process variation known as seeding; and 3) evaluation of alternative atomization systems. The development of a long-range cost-reduction plan was a major milestone.

The development of an NDE technique included work toward objectives of: 1) characterization of electrolyte flaws; 2) fracture data acquisition and correlation with characterization data; and 3) development of a proof-pressure test.

3.2.5 SUPPORTING RESEARCH (TASK 5)

Under the tripartite contract in place since 1979, Ford Motor Company has carried out supporting research activities. By the beginning of Phase VB, preliminary corrosion and conductivity tests indicated promise for chromium oxides and perovskites as possible coating materials to provide corrosion-resistant cathode containers.

Phase VB objectives included: 1) identification of additional materials candidates; 2) development of methods for forming coatings from chromium oxides and perovskites; and 3) continued testing of promising materials.

SECTION 4

CELL DEVELOPMENT

During Phase VB, two major sodium-sulfur (Na/S) cell development efforts were pursued: the development of high power density cells for electric vehicle (EV) applications; and development of improved components generic to Na/S technology. Cells for stationary energy storage (SES) applications received less development emphasis, although evaluation of Mark-IID cells continued, and the feasibility of higher energy cells for weekly storage cycles was demonstrated. Approximately 90 cells fabricated in Phase VB were evaluated for SES applications.

EV cell development was based on a systems approach involving design and analysis at the battery level coordinated with cell component development and thorough product evaluation. Two generations of cells resulted: the horizontal Electric Vehicle Engineering Model-1 (EVEM-1) cell which permits dense packint and low-resistance interconnection of cells into modules; and the vertical ETX cell* which provides opportunity for maintenance without battery cooldown. Both cells provide excellent power density at the cell and battery level, together with many other favorable performance characteristics and safety attributes. Approximately 150 EVEM-1 and 140 ETX cells were fabricated and evaluated during Phase VB in direct support of EV cell development, in addition to over 700 cells evaluated as cell groups, modules, or batteries.

Approximately 100 exploratory cells were fabricated to support in-situ evaluation of alternate full-size cell components. These studies addressed variations in the electrolyte, sulfur electrode, safety devices, sodium reservoirs, and the cathode container/current collector. The experimental approach consisted of evaluation of exploratory cell performance and comparison to results from baseline cells, followed by post-test examination of individual components, and supported, as necessary, by basic studies of material properties. This work was augmented by post-test analysis programs at both Argonne National Laboratory (ANL) and Sandia National Laboratories (SNL) in which components and tested cells from the Ford Aerospace program were examined.

Details of these cell development efforts are given below.

4.1 EV CELL DEVELOPMENT

Interest in pursuing the EV application for Na/S batteries was heightened by the exceptional performance shown by laboratory cells at the close of Phase VA. Power densities exceeding 220 W/kg and 450 W/l (30-s pulse, maximum power) were achieved by individual cells along with a specific energy of 140 W/kg at the 3-h rate. Except for product safety, high power density has been recognized as the most critical technical parameter for an EV battery and is the feature most generally lacking in state-of-the-art batteries. With the encouraging cell results, a systems study for a possible in-vehicle experimental battery was performed. The existing test vehicle and power train set the approximate requirements for energy, power, weight, volume and voltage level. (Further discussion of battery issues can be found in Section 6.)

*Cell for a battery to be built and tested in the DOE/Ford Experimental Transaxle (ETX) Program.

These studies were used to select the goals for the initial EVEM-1 cell. The cell is shown in Figure 4-1 and its design ratings are summarized in Table 4-1. Based on its safety, ruggedness and performance characteristics, the development of the EVEM-1 cell was very successful. However, it suffered from a small infant mortality rate and an inadequate reliability with respect to repeated freeze-thaw cycling ($\sim$3 percent mortality per freeze-thaw cycle). The cell interconnection circuit employed in the EVEM-1 module heightened sensitivity of battery performance deterioration to cell failure, causing the reliability to be poor and thwarting full battery evaluation, as discussed in Section 6.

A second generation cell design was developed for the ETX battery being developed in another program. The ETX cell retained the good features of the EVEM-1 cell and improved on its shortcomings. Higher cell reliability, fewer cells and capability to perform limited maintenance without battery cooldown lead to the design and specifications for the vertical ETX cell, shown in Figure 4-2 and Table 4-1, respectively. While both cells have similar high specific energy and power density ratings, preliminary results indicated that the ETX cell is substantially more tolerant of freeze-thaw cycles. Details of these cell developments are discussed below.

FIGURE 4-1. THE EVEM-1 CELL (RATED AT 77 Wh, 145 Wh/kg AT C/3)

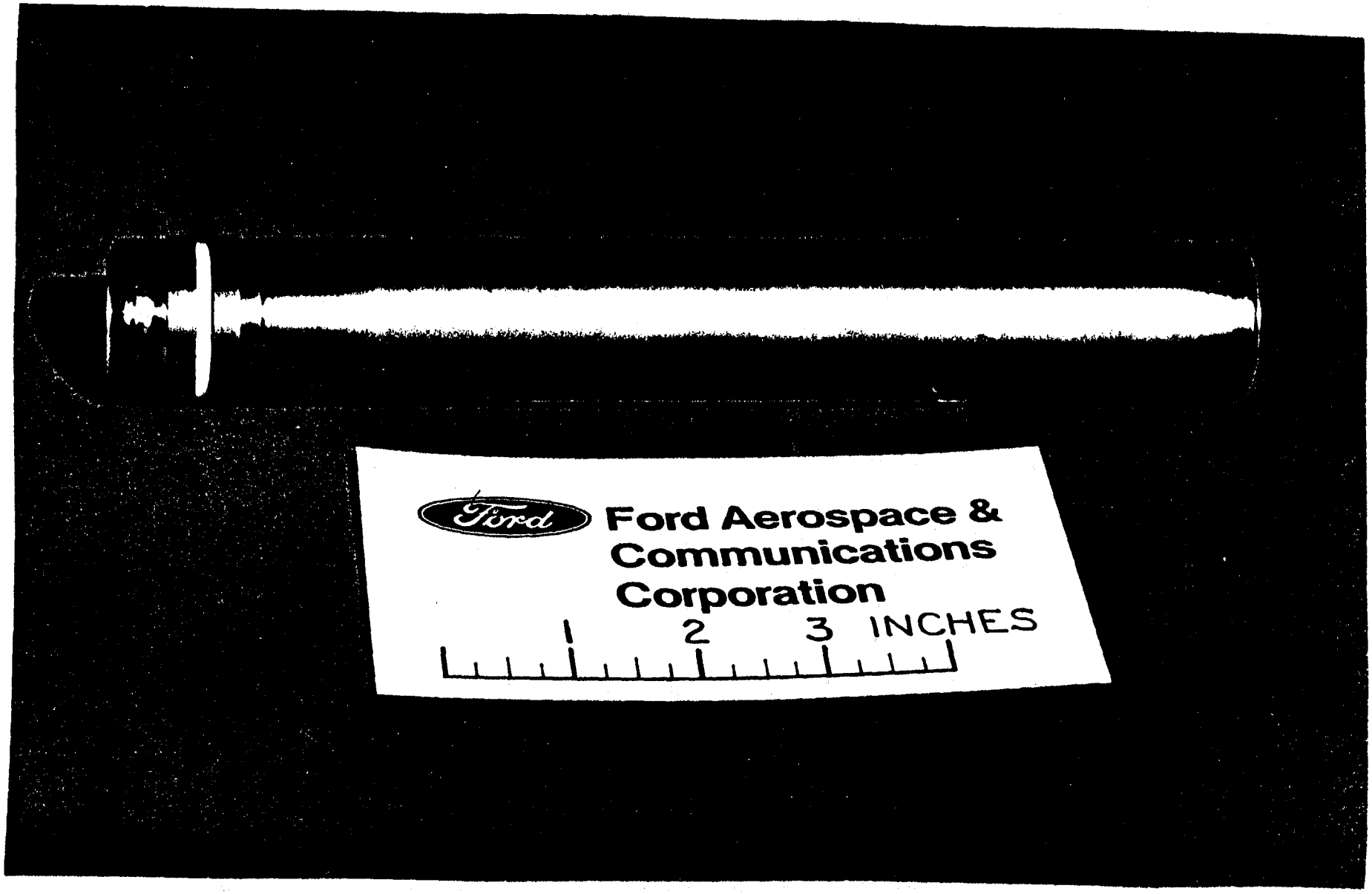
Ford
Ford Aerospace &
Communications
Corporation
1 2 3 INCHES

Figure 4-1

TABLE 4-1. ELECTRIC VEHICLE CELL DESIGNS

	EVEM-1	ETX
Size and Weight		
Dimensions, cm		
OD	3.6	3.8
L	25.2	33.1
Volume, cm^3	260	380
Weight, g	529	750
Ratings		
Resistance, mΩ		
Steady	9.3	7.8
Pulse	<8	<6.7
Capacity at C/3, Ah	41.5	55.0
Energy at C/3, Wh	77	102
30-s Pulse power, W		
0-50% DOD	140	-
at 80% DOD	114	135
Specific energy at C/3, Wh/kg	145	136
Power density at 80% DOD, W/l	420	355

FIGURE 4-2. THE ETX CELL (RATED AT 102 Wh, 136 Wh/kg at C/3)

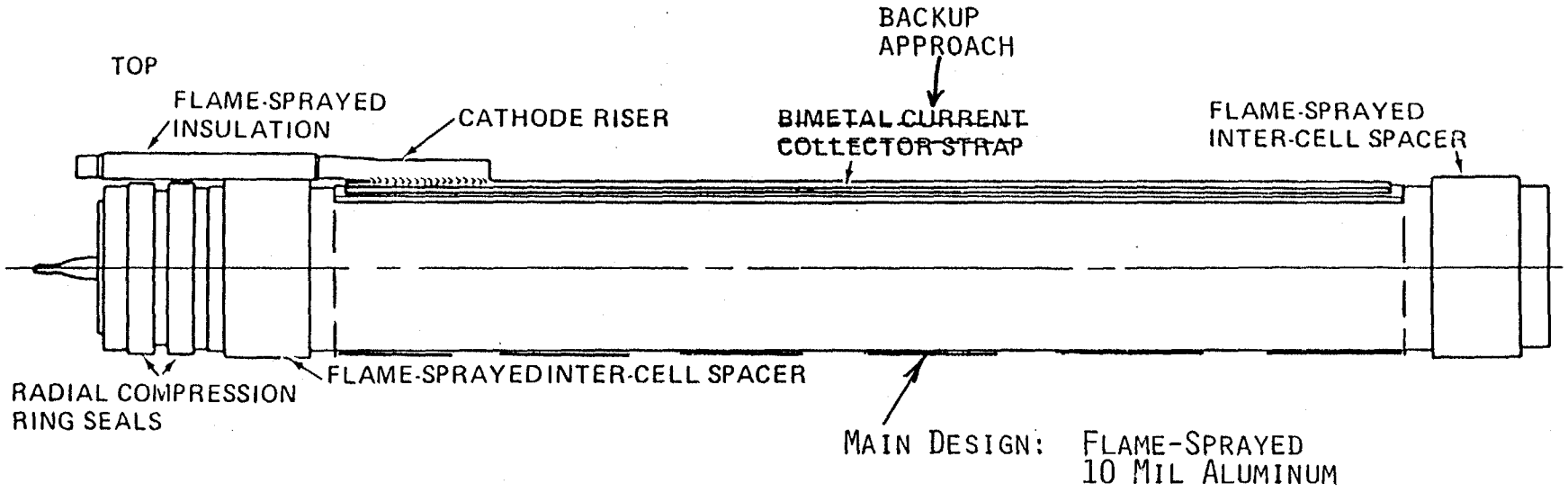

Use Photo

Figure 4-2

4.1.1 EVEM-1 CELLS

The design of the EVEM-1 cell resulted from extensive trade studies in which specific energy and power density were maximized, subject to numerous physical constraints imposed by battery considerations. The dominant variables in these trade studies were the dimensions of the ceramic electrolyte and the major constraints were the size and shape of the battery package.

4.1.1.1 Design. Because of the high voltage (240 V) and low capacity of the EVEM-1 battery (166 Ah), only a few discrete values for cell capacity could be considered, determined by the number of cells or strings in parallel (N). (Cell capacity equals 166/N.) Very large capacity EV cells (e.g., 166 or 83 Ah for N equals 1 or 2) were not practical due to excessive length, high ohmic losses along container, mechanical fragility, and manufacturing difficulties. Likewise, very small capacity cells (N>6) provided poor specific energy and power density as a result of the sizable inert weight and volume associated with the radial-compression ring seal. In addition, small cells would introduce an extremely large "parts count" for the battery.

Cell designs for intermediate capacities (e.g., 55, 42, or 33 Ah for N=3, 4, or 5) were analyzed in more detail. The 42-Ah EVEM-1 design was selected because:

1) It provides the proper ratio of power to energy in a small volume.

2) The electrolyte diameter eliminates the requirement for an external sodium reservoir.

3) The moderate cell length controls the thermal gradients and ohmic losses and provides a rugged shape.

4) The horizontal orientation permits "head-to-toe" low-resistance interconnections which are necessary to maintain high peak power capability.

5) It provides a shape for efficiently packaging 480 cells into the battery's thermal enclosure.

The design of a horizontally operating cell placed severe demands on the sodium storage and protection devices to assure: 1) full and continued coverage of the electrolyte's inner surface by sodium independent of the level of remaining reactant; and 2) minimization of the annular volume outside the protection tube to control cell safety and reduce the tolerances on the weight of sodium.

4.1.1.2 Fabrication. The principal cell fabrication issue was the control of dimensional tolerances and electrolyte alignment. The electrolyte dimensions were especially critical since ovality, bow or undersize diameter would prevent insertion of the sodium reservoir; and misalignment or oversize diameter would interfere with the sulfur electrode. Special tooling and fixtures were developed for cell fabrication and inspection.

The materials of construction were the same as those in the Mark-II cell with the exception that because of the limited availability of E-Brite stain-

less steel, the sulfur container was of Type 410 stainless steel (electroplated with chromium). Difficulties were encountered with welding and glassing operations as a result of a martensitic transformation in the stainless steel. In addition, the material provided less corrosion resistance near coating defects and in unprotected areas than had the E-Brite stainless steel of previous cells.

Development of an effective sodium storage and feed system proved difficult because of the close dimensional tolerances. Exploratory cells were fabricated with a series of design changes to evaluate their safety and effectiveness. Unfortunately, the problem of erratic performance persisted into the initial production of battery cells and required continuing cell modifications. Ultimately, more than 800 cells were fabricated. Although one cell of each lot of 25 cells was designated for QA testing, most of these cells were reassigned to support the assembly of the prototype module and the EVEM-1 battery.

4.1.1.3 Cell Evaluation. Following resolution of the sodium storage and feed problem and confirmation of cell safety, the EVEM-1 cells were evaluated for performance under steady and pulsed loads as a function of temperature and orientation. Cycle life, durability under vibration and shock conditions, and freeze-thaw and post-failure conductance characteristics were also evaluated.

The performance of the EVEM-1 cell was excellent. The response to various levels of steady discharge and charge currents is shown in Figure 4-3, showing the full capacity and nearly constant resistance properties of the cell. The corresponding Ragone diagram, Figure 4-4, compares the high specific energy (~165 Wh/kg at C/3) with that achieved by previous exploratory EV cells. The response at 30-s pulse loads showed a very high peak power density (132 W/260 cm, 500 W/l fully charged) that decreased slowly with state-of-charge (>400 W/l at 80 percent depth of discharge) and was nearly independent of orientation, as shown in Figure 4-5.

Because of the small number of cells for single-cell testing, a statistically significant cycle life test was not accomplished. However, the longest cycle life test was not accomplished. However, the longest cycle life exceeded 2000 cycles, with acceptable performance continuing beyond 1500 cycles, as shown in Figure 4-6. In another test all of a group of five cells surpassed 1000 cycles operating vertically, with four cells remaining on test at the end of the program.

The EVEM-1 cell also proved durable to shock and vibration loads exceeding those expected in normal vehicle operation. Five cells were subjected to shock loads (11-ms half-sine, up to 24 g), sine-sweeps (up to 30 g at resonances), and random vibrations (to 9 g rms) with the cells at their operating temperature and the loads applied perpendicular to the tube axis. No cell damage was observed in any of the cells.

A successful test of freeze-thaw characteristics was made on a few cells prior to battery assembly. Following the observation of a high cell failure rate in the battery associated with freeze-thaw cycles (about 3 percent per freeze-thaw cycle), more extensive testing was performed using previously tested cells. These data showed higher failure rates to be associated with

FIGURE 4-3. VOLTAGE CHARACTERISTICS OF EVEM-1 CELLS

FIGURE 4-4. RAGONE DIAGRAM

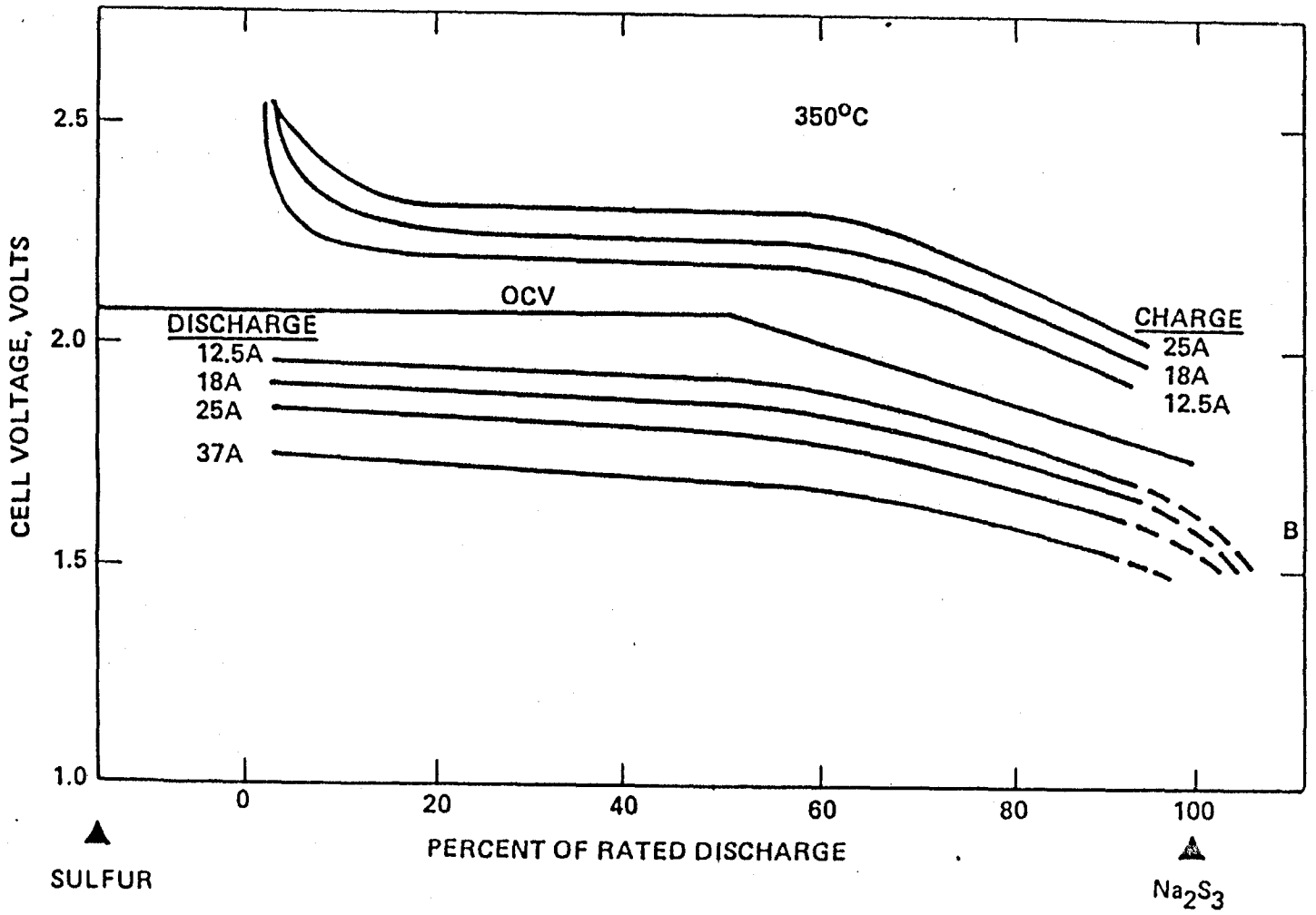
350°C
OCV
DISCHARGE
12.5A
18A
25A
37A
CHARGE
25A
18A
12.5A
B
CELL VOLTAGE, VOLTS
2.5
2.0
1.5
1.0
0
20
40
60
80
100
PERCENT OF RATED DISCHARGE
SULFUR
Na_2S_3

Figure 4-3

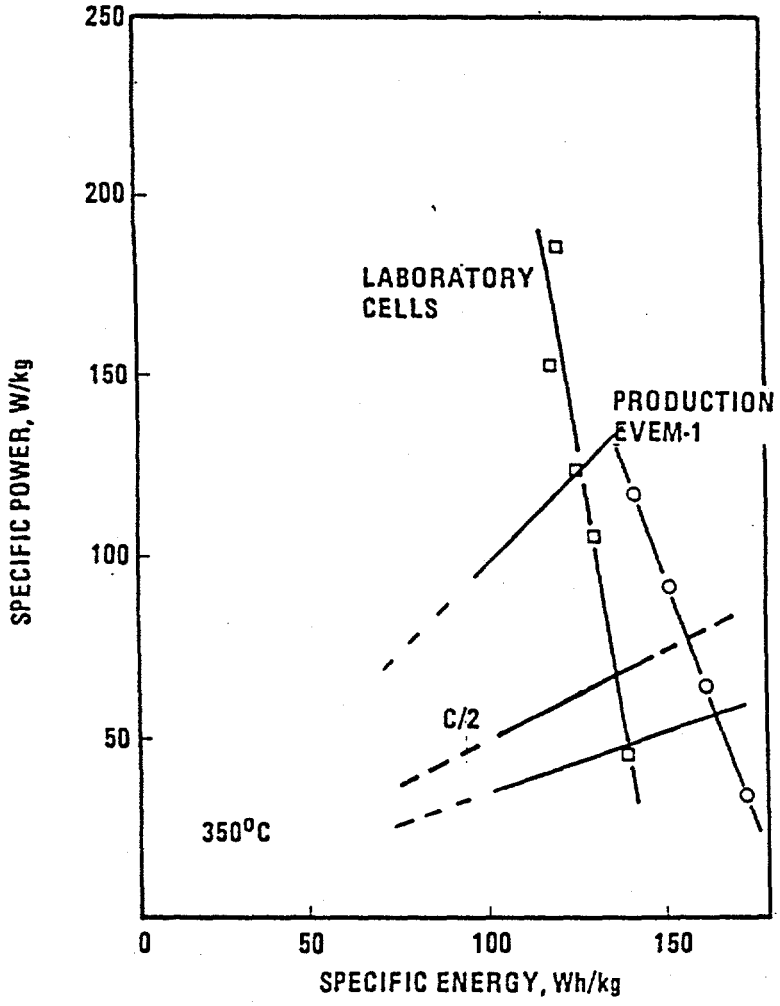
250
200
150
100
50
0
50
100
150
SPECIFIC POWER, W/kg
SPECIFIC ENERGY, Wh/kg
LABORATORY CELLS
PRODUCTION EVEM-1
C/2
350°C

Figure 4-4

FIGURE 4-5. PULSE RESPONSE OF EVEM-1 CELLS

FIGURE 4-6. LONG CYCLE LIFE CELL

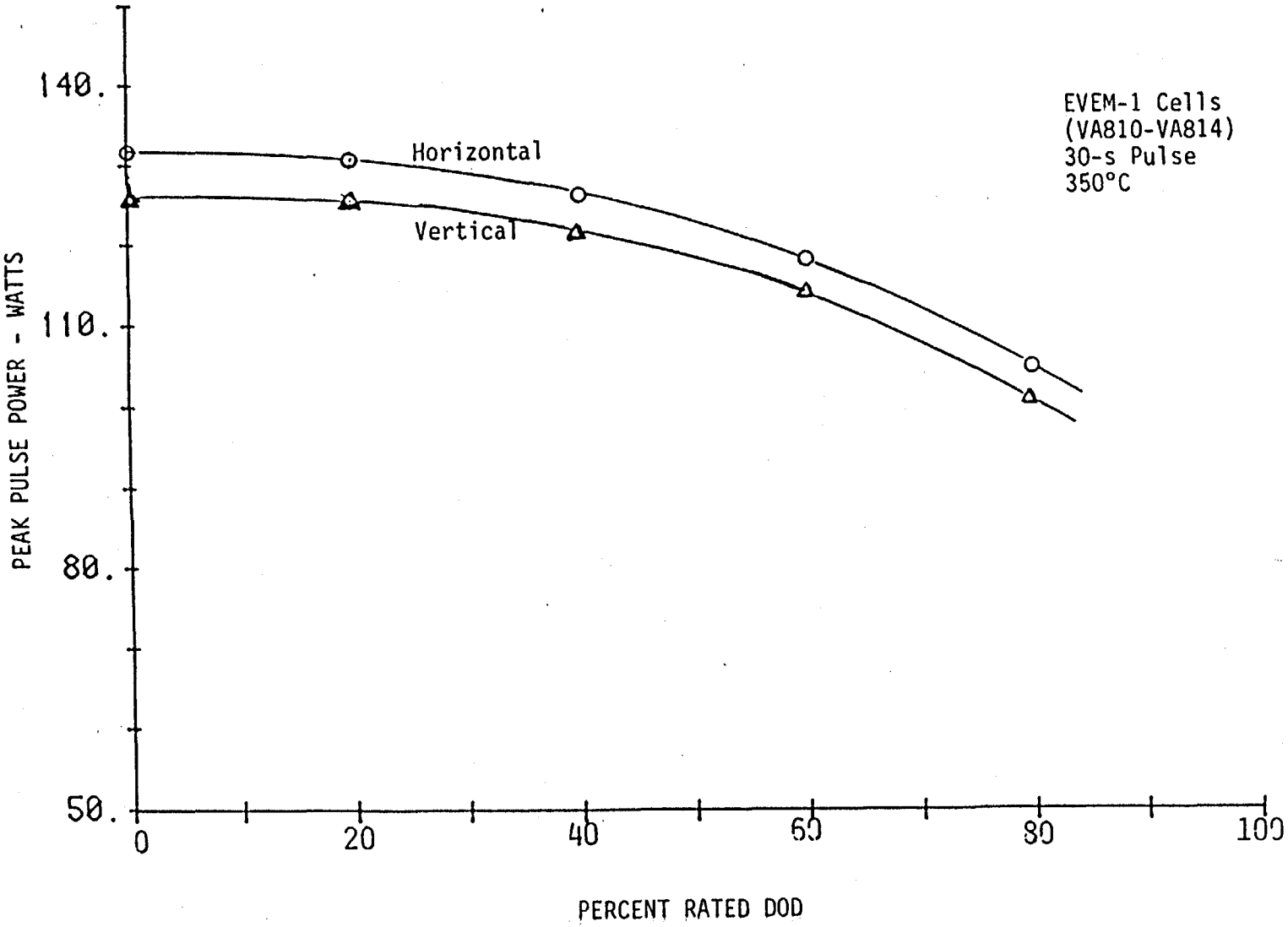
140.
110.
80.
50.
PEAK PULSE POWER - WATTS
Horizontal
Vertical
EVEM-1 Cells
(VA810-VA814)
30-s Pulse
350°C
0
20
40
60
80
100
PERCENT RATED DOD

Figure V-5

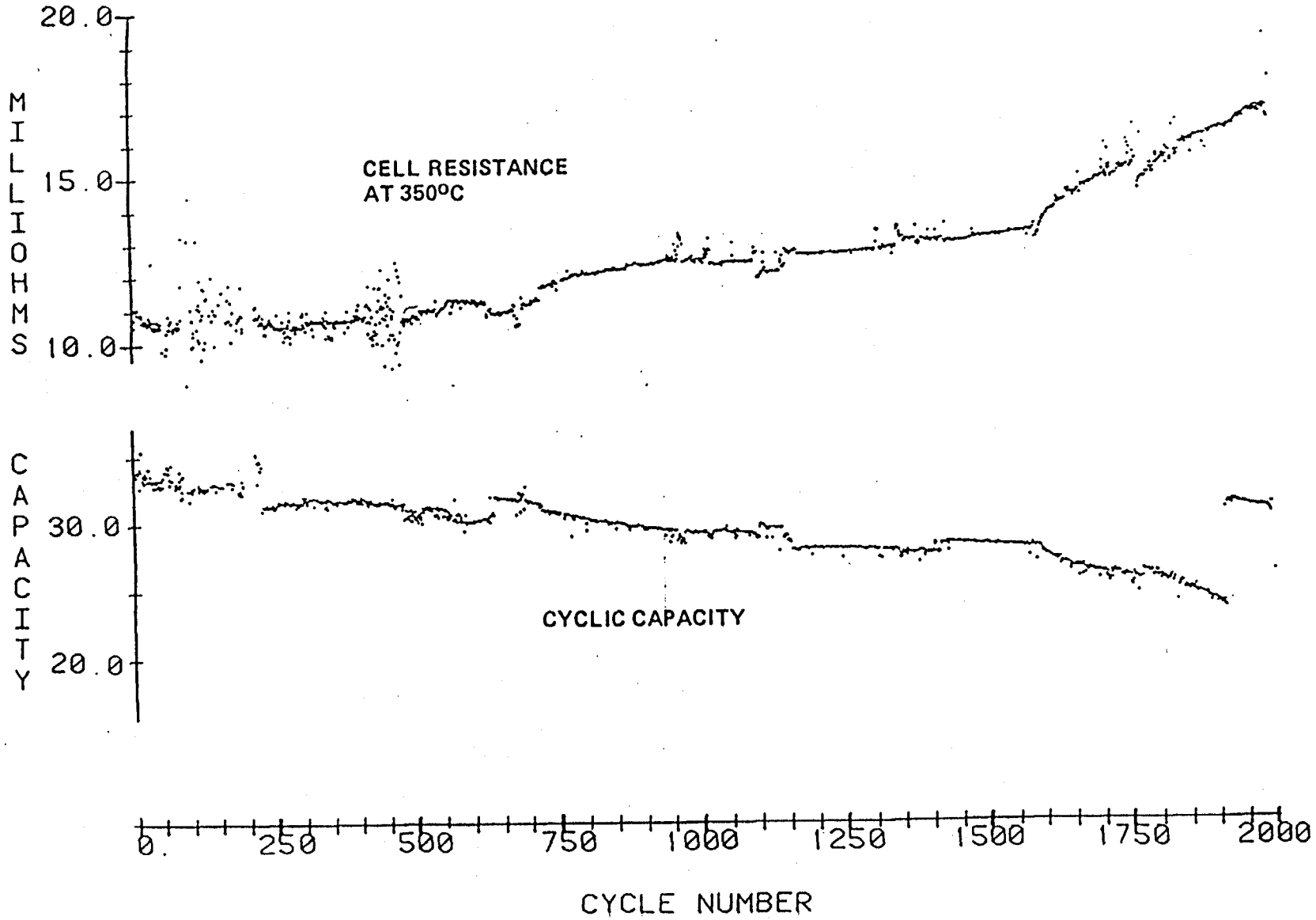
20.0
15.0
10.0
MILLIOHMS
CELL RESISTANCE
AT 350°C
30.0
20.0
CAPACITY
CYCLIC CAPACITY
0.
250
500
750
1000
1250
1500
1750
2000
CYCLE NUMBER

Figure 4-6

horizontal orientation, probably due to lack of cylindrical symmetry of stresses on the electrolyte. Very high failure rates were encountered upon reheating those cells which had been frozen when horizontal and in a completely discharged state. Less than half of the 120 cells survived reheating under these conditions.

In addition to fracture of its electrolyte, the EVEM-1 cell exhibited loss of performance as a result of thermal cycling, probably a result of delamination of the corrosion product layer from the container. This effect was more severe for older cells, or for cells frozen when deeply discharged. Poor ability to survive freeze thaw was one of two practical shortcomings of the EVEM-1 cell designs.

The second concern from a battery viewpoint was the high resistance of failed cells which seriously reduced the peak-power capability of a string of cells in series. Typical values of post-failure resistance ranged from 20 to 160 milliohms, and were not stable with time. Post-failure resistance is discussed in more detail in Section 4.3.4.4.

In summary, the EVEM-1 cell proved safe and had excellent power and energy. However, its poor reliability with respect to sodium supply (capacity), freeze-thaw survival and post-failure conductance defined specific areas for improvement in the next generation cell for the ETX battery. Development of the ETX cell is summarized in Section 4.1.2.

4.1.2 ETX CELLS

The longer, vertically oriented ETX cell was designed to incorporate the favorable performance features of the EVEM-1 cell while providing improved freeze-thaw and sodium-feed reliability. The cell capacity was increased to 55 Ah, thereby reducing the number of cells required for the battery from 480 to 360, and lowering the complexity and cost of the battery.

4.1.2.1 Design. The ETX cell design maintained many of the critical features of the EVEM-1 cell, including the diameter and wall thickness of the electrolyte, all seal geometries, and the diameter of the cell. The principal change was the specification for vertical orientation in order to: 1) provide improved symmetry of stresses associated with freeze-thaw cycles; 2) assure better control of the sodium-feed supply; and 3) provide a convenient location of cell terminals for partial battery maintenance (cell bypass) without cooling and dismantling the battery.

Vertical cell operation introduced two significant design issues related to the method of attachment and increased resistance of the longer intercell connector. The increased lead resistance proportionally reduced peak-power capability, and had to be balanced against an increased conductor cross-section which interfered with cell-to-cell packing density, even with an aluminum conductor. Attachment of the conductor to the side of the container near the top seals was preferable to reduce its length, and it had to be electrically insulated passing the anode container and seal.

The 33 percent higher cell capacity required a proportionately longer electrolyte and cell. To avoid sizable electric resistance losses and maintain uniform electrical operation along the cathode container without serious weight penalty, a conductive shunt was added to the outside of the container. Two alternate approaches were developed--a flame-sprayed aluminum coating and a narrow bimetal (steel/aluminum) strap seam welded to the container. Either method provided a convenient anchor for attaching the cathode lead. The flame-sprayed aluminum coating was selected for the preproduction cells.

Apart from the vertical orientation and increased length, other major design changes included: 1) use of an E-Brite stainless steel cathode container for improved cycle life; 2) plasma-sprayed zirconia bands for intercell spacers; and 3) a flexibly connected sodium reservoir to eliminate possible mechanical stresses on the electrolyte due to misalignment or interference. A schematic of the cell and its performance ratings were presented previously in Figure 4-2 and Table 4-1.

4.1.2.2 Manufacturing. Developmental ETX cells were fabricated incorporating various aspects of the overall design as the components became available. A comparison of the salient features of these cells is presented in Table 4-2. Tooling, gauges and fixtures were modified for the new size. Despite tighter dimensional tolerances on the electrolyte assembly because of its increased length, dimensional control and uniformity of the electrolyte was markedly improved by Ceramatec, Inc., resulting in a high yield and routine QC acceptance.

TABLE 4-2. DEVELOPMENTAL ETX CELLS

Series Designation	No. of Cells	Sulfur Electrode Length	Conductive Shunt	Ceramic Spacer	Other
Exploratory					
A	6	2 segments	No	No	Floating sodium reservoir
B	9	2 segments	No	No	Flexible sodium reservoir (FLEX)
C	30	2 segments	No	No	FLEX; shortened container
Prototype					
D	55	Continuous	Flame-sprayed	Yes	FLEX; design length
Preproduction					
E	25	Continuous	Flame-sprayed	Yes	FLEX; reduced length
Alternate					
F	23	Continuous	Bimetal	Yes	FLEX; reduced length

4.1.2.3 Cell Evaluation. The initial evaluation focused on confirming safety and assuring nominal rated output. Excellent safety was achieved with all design variations; however, the cell output was inadequate for the cells of Series A and B. Full rated capacity and nearly rated peak power were obtained from the Series C cells, even without the conductive shunt. Five of these cells were evaluated for ability to withstand repeated freeze-thaw cycles. Each cell successfully completed 40 freeze-thaw cycles in a fully charged state, with no electrolyte fracture and only minor loss in performance (5 percent capacity decline, 13 percent resistance increase).

The thermal cycle evaluation was repeated on cells of Series D that incorporated the flame-sprayed aluminum shunt and the plasma-sprayed zirconia bands. Fourteen cells were assigned to the test and completed 14 to 16 freeze-thaw cycles with no electrolyte failures, minor performance change, and no delamination of the aluminum or ceramic insulating bands. The test was aborted because the cells were damaged during a repair of their cathode terminal. Fifteen additional cells of this design that had completed ∿100 electrical cycles were reassigned to freeze-thaw testing. This test was structured to address the effects of depth-of-discharge (DOD), with 5 cells each at 0, 5, and 100 percent DOD. Preliminary results after 5 freeze-thaw cycles showed no deterioration for charged or half-charged cells, but substantial failure rates for cells frozen at ∿100 percent DOD.

Post-failure resistance of the exploratory and prototype cells was variable and high, enforcing the conclusion that development of an external failed-cell bypass is necessary. (See Section 4.3.4.4 for a discussion of post-failure resistance of EVEM-1 cells.)

The performance characteristics of developmental ETX cells under steady loads are compared in the Ragone plot, Figure 4-7. Although the exploratory cells (Series C) did not have aluminum shunts or the proper full-length sulfur electrode, their performance was excellent. It met the ETX design goal for energy (136 Wh/kg at C/3) and exceeded the rated peak power (180 W/kg) to beyond 75 percent DOD.

The performance of the prototype cells, Series D, with conductive shunts and improved sulfur electrodes, fell about 10 percent short of the goals for both energy and power. This relatively poor performance resulted from a design feature that provided excess volume at the bottom of the cell. As a consequence, some reactant remained inactive, reducing available capacity.

The excess volume at the bottom of the cell was present to accommodate the anticipated worst-case tolerance stackup of component dimensions and reactant volume expansion in the event of electrolyte fracture. A review of the tolerances based on actual hardware dimensions and reactant amounts showed that the ullage allowance far exceeded the requirements. The preproduction cells, Series E, incorporated a modified end cap to reduce the volume at the bottom of the cell.

The performance of the preproduction cells showed excellent response to both steady and pulsed loads. Preliminary data are presented in Table 4-3 and Figure 4-8. The high peak pulse power resulted from a low pulse resistance

independent of DOD. A comparison of cell resistance during steady and pulsed discharge is presented in Figure 4-9 for a preproduction cell. During steady discharge, concentration polarization losses increased the effective resistance at mid-cycle.

Cycle life tests were in progress on a number of cells of different designs at the end of Phase VB. The cells have shown excellent chargeability and stable performance over the limited duration of the test. The status of these tests is summarized in Table 4-4.

In summary, preliminary evaluation of the ETX preproduction cells indicates that all design objectives have been accomplished. The cells are safe and very durable with respect to repeated freeze-thaw cycles when charged, and provide very high specific energy and power density. Post-failure resistance is yet to be evaluated, as is the tolerance to vibration and shock loads.

FIGURE 4-7. PERFORMANCE OF ETX DEVELOPMENT CELLS

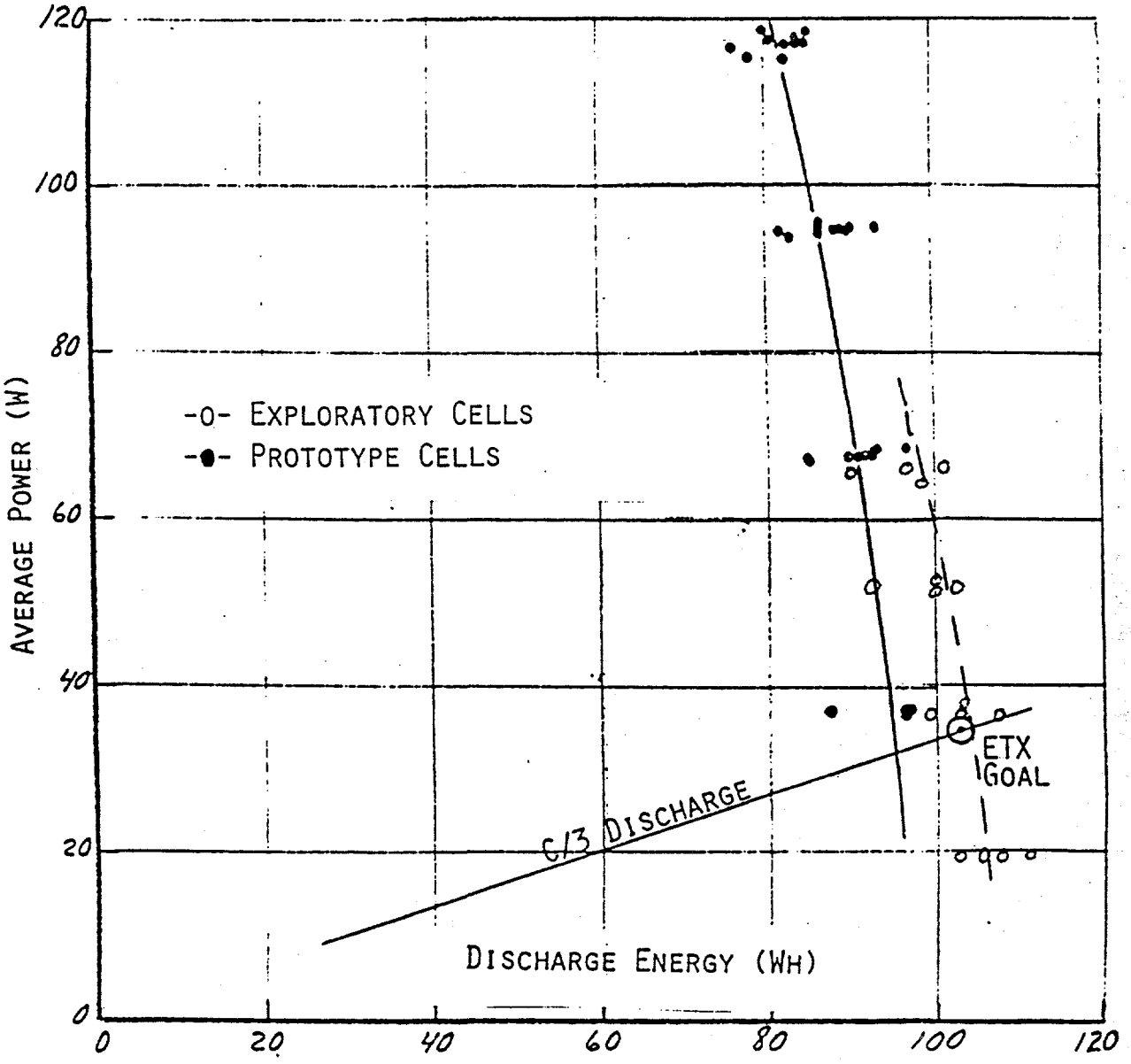
120
100
80
60
40
20
0
AVERAGE POWER (W)
-o- EXPLORATORY CELLS
-●- PROTOTYPE CELLS
C/3 DISCHARGE
ETX GOAL
0
20
40
60
80
100
120
DISCHARGE ENERGY (WH)

Figure 4-7

TABLE 4-3. PREPRODUCTION CELL PERFORMANCE

	No. VRA-37	ETX Goals
Resistance (mΩ)	7.69	7.8
Capacity (Ah)	56.7	55
Charge Limit	.08	0.15
Pulse Power (W) @ 80% DOD	139	135

FIGURE 4-8. PEAK PULSE POWER OF PREPRODUCTION CELLS

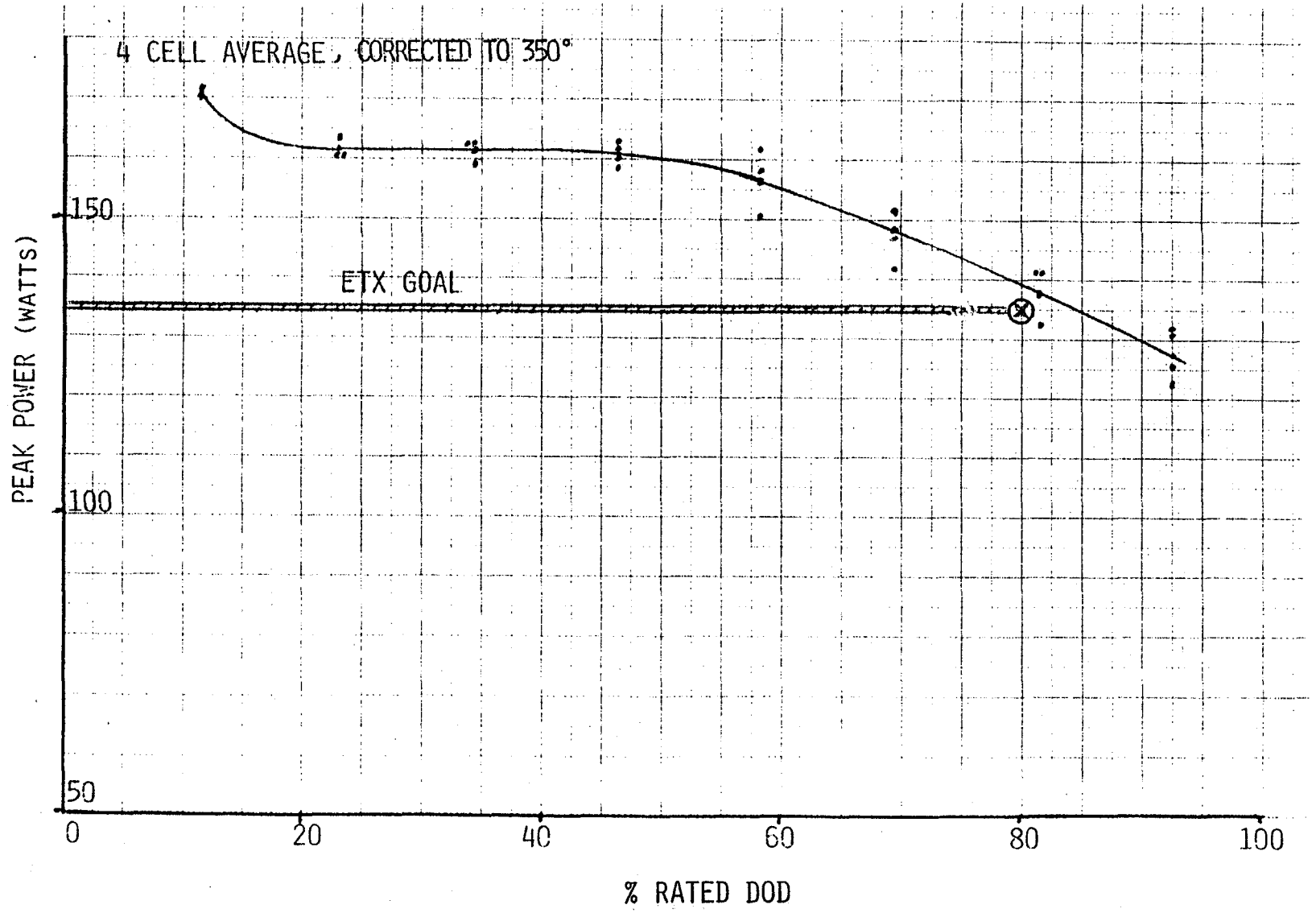
4 CELL AVERAGE, CORRECTED TO 350°
ETX GOAL
PEAK POWER (WATTS)
150
100
50
0
20
40
60
80
100
% RATED DOD

Figure 4-8

FIGURE 4-9. CELL RESISTANCE DURING STEADY AND PULSED DISCHARGES

TABLE 4-4. STATUS OF CYCLE LIFE TESTS

	Initial Value	Present Value	Change per Cycle [ΔX/X]/N
Exploratory Cells (Series C)			
4 Cells; 1.7 V Cutoff			
Cycle No.	∿10	∿358	
R (mΩ)	9.05	9.25	$+0.61 \times 10^{-4}$
Cap (Ah)	48.72	48.37	-0.21×10^{-4}
Chargeability*	8.4	8.3	
8 Cells; 1.6 V Cutoff			
Cycle No.	∿40	∿298	
R (mΩ)	9.03	8.65	-1.70×10^{-4}
Cap (Ah)	59.15	59.50	$+0.23 \times 10^{-4}$
Chargeability*	7.8	7.1	
Prototype Cells			
20 Cells; 1.75 V Cutoff			
Cycle No.	∿15	∿159	
R (mΩ)	8.77	8.46	-2.5×10^{-4}
Cap (Ah)	41.56	43.23	$+2.7 \times 10^{-4}$
Chargeability*	14.4	15.8	

*Percent of theoretical capacity. (Design value is 15.0 percent.)

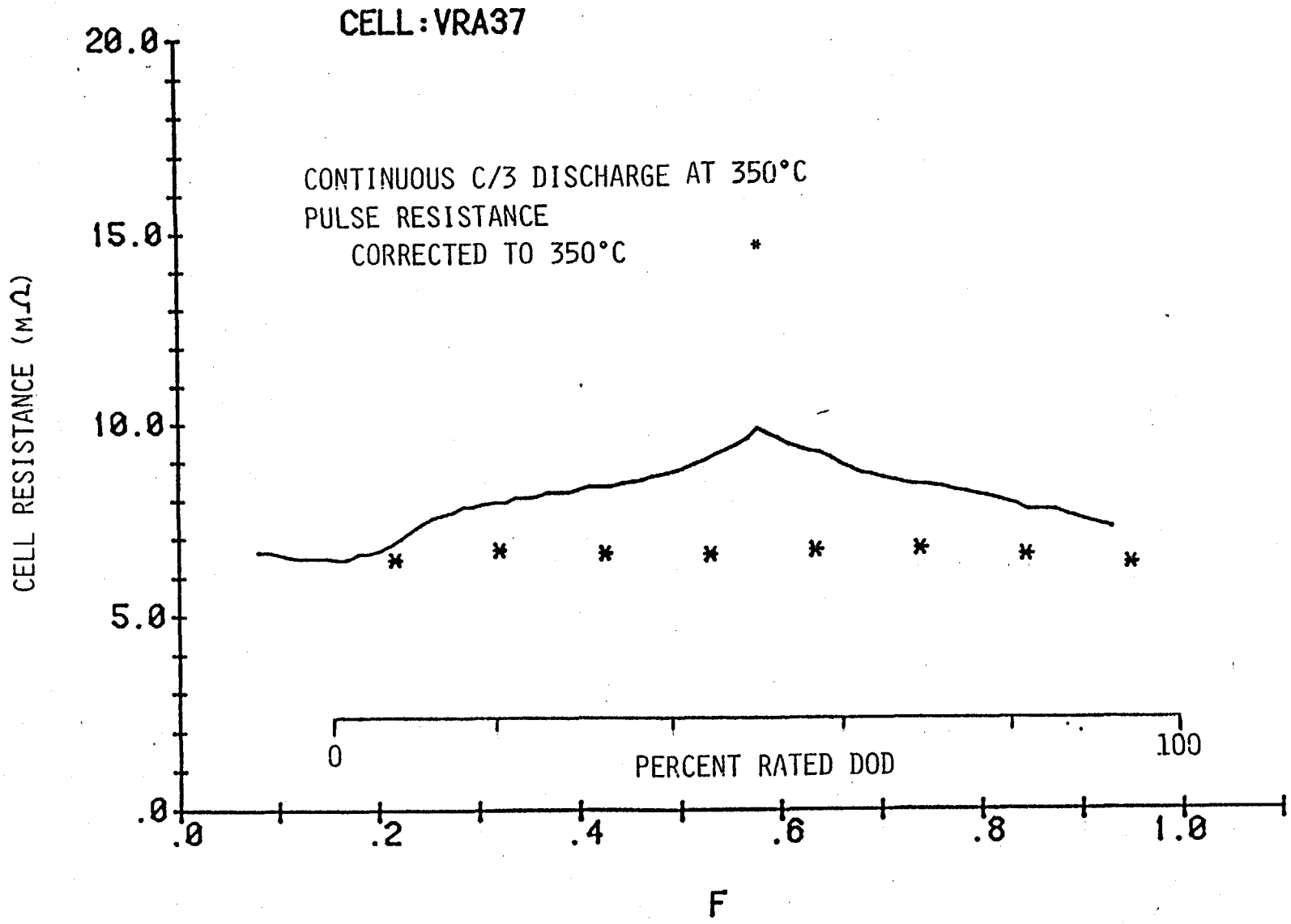
CELL: VRA37
CONTINUOUS C/3 DISCHARGE AT 350°C
PULSE RESISTANCE
CORRECTED TO 350°C
*
CELL RESISTANCE (mΩ)
20.0
15.0
10.0
5.0
.0
0
100
PERCENT RATED DOD
.0
.2
.4
.6
.8
1.0
F

Figure 4-9

4.2 SES CELL DEVELOPMENT

SES cell development efforts were directed toward: 1) durability testing of Mark-II cells; and 2) design, fabrication, and evaluation of high-energy cells for weekly storage cycles, as summarized in Sections 4.2.1 and 4.2.2, respectively.

4.2.1 MARK-IID Cells

Since August 1980 the Mark-IID has been the program's standard load-leveling cell. Extensive discussion of its design, characteristics and performance can be found in previous reports.[1] The present report discusses the outcome of life tests extending over the last four years. Sections 4.2.1.1 and 4.2.1.2 summarize a 20-cell life test and the post-test analysis of a surviving cell, respectively. Section 6.2 discusses tests of a battery constructed from 512 Mark-IID cells.

4.2.1.1 Life Tests. In August 1980, 20 of the first 50 Mark-IID cells were placed in a box oven and electrically cycled twice daily in a life test, which lasted until May 1982 when the belt on a circulating-air fan failed, causing the control system to cool the oven and resulting in conclusion of the test. Table 4-5 summarizes the outcome.

TABLE 4-5. OUTCOME OF 20-CELL TEST

STATUS (End of Test, May 9, 1982)	NUMBER OF CELLS	
o Operating satisfactorily*	5	
After 1182 cycles		4
After 704 cycles**		1
o Capacity (Q) less than 60% of theoretical	7	
o Ceramic failure	5	
Occurred when Q >60%		4
Occurred when Q <60%		1
o Probable equipment-induced failures	2	
o Never operated (no-start cell)	1	
TOTAL	20	

*Cycled twice daily at 320°C, discharged 5 h at 24 A and charged at 18 A to 2.3 V; Q >60% of theoretical.
**Presumed failed and idled for 260 days (at 320°C) after 390 cycles then restarted.

Of the five cells which were operating satisfactorily when the oven cooled, one was dissected for the post-test analysis described in Section 4.2.1.2. The remaining four cells were reheated in individual ovens for additional testing. Three have subsequently failed; one (No. LL181) continues to operate satisfactorily after 53 months. The causes of the three failures are as follows:

Cell No.	Time on Test Cycle	Time on Test Mo.	Cause of Failure
LL182	815	24	Equipment-induced
LL183	1257	24	Electrolyte failure
LL196	1470	30	Loss of capacity

Cell No. LL181 has completed over 2300 cycles. (The goal is 2500 cycles.) As it ages, performance is becoming very temperature sensitive. Figure 4-10 charts the variation in resistance over the cell's life. At temperatures above 330°C, the resistance is less than 14.4 mΩ, the original goal for a Mark-IID cell at the end of life. Its capacity also remains above 60 percent of theoretical if the temperature is above 330°C.

Figure 4-11 is a Weibull probability plot summarizing the statistical analysis of cell-life data from testing these 20 cells. The analysis considers electrolyte fracture as the sole failure mode. In the plot the four failures occurring in the box oven are shown as black dots, and the failure which occurred later during the extended testing of the surviving five cells is shown as an open dot. All five dots fall along a straight line, indicating they probably are due to the same failure mechanism. The Weibull parameter α, which is estimated to be about 1730 cycles, infers that 63 percent of the cells (in a test without replacements) will fail (due to electrolyte fractures) by 1730 cycles. The parameter β is 1.37, indicating the rate of failure is increasing slowly with time.

Figure 4-11 supercedes the Weibull plot presented as Figure 3-23 in the Interim Report[1], which is in error because at that time one cell was presumed to have failed in its 390th cycle. Actually the cell was operable, and eventually cycling was renewed after 260 days at idle.

4.2.1.2 Post-Test Analysis. Cell No. LL198--one of the 5 cells operating acceptably at the conclusion of the 20-cell oven test--was dissected to examine the electrolyte and sulfur container for signs of degradation. Diametral strength tests on 12 rings cut from the electrolyte showed the mean breaking strength was 237 ± 12 MPa (34.4 ± 1.7 kpsi). (The breaking strength of as-received β"-alumina is about 250 MPa.) Electrolyte coloration extended to a depth of 1 mm on the sodium side while the sulfur side was relatively free of stains. No internal sodium precipitation was detected. The electrolyte was cut into three sections for post-test analysis. One section developed a longitudinal crack coincident with the location of a lontigudinal gap in the electrode felt, suggesting that electrode gaps cause high stress buildup in electrolytes. Mild chromium-coating corrosion was noted with very small regions of penetration to the E-Brite substrate.

FIGURE 4-10. CELL RESISTANCE AS A FUNCTION OF CYCLE LIFE

FIGURE 4-11. WEIBULL PROBABILITY PLOT FOR ELECTROLYTE FAILURES IN 20-CELL LIFE TEST

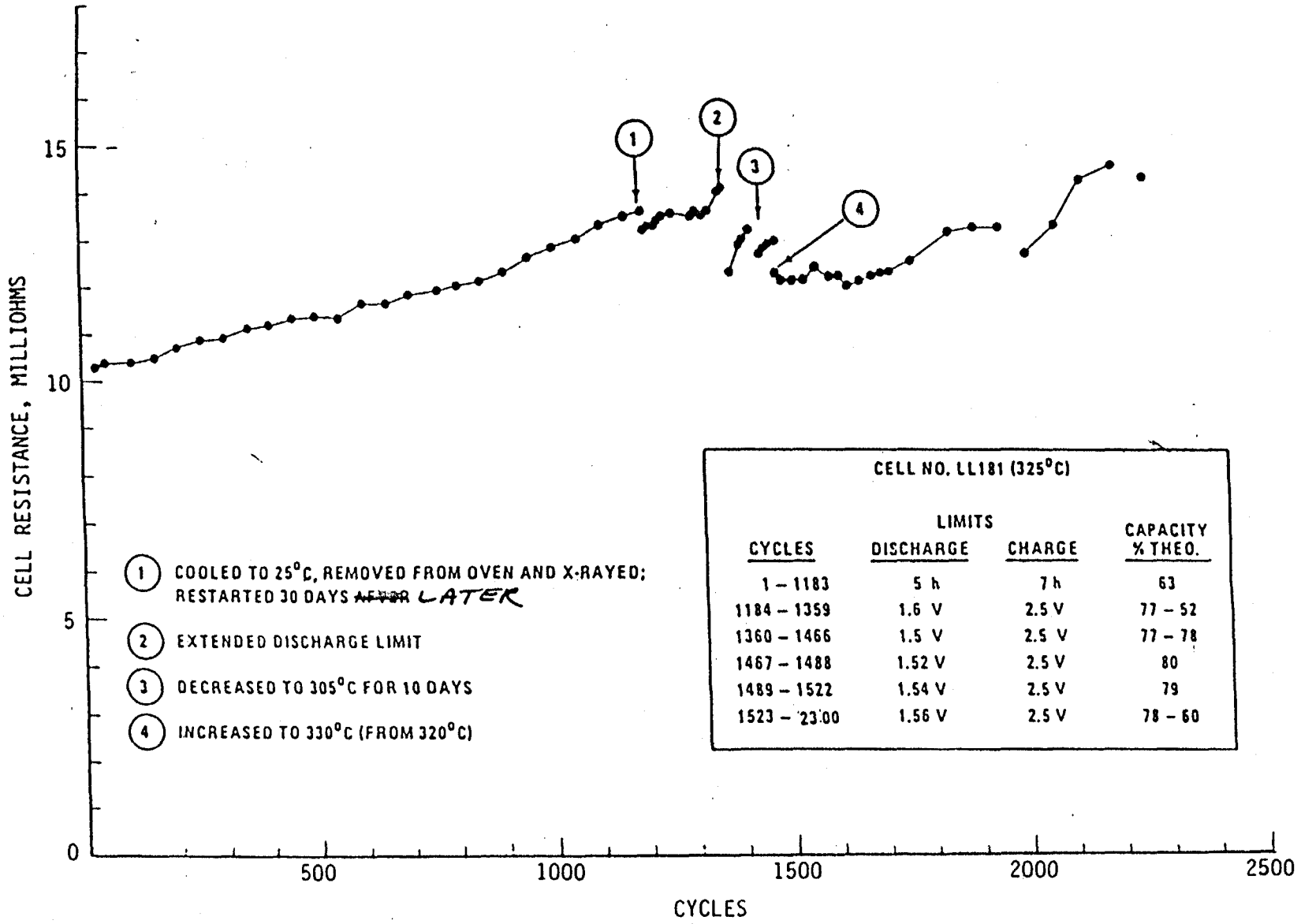
CELL RESISTANCE, MILLIOHMS
15
10
5
0
500
1000
1500
2000
2500
CYCLES
1
2
3
4
1 COOLED TO 25°C, REMOVED FROM OVEN AND X-RAYED; RESTARTED 30 DAYS ~~AFTER~~ LATER
2 EXTENDED DISCHARGE LIMIT
3 DECREASED TO 305°C FOR 10 DAYS
4 INCREASED TO 330°C (FROM 320°C)
CELL NO. LL181 (325°C)
CYCLES | LIMITS DISCHARGE | LIMITS CHARGE | CAPACITY % THEO.
1 – 1183 | 5 h | 7 h | 63
1184 – 1359 | 1.6 V | 2.5 V | 77 – 52
1360 – 1466 | 1.5 V | 2.5 V | 77 – 78
1467 – 1488 | 1.52 V | 2.5 V | 80
1489 – 1522 | 1.54 V | 2.5 V | 79
1523 – 2300 | 1.56 V | 2.5 V | 78 – 60

Figure 4-10

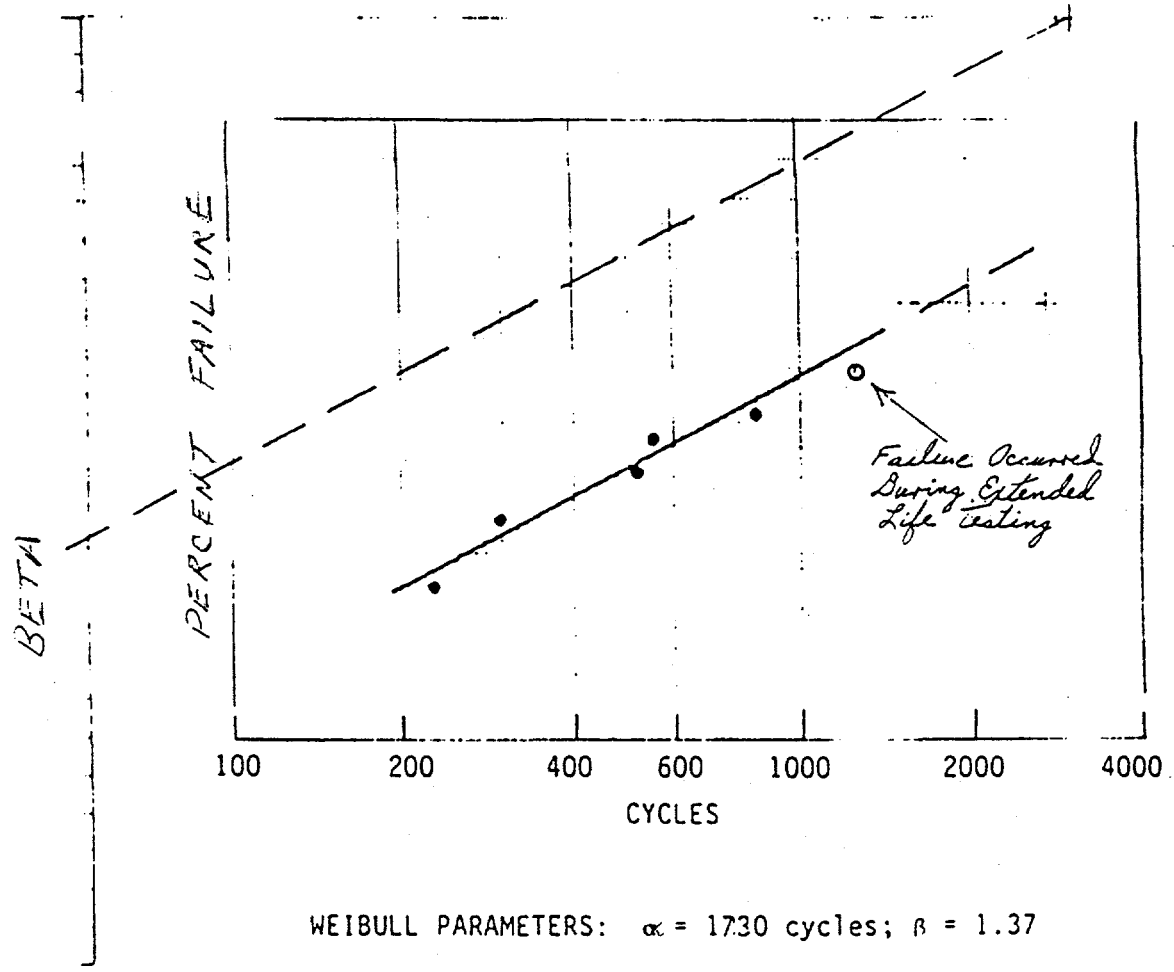

WEIBULL PARAMETERS: α = 1730 cycles; β = 1.37

Figure 4-11

4.2.2 HIGH-ENERGY CELLS

High-energy cells are projected to be economically advantageous for applications such as storage for renewable energy sources and utility applications using weekend charging. Previously excellent performance had been demonstrated by cells with a theoretical capacity of 575 Ah. In Phase VB, 46 additional high-energy cells were fabricated: two 575-Ah (theoretical) cells using Mark-II size electrolytes, two 1785-Ah (theoretical) super-energy cells using double length electrolytes of Mark-II diameter, and forty-two 700-Ah (theoretical) cells using Mark-II electrolytes. The electrode thicknesses for these cells were 21.4, 30.3, and 24.3 mm, respectively. By comparison, the electrode thickness in a Mark-II cell is 9.0 mm. Rated performance based on tests for the first two of these cell sizes is compared to that of a Mark-II load-leveling cell in Table 4-6.

TABLE 4-6. RATED PERFORMANCE OF STATIONARY ENERGY STORAGE CELLS

Cell Type	Capacity Ah	Energy Wh	Efficiency %	Discharge/Charge h
Super-Energy	1250	2250	85	40/60
High-Energy	440	810	85	20/40
Mark-II	150	250	75	5/7

A high-energy cell was used to demonstrate a weekly cycle comprising weekday discharges of 10 h and charges of 7 h with a weekend charge back of 42 h as shown in Figure 4-12. The short daily segments dramatized the effect of cathode polarization. Cycle efficiency was significantly improved with the segmented-operation mode. Even with a 21.4-mm thick electrode, the cell had excellent chargeability to about 6 percent of theoretical capacity. An electrolyte current density of 47 mA/cm^2 was used during charge to a cutoff voltage of 2.5 V. Discharging to about midway between the Na_2S_4 and Na_2S_3 compositions, this cell operated to over 81 percent of its theoretical capacity.

Cycle voltage is shown in Figure 4-13 for a super-energy cell operated at an electrolyte current density of 42 mA/cm^2. Electrode thickness in this cell was 30.3 mm. The cycle-averaged resistance was 7.9 milliohms, higher than expected ($\sim$6 milliohms). The high resistance was attributed to a temperature gradient along the cathode from a low of 315°C to a maximum of 350°C which was the result of an inadequate test oven size for the unusually large cell. Following a 5-h taper charge, the cell delivered 80 percent of its theoretical capacity when discharged to an OCV of 1.85 V, in spite of the thermal handicap.

Figure 4-14 presents discharge performance of a super-energy cell. Taper charging at 10 A was carried out before each discharge. At 8.8 A the cell discharged for 180 h, while at 50 A (104 mA/cm^2 of electrolyte) the discharge period was 27.5 h. Discharge cutoff voltages were somewhat arbitrary for this test, and each discharge curve could have been extended to at least the 1500-Ah mark representing 84 percent of the theoretical capacity.

FIGURE 4-12. HIGH-ENERGY CELL WEEKLY CYCLE

FIGURE 4-13. SUPER-ENERGY CELL PERFORMANCE

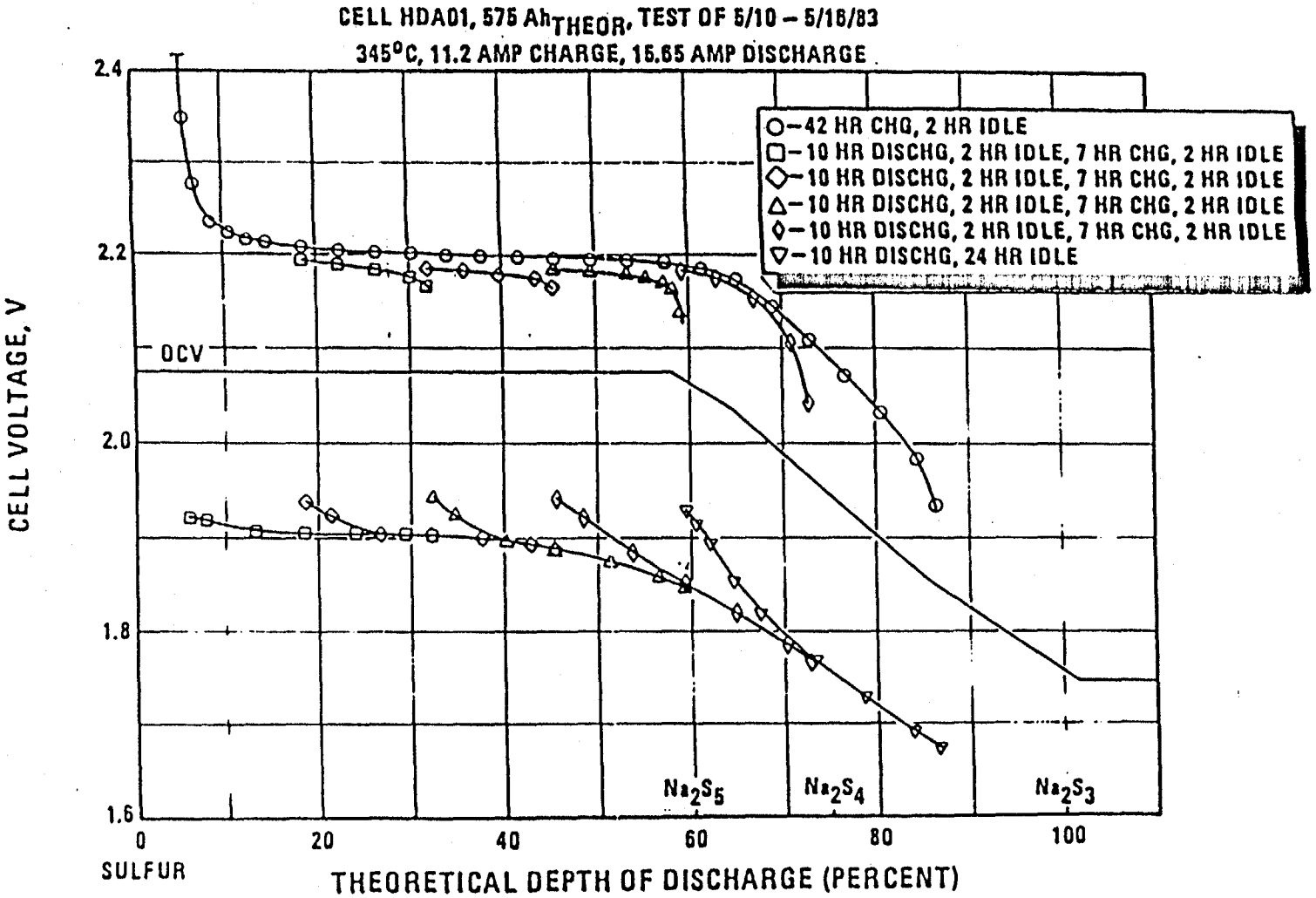
CELL HDA01, 575 Ah THEOR, TEST OF 5/10 – 5/16/83
345°C, 11.2 AMP CHARGE, 15.65 AMP DISCHARGE
O–42 HR CHG, 2 HR IDLE
□–10 HR DISCHG, 2 HR IDLE, 7 HR CHG, 2 HR IDLE
◇–10 HR DISCHG, 2 HR IDLE, 7 HR CHG, 2 HR IDLE
△–10 HR DISCHG, 2 HR IDLE, 7 HR CHG, 2 HR IDLE
◊–10 HR DISCHG, 2 HR IDLE, 7 HR CHG, 2 HR IDLE
▽–10 HR DISCHG, 24 HR IDLE
CELL VOLTAGE, V
2.4
2.2
2.0
1.8
1.6
OCV
Na2S5
Na2S4
Na2S3
0
20
40
60
80
100
SULFUR
THEORETICAL DEPTH OF DISCHARGE (PERCENT)

Figure 4-12

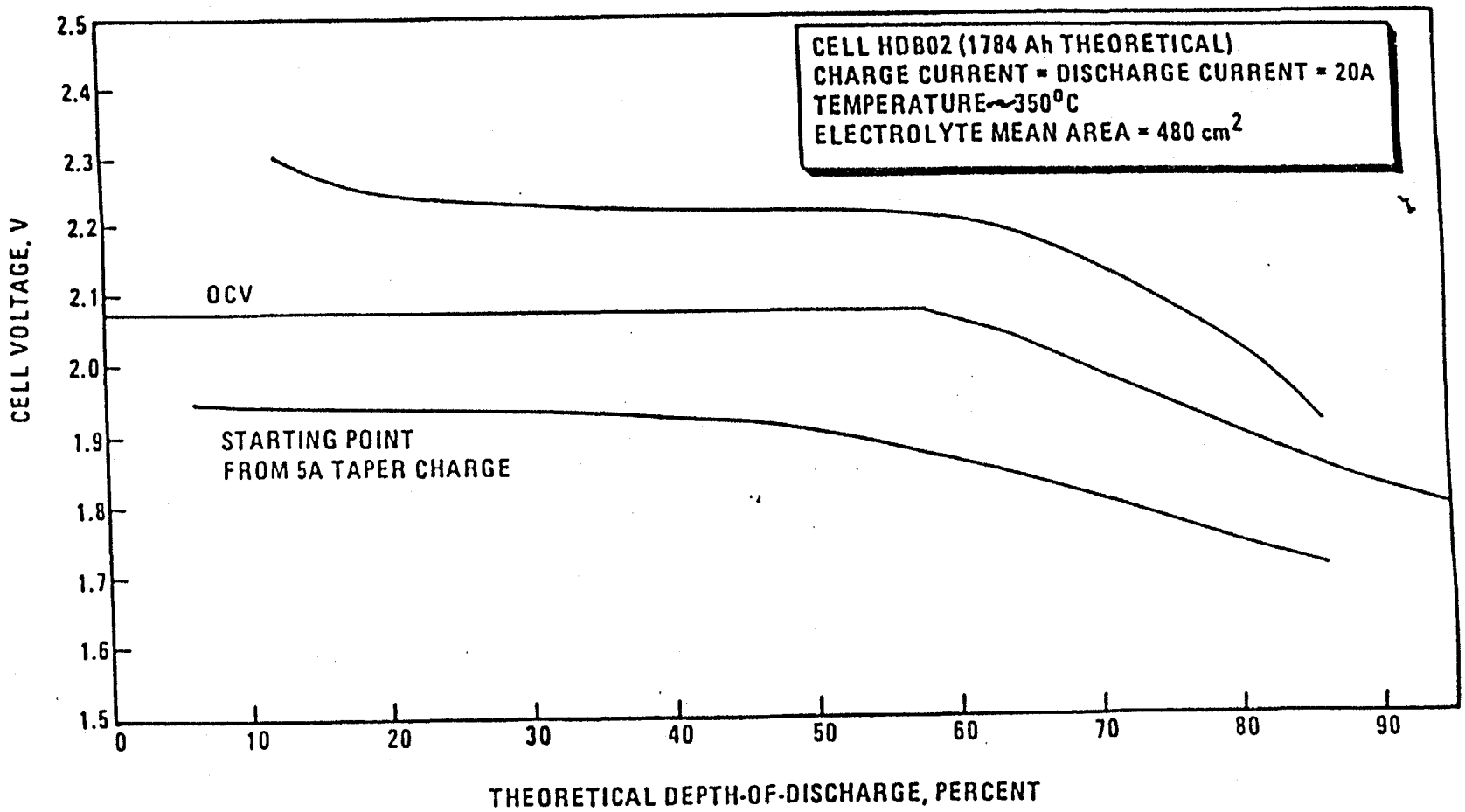
CELL HDB02 (1784 Ah THEORETICAL)
CHARGE CURRENT = DISCHARGE CURRENT = 20A
TEMPERATURE~350°C
ELECTROLYTE MEAN AREA = 480 cm²
OCV
STARTING POINT
FROM 5A TAPER CHARGE
CELL VOLTAGE, V
2.5
2.4
2.3
2.2
2.1
2.0
1.9
1.8
1.7
1.6
1.5
0
10
20
30
40
50
60
70
80
90
THEORETICAL DEPTH-OF-DISCHARGE, PERCENT

Figure 4-13

FIGURE 4-14. DISCHARGE CHARACTERISTICS OF SUPER-ENERGY CELL

Near the end of Phase VB, intermediate-size (700-Ah, theoretical) cells were fabricated and tested. These cells had radial-compression type seals while the previous cells utilized a type of axial-compression seal. Three of these cells were safety tested with very benign, safe results. Thirteen cells of this type were tested as single cells, and twenty cells were tested in two-cell strings as additional validation of a short-series string concept described in Section 6.2.2. About one-third of the 700-Ah cells failed early in the test (24 to 87 days) due to manufacturing problems which were identified. Corrective actions were planned but not implemented before the end of the program.

In summary, high-energy cells were found to be safe and very efficient in spite of thick electrodes. These cells offer added advantages due to long-term discharge and weekend charging capability.

4.3 EXPLORATORY CELLS

During Phase VB 446 exploratory cells were tested as individual cells (as differentiated from tests of groups of cells). Seventy of the exploratory cell tests involved cells carried over from Phase VA. These included two electric vehicle cells, 67 load-leveling cells and one high-energy cell. One cell was of a sulfur-core design. It operated for 1784 cycles over 1076 days. Ten cells were specifically for cathode container material studies (nine to test conductive glass coatings, and one to test a chromium oxide-coated current collector. The latter cell operated for 1139 cycles over 1013 days. One cell had the old Mark-I axial-type seal, and survived for 1525 cycles and

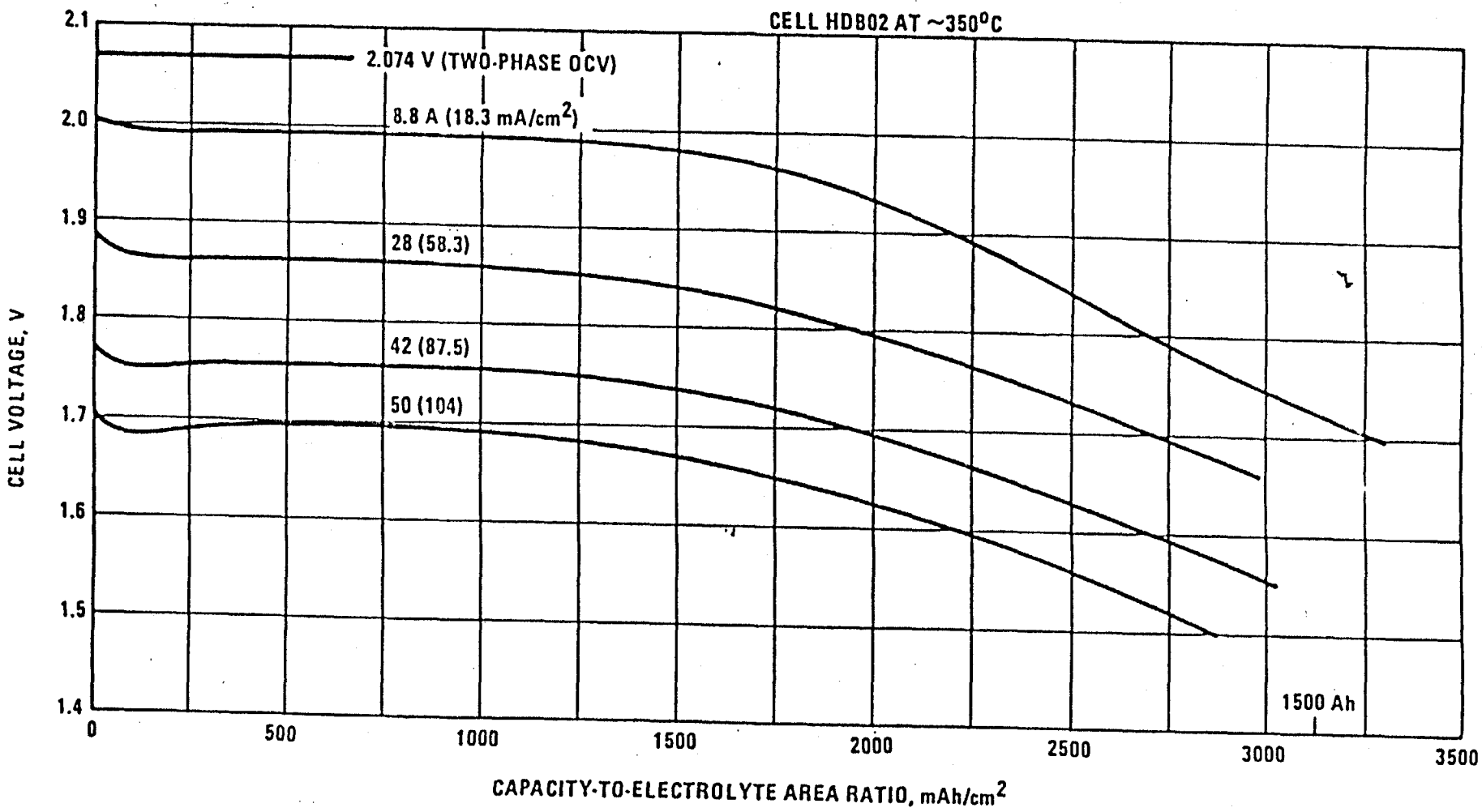

4-19a

Figure 4-14

1014 days. A load-leveling cell from the 100-kWh SES battery production run was still on test at the end of Phase VB, having accumulated 2340 cycles in 1192 days.

The 376 cells fabricated in Phase VB and tested as individual cells included a number of exploratory cells addressing generic issues such as current collector coatings, electrolyte quality, sulfur electrodes, and safety features. Many other cells were evaluated for performance, cycle life, ability to withstand vibration and freeze-thaw, and post-failure charactistics in direct support of this EV application. The cells were classifed as shown in Table 4-7.

TABLE 4-7. CELL CLASSIFICATIONS

Purpose		Design	
a. Electric Vehicle	297	a. Sodium-Core	367
b. Load-Leveling	51	b. Sulfur-Core	1
c. High-Energy	20	c. Sodium/Sodium	8
d. Sodium/Sodium	8		
Orientation		**Current-Collector Coating**	
a. Vertical	206	a. Chromium Plate	324
b. Horizontal	170	b. Conductive Glass	39
		c. CVD Molybdenum	5
		d. Not applicable (sodium/sodium)	8

Of the 371 cells, 36 incorporated variations in sulfur purity, amount of sulfur, or fiber materials. Fifteen were special cells with fixed chemistry for thermal cycling studies. Most of the cells were tested under duty cycles typical of the intended application, but many special tests were also performed as described throughout this report.

4.3.1 ALTERNATIVE SULFUR CONTAINERS

Cathode current collectors, the sulfur container in the case of sodium-core cells, must be protected against electrochemical corrosion by the sodium polysulfide catholyte. The corrosion-protection system must afford adequate lifetime and be economically viable as well. Additionally, the accumulation of corrosion products must not adversely affect cell performance. In Phase VB, Ford Motor Company conducted research on new candidates for sulfur-container corrosion protection, the most exciting candidate being a SiC/Al composite (see Appendix A). Ford Aerospace continued to evaluate chromium, conductive glass and molybdenum coatings in operating cells.

Chromium plate has been traditionally used as a coating on stainless steels containing high percentages of chromium (E-Brite with 26 percent chromium being preferred). These substrates afford good protection in the event the chromium has been corroded through or otherwise violated. Less expensive stainless steels like Type 410 were found to have poorer qualities in this respect. While it was once thought that iron or carbon steels would not be viable as substrate materials, experience with such materials with the conductive glass

has shown otherwise. The formation of a well-adhered duplex corrosion layer of FeS next to the substrate metal and FeS_2 next to the sulfur electrode was found to protect the substrate very well. [2]Corrosion associated with a pit was found to proceed transversely an order of magnitude faster than it did directly through an iron container wall because of spalling of the protective layer at the edges of the pit and the formation of protective sulfides at the bottom.

The conductive glass, a proprietary process developed over the past five years, continued to show promise. The coating was shown to corrode at a slower rate than does chromium plate. Also, the glass coating can be applied more thickly and at less cost than chromium plate.

Except at low charging rates chemically vapor deposited (CVD) molybdenum presented a somewhat unpredictable chargeability problem, and received little emphasis because of the perception that its economics will be less favorable than those of chromium and conductive glass coatings.

Highlights of the most promising results of in-cell testing with chromium, conductive glass and molybdenum are presented here. There are still strong indications that all of these systems could be viable. In order of cheapest to most expensive, these materials are ranked: conductive glass, chromium, CVD molybdenum. In order of ability to perform in a predicted manner, the order appears to be chromium, conductive glass, and CVD molybdenum.

4.3.1.1 Chromium Coatings. In June 1984 testing of 20 new EVEM-1 size cells began to evaluate a new chromium plate based on research work at Ford Motor Company. Substrates (containers) included E-Brite stainless steel, Type 410 stainless steel, and low-carbon steel. At the end of Phase VB, 8 cells remained on test with good performance, having reached an average of ~620 cycles. Post-test analyses of 8 cells voluntarily removed from the test at intervals indicated excellent corrosion resistance independent of substrate, although longer tests are required to demonstrate adequate life. Also, four cells to evaluate chromium plating (on E-Brite stainless steel) supplied by Sandia National Laboratories (Livermore) had operated for ~435 cycles in six months with good performance.

Detailed analysis of the chromium plate in Mark-II load-leveling cells was made to compare six cells from the 100-kWh battery with six cells from a 26 month storage test (described in Section 4.3.4.2). Three cells which had undergone daily electrical cycles as exploratory cells were included in the comparison to provide a reference. Except for one of the exploratory cells, none of these cells suffered from substrate corrosion.

In the one exception, corrosion was extensive along the edges of a gap between the semicylindrical precast electrode structures as seen in Figures 4-15 and 4-16. Figure 4-15 is a view of the chromium surface showing unattacked chromium in the electrode-gap region; deep attack at the edges of the gap believed to be due to current focusing; and the usual mild pitting under the electrode (left and right edges in the photo). The cross-section of the deeply corroded region of Figure 4-16 shows some attack of the E-Brite steel substrate. However, the substrate corrosion was not accelerated as evidenced by lack of undercutting of the chromium plate. This cell operated for 1182 cycles over 630 days at 320°C and had acceptable performance at the end of a 20-cell durability test described in Section 4.2.1.1.

FIGURE 4-15. CHROMIUM SURFACE IN ELECTRODE GAP REGION

FIGURE 4-16. CORROSION AT EDGE OF ELECTRODE GAP

UNATTACKED SURFACE CORRESPONDS TO GAP IN ELECTRODE

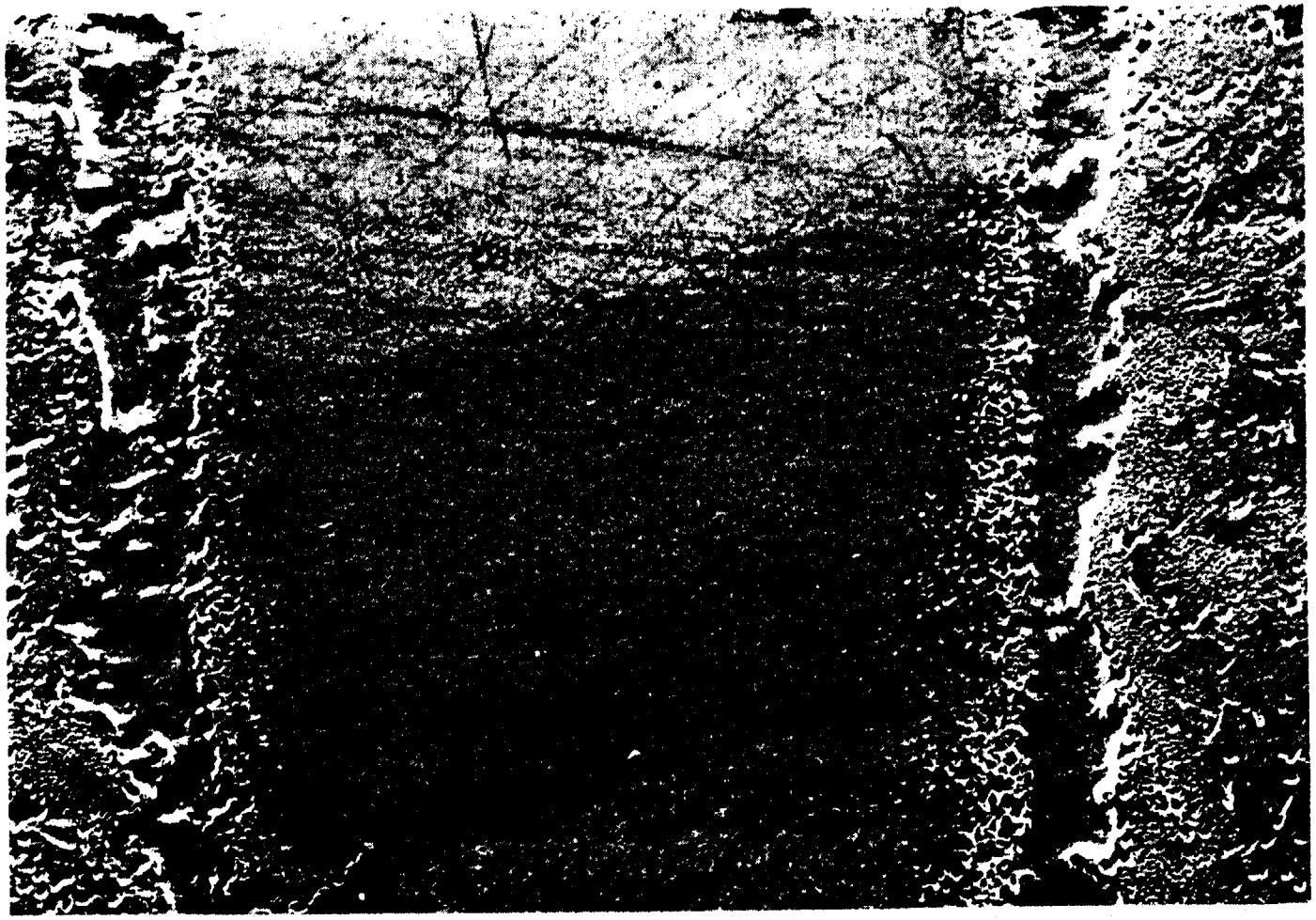

Figure 4-15

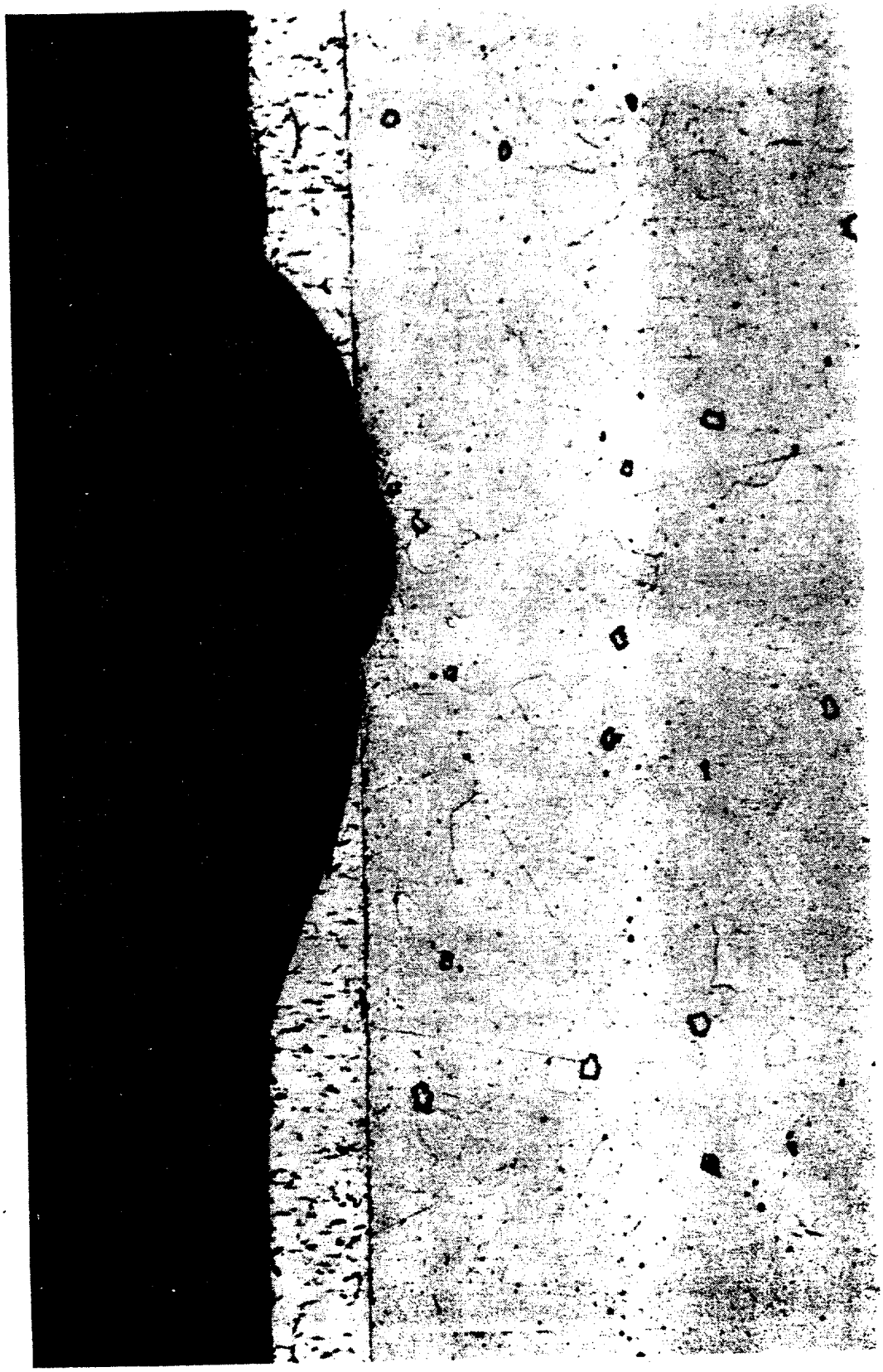

Figure 4-16

Figure 4-17 presents the surface appearance of microcracked chromium. Microcracks are short cracks that do not extend completely through the chromium (compared to macrocracks which do extend through the plate). The chromium plate shown in this figure is from a cell that operated for more than 2.5 years in the 100-kWh SES battery. The cracks were a maximum of about 3 μm wide, widened somewhat by corrosion. No significant pitting was observed. A few large-grain nodules appeared to coalesce the cracks. In cells with corrosion-widened macrocracks extending to the substrate, no evidence of substrate attack was observed.

Figure 4-18 shows photomicrographs of sections taken from the top, middle and bottom of a cell which was tested for 675 cycles in the 100-kWh battery. The worst corrosion was observed in the middle region, confirming previously reported results.[5]

Results from six cells stored for 26 months with electrical cycles varying from 19 to 113 revealed very slight corrosion to a depth of from 2 to 5 μm. The storage test matrix included storage at 300 and 350°C with some cells charged and some discharged. There was no obvious difference in corrosion under charged and discharged conditions. Corrosion appeared to be lessened by the lower temperature.

FIGURE 4-17. TYPICAL CHROMIUM PLATE CONDITION AFTER ~2.5 YEARS OPERATION IN 100-kWh BATTERY

Figure 4-17

FIGURE 4-18. CHROMIUM PLATE CONDITION IN CELL OPERATED FOR ~2.5 YEARS IN 100-kWh BATTERY

Comparing the worst observed corrosion for the stored cells against the worst case for cells from the 100-kWh battery, it appeared that corrosion rates were attenuated by a factor of about eight by limiting electrical cycles. This factor could be even greater for cells stored hot and not cycled at all.

An EVEM-1 cell with a chromium-plated Type 410 stainless steel cathode container had remarkably little corrosion. The chromium plate, of the microcracked type, was uniformly corroded to a depth of about 10 μm. Some surface cracks were widened and appeared to offer some surface corrosion resistance, as evidenced by less thinning of the plate in the crack areas. Figure 4-19 shows corrosion typical of this cell in which the chromium plate had a slightly scalloped appearance between the major surface cracks. This cell operated for 2022 cycles over 772 days at 350°C before testing was discontinued voluntarily for post-test analysis.

Because of observations made during post-test analyses of chromium plates, emphasis was placed on the fabrication of electrodes without gap spaces and on improvements in the chromium-plating process to reduce local corrosion effects. As chromium corrosion effects are better understood, it appears evident that chromium is a viable corrosion protection system. This has been observed on load-leveling cells for at least 1000 cycles and electric vehicle cells for at least 2000 cycles. With a better understanding of the corrosion mechanism in sodium-sulfur cells, these limits may be extended significantly further for chromium.

SCALE: 100 μ

TOP

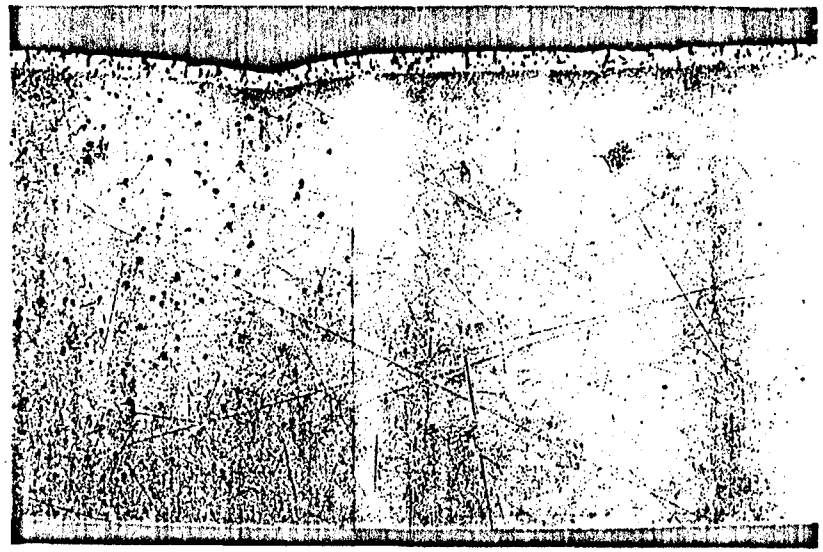

LL 460

675 CYCLES
32 MONTHS

MIDDLE

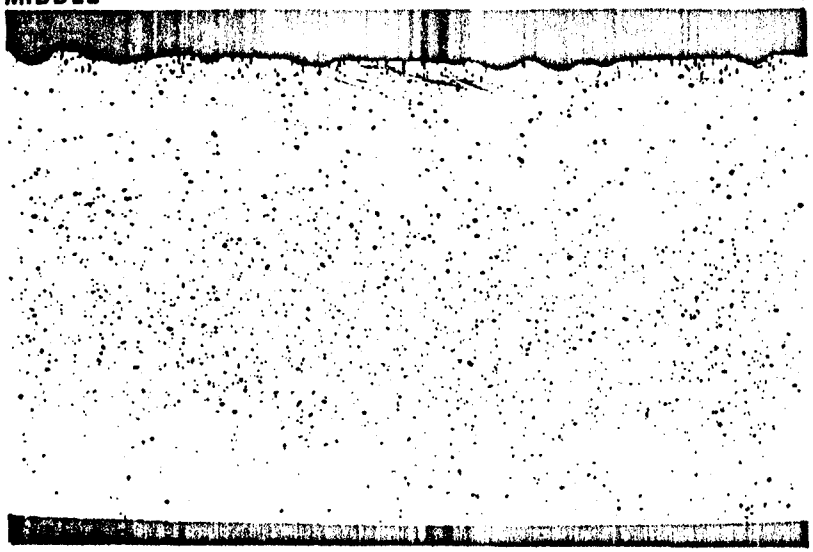

BOTTOM

Figure V-18

FIGURE 4-19. CROSS-SECTION OF CHROMIUM PLATE ON TYPE 410 STAINLESS STEEL AFTER 2022 CYCLES

4.3.1.2 Conductive Glass Coatings. In-cell evaluation of proprietary low-cost conductive glass coatings continued in Phase VB at a moderate level of effort. Earlier development utilized the Mark-II load-leveling cell. As part of a cost-reduction effort, iron (Univet) substrate replaced E-Brite stainless steel. However, the iron was left exposed in the seal area due to damage of the coating in the sealing step, and frequently corrosion problems arose at the cathode seal.

Eleven new EVEM-1 size cells to test the conductive coating were fabricated in January 1984. At the end of Phase VB, four cells remained on test with good performance after more than 1070 cycles, and another cell had operated for 815 cycles. However, the other cells had failed primarily due to leaks in the seal areas attributed to damage to the glass coating during cell fabrication. Also in some cells, cracked coatings were found underneath jaw chuck marks resulting from lathe operation. The glass coating was found to be susceptible to damage from relatively minor metal substrate distortion during fabrication.

Ford Aerospace funded a component development program which resulted in improved cathode seal-area protection and in identification of tooling changes for use with the conductive glass-coated containers. By the end of Phase VB, testing was in progress on EV cells constructed with the improved cathode seal. The identified special handling requirements should have only a modest effect on production costs. The conductive glass coating is still considered a viable alternative to chromium plating.

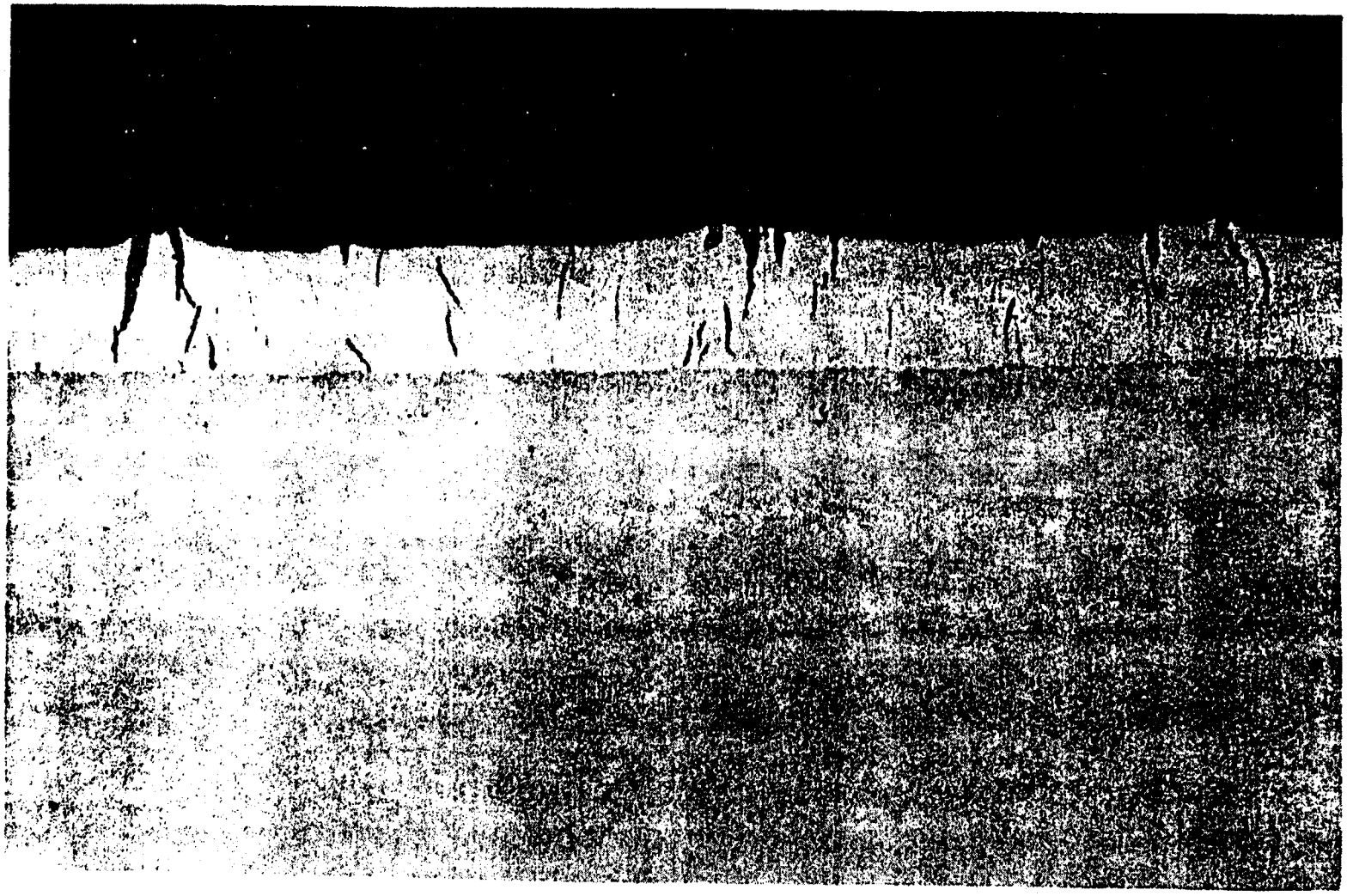

Figure 4-19

4.3.1.3 Molybdenum Coatings. Previously test results of 12 exploratory cells involving molybdenum were reported.[1] Included were sulfur containers made of solid molybdenum, CVD molybdenum coatings on steel, and diffused molybdenum on steel. Operated at high charge rates, more than half of these cells developed severe two-phase chargeability problems. Other cells which appeared to operate normally failed before reaching 150 cycles. It appeared that the chargeability problem was related to sulfur formed on the positive (charge) electrode, resulting in a high-resistance blocking layer at high charge rates. The problem was avoided by using reduced charge rates, rates which may not be practical for many applications.

The results shown in Table 4-8 were obtained with five additional Mark-II cells when operated at a load-leveling charge rate of C/6. These cells had CVD molybdenum coatings on E-Brite stainless steel. In the table, percentage values are relative to theoretical capacity.

TABLE 4-8. RESULTS FOR CELLS WITH CVD MOLYBDENUM CORROSION PROTECTION

Cell No.	Cycles Tested	Performance
MKD01	566	Capacity dropped to below 50% by Cycle No. 110. Testing stopped voluntarily.
MKD02	355	Initial capacity below 30%. Increased to 50% by Cycle No. 70 and to 75% by Cycle No. 250. Cell became nonfaradaic.
MKD03	616	Capacity dropped to below 50% by Cycle No. 205. Cell became nonfaradaic.
MKD04	690	Capacity dropped to below 50% by Cycle No. 170. Testing stopped voluntarily.
MKD05	688	Capacity dropped to below 50% by Cycle No. 350. Testing stopped voluntarily.

In summary, cells with CVD molybdenum corrosion protection continued to exhibit irreproducible chargeability, although some cells have exhibited good performance.

4.3.2 ALTERNATIVE ELECTRODES

Electrode development proceeded toward two objectives: 1) to qualify substitute low-cost electrode fiber materials; and 2) to develop alternative-size electrodes for EV and weekly storage applications. Union Carbide WDF, a graphitized felt from a rayon precursor, has been the standard material used in developmental cells. In 1984 small quantities of this material cost approximately $0.28/g. A graphitized pitch-precursor material with a 1984 small-quantity cost of about $0.06/g was assembled into cells and successfully tested during Phase VB. Also, cell sizes corresponding to a factor of ten variation in electrode thickness were successfully fabricated and tested.

4.3.2.1 Cost-Effective Electrode Materials. The pitch-precursor fiber was in the form of a loose mat with the fibers oriented two dimensionally. Its cost was less than one-fourth that of the three-dimensional WDF material, but it was considerably more difficult to handle. Also, the two-dimensionality of the pitch-based fibers resulted in poorer electronic conductivity normal to the plane of the fiber orientation. Two types of in-cell experiments were carried out. The first involved using the pitch-based fibers as a circumferential wrap in EVEM-1 cells, there being essentially no radially directed fibers to enhance electronic conductivity between the electrolyte and current collector surfaces. The second involved rotating the mat for radial fiber orientation in high-energy cells.

Five EVEM-1 cells with a circumferential wrap of pitch-based fibers were tested. One developed a sodium-supply problem after 570 cycles, testing of one was voluntarily stopped after 703 cycles to examine the fibers, one developed a cathode container leak after 849 cycles, and two cells remained on test with 1075 cycles at the end of the program. Because of the reduced radial conductivity, the cycle-averaged resistance was high (13 to 14 milliohms) compared to that of the same size cells with electrodes of WDF material (9 to 10 milliohms). Chargeability was improved, probably due to increased resistance within the electrode. Early data (Cycle No. 48) for these cells are shown in Table 4-9. The cells were cycled in a horizontal position at 350°C discharging at 100 mA/cm^2 to 1.66 V, and charging at 67 mA/cm^2 to 2.35 V. Data for similar cells with WDF electrodes are shown in Section 4.3.4.1.

Table 4-9. PERFORMANCE OF EVEM-1 CELLS WITH PITCH-BASED ELECTRODE MATERIAL

	Depth-of-Discharge (% of Theoretical)			Cycle-Averaged
Cell No.	End of Charge	End of Discharge	Cycle Capacity	Resistance, milliohms
VEA01	8.0	91.5	83.5	13.0
VEA02	7.6	90.7	83.1	12.8
VEA03	6.1	89.5	83.4	13.9
VEA04	4.9	89.1	84.2	14.0
VEA06	5.5	89.5	84.0	13.8
Mean	6.4	90.1	83.6	13.5
RSD, %	21	1.1	0.5	4.1

The cells with WDF electrodes (also at Cycle No. 48 and tested horizontally) operated on the average between depths of discharge of 9.6 and 88 percent of theoretical. Slightly extended cutoff voltages were used for the cells with pitch-based electrodes to compensate for the higher resistance.

The thicker electrodes of high-energy cells allowed cutting the fiber mat into strips to be turned on edge in precasting, resulting in the fibers being oriented radially and longitundinally in the cell. Data for the high-energy cells with the radially orientated pitch-precursor electrodes were presented in Section 4.2.2. From these results and those of the above EVEM-1 cells described above, confidence was developed that a change to the lower cost electrode can be made without a significant sacrifice in performance. Suitable tooling will permit orienting pitch-precursor fibers radially in even the small electrodes of electric vehicle cells.

However it should be kept in mind that the economic trade off between rayon- and pitch-based fibers involves not only the material costs but fabrication costs as well. Fabrication costs may be higher for the pitch-based fibers because of considerably poorer handling characteristics.

4.3.2.2 Development of Alternate-Sized Electrodes. Most prior cell development was accomplished using Mark-II cells with 9.0-mm thick electrodes. For electric vehicle applications the electrode thickness was scaled down to 3 to 4 mm to provide a higher power-to-energy ratio. High-energy cells for weekly storage were scaled upward to an electrode thickness of 30.3 mm in the super-enegy cell (see Section 4.2.2). This order of magnitude scaling in electrode thickness was accomplished with excellent results in each of the cell sizes. The scale-up to high-energy cells resulted in a low cycle-averaged resistance. The high-energy cells, therefore, had an exceptionally good energy efficiency, making them attractive not only because of their weekend charge capability, but also from economic considerations related to energy.

The ability of sodium-sulfur cells to operate efficiently with very thick electrodes offers wide design flexibility for adjusting power-to-energy ratio to a desired application. This attribute is best demonstrated by a modified Ragone plot (Figure 4-20) which shows the average power vs. the total output energy for high-energy and other classes of cells, where all data were obtained at constant currents. The stored energies for the cell classes are indicated by the notations on the abscissa. Uniform proximity of the curves to the corresponding notations demonstrates the ability of the sodium-sulfur cell to utilize most of its reactants, independent of cell size. Cells demonstrated efficient high-rate cathode operation during both charge and discharge for all electrode thicknesses tested.

4.3.3 ALTERNATIVE ELECTROLYTES

The majority of cells tested in Phase VB utilized electrolytes made by the standard zeta process. Seventeen cells were fabricated and tested to evaluate electrolytes made by the slurry-solution spray drying (S^3D) process still under development by Ceramatec, Inc. This process which has the potential for reducing ceramic fabrication cost is discussed in detail in Section 5.2.1. Eight of the cells with S^3D electrolytes were of the Mark-II load-leveling size. These electrolytes were the first processed by the new technique and appeared to be flawed by normal standards. When "candled" by internal light, they appeared to have a swirl pattern suggesting nonhomogeneity in density and/or wall thickness. Nine of the S^3D electrolytes were tested in EVEM-1 size electric vehicle cells. These electrolytes appeared to be of good quality. Good results were obtained with both groups of electrolytes as described below.

FIGURE 4-20. SODIUM-SULFUR CELL CAPABILITIES

4.3.3.1 In-Cell Performance. The status of the Mark-II cells with S^3D electrolytes as of the end of Phase VB is summarized in Table 4-10. Of the three cells which failed for reasons other than equipment problems, No. MBA01 and No. MBA03 appeared to be functioning normally prior to failure. Cell No. MBA07, however, had an abnormally high resistance (15 rather than 10 to 12 milliohms) over its entire life suggesting either an electrolyte processing anomally or a sodium-supply problem which could have caused abnormal stressing of the electrolyte. A similar summary of the nine electric vehicle cells is shown in Table 4-11. One cell, No. VBB12, became nonfaradaic after completing 1238 cycles. The other three failures were for reasons not related to the electrolyte. The cathode seal-leakage problem was common in early EVEM-1 size cells, before corrosion protection in the seal area was improved in later model cells.

The results of the electric vehicle cell test suggest that S^3D electrolytes have potential for good lifetime. This is particularly encouraging since the tested electrolytes were early process specimens.

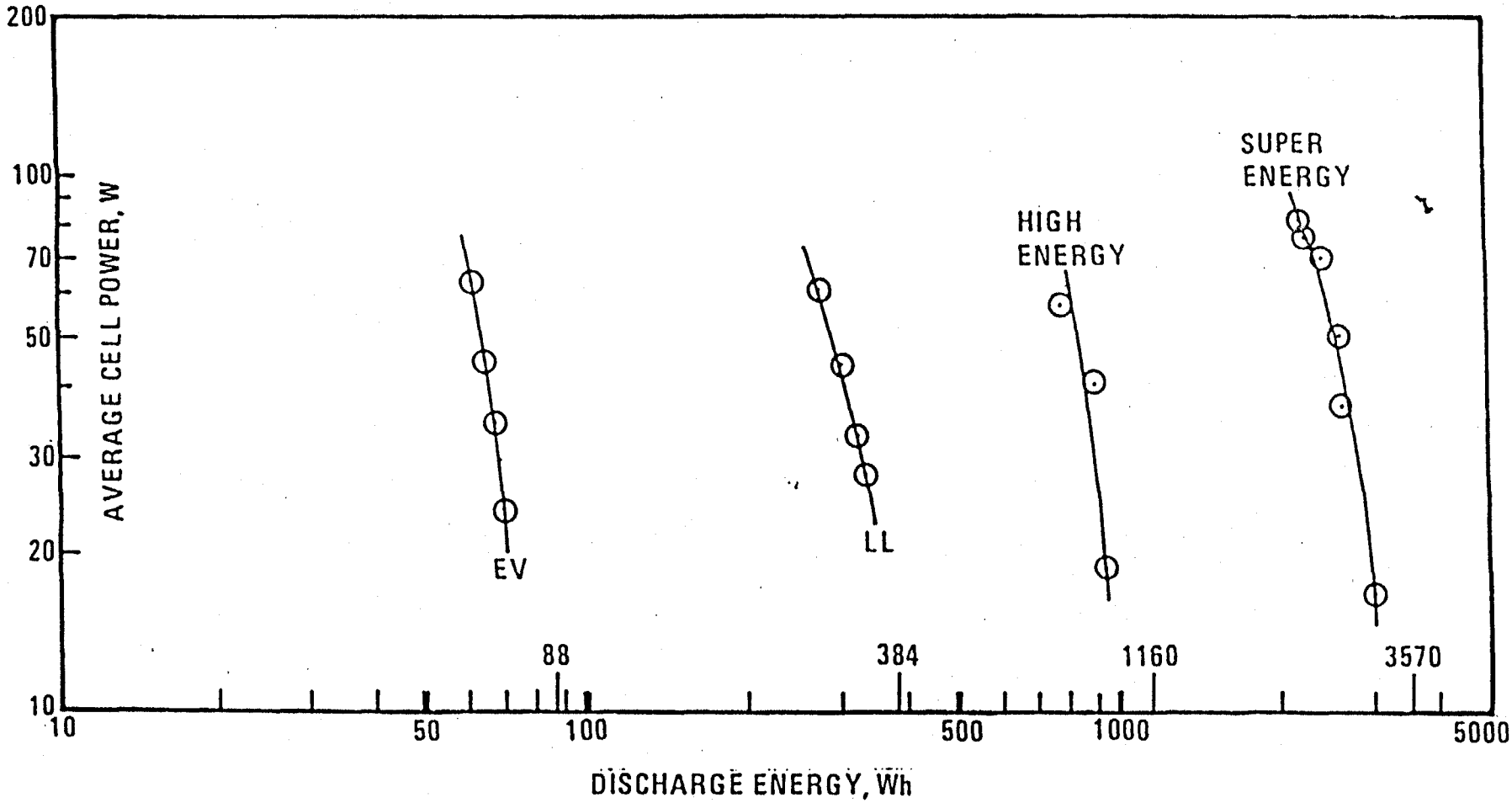
200
100
70
50
30
20
10
AVERAGE CELL POWER, W
EV
LL
HIGH ENERGY
SUPER ENERGY
88
384
1160
3570
10
50
100
500
1000
5000
DISCHARGE ENERGY, Wh

Figure 4-20

TABLE 4-10. STATUS OF MARK-II CELL TESTS OF S^3D ELECTROLYTES

Cell No.	Cycle Completed	Days Tested	Status
MBA01	144	138	Became nonfaradaic
MBA02	90	108	Became nonfaradaic due to control malfunction
MBA03	510	455	Became nonfaradaic
MBA04	676	580	Still on test
MBA05	660	580	Still on test
MBA06	683	580	Still on test
MBA07	530	470	Became nonfaradaic
MBA08	15	8	Became nonfaradaic due to control malfunction

TABLE 4-11. STATUS OF EVEM-1 CELL TESTS OF S^3D ELECTROLYTES

Cell No.	Cycle Completed	Days Tested	Status
VBB02	772	231	Developed a sodium supply problem
VBB04	861	262	Cathode seal leaked
VBB05	1317	435	Still on test
VBB06	1331	435	Still on test
VBB07	1331	435	Still on test
VBB09	1301	431	Still on test
VBB10	1303	435	Still on test
VBB12	1238	426	Became nonfaradaic
VBB13	795	335	Cathode seal leaked

4.3.3.2 Electrolyte Resistance. The resistances of standard zeta-processes EVEM-1 electrolytes were measured in special sodium-sodium tests. EVEM-1 cells were constructed normally except that the cathode containers were submerged in sodium. This provided for direct in-cell measurement of electrolyte resistance. From comparison with sodium-sulfur cell resistance, the resistance of the sulfur electrode could be determined. Additionally, this in-situ radial measurement provided data for comparison with Ceramatec's axial resistivity data. The measurement was made in a dry box containing argon with less than 2 ppm oxygen. An 8-kg copper crucible in an isothermal oven provided good thermal control. The electrolytes were 25 mm in diameter by 220 mm long with 1.4 mm wall thickness.

The observed resistivity is shown over a temperature range of 240 to 400°C in Figure 4-21. When plotted in the form of the Arrhenius equation, ρ/T versus $1/T$ where ρ is the resistivity and T is the temperature in degrees Kelvin, the usually seen two straight-line segments resulted. From linear regression correlation fits to the data, the following equations were found:

FIGURE 4-21. RESISTIVITY AS A FUNCTION OF TEMPERATURE

1. Electrolyte No. CAB1104407LM9U (13 data points)
   a. $\ln (\rho/T) = 3041.33\ (1/T) - 9.9457$ for $T \leq 310.6°C$
   b. $\ln (\rho/T) = 2505.28\ (1/T) - 9.0273$ for $T \geq 310.6°C$

2. Electrolyte No. CAB1104415LM9U (19 data points)
   a. $\ln (\rho/T) = 3018.32\ (1/T) - 9.9336$ for $T < 314.6°C$
   b. $\ln (\rho/T) - 2415.93\ (1/T) - 8.9084$ for $T \geq 314.6°C$

These equations fit the observed data to within ±0.7 percent and ±1.0 percent, respectively, for the two electrolytes. The maximum overall error in the data in terms of computed resistivity was estimated to be as follows:

1. Low-temperature range:
   a. At 240°C, ±3.1 percent
   b. At 312°C, ±2.7 percent

2. High-temperature range
   a. At 312°C, ±2.3 percent
   b. At 400°C, ±2.6 percent

Included in the error estimation, were effects of current, voltage, temperature, and electrolyte geometry measurements.

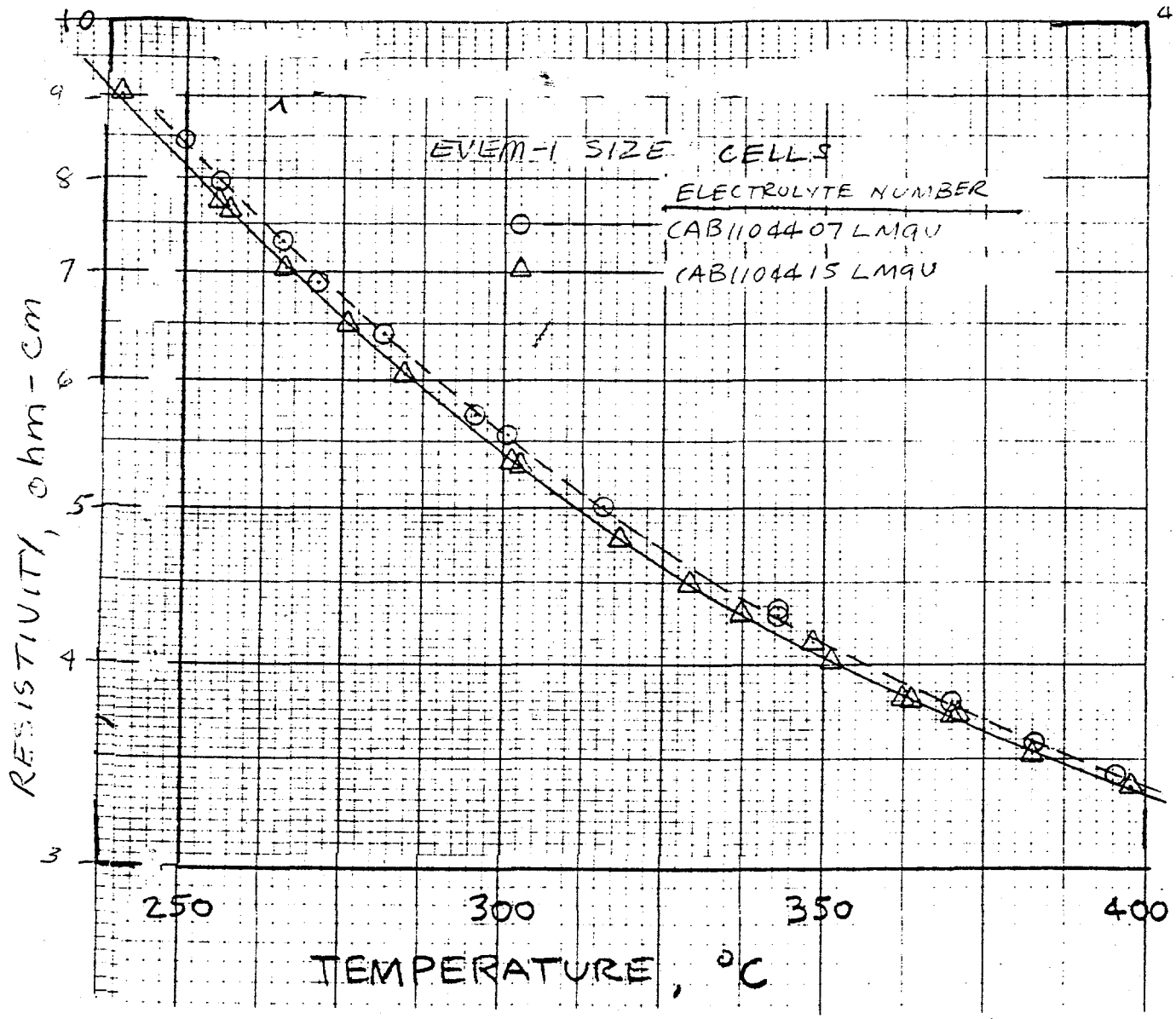
EVEM-1 SIZE CELLS
ELECTROLYTE NUMBER
CAB1104407LM9U
CAB1104415LM9U
RESISTIVITY, ohm-cm
TEMPERATURE, °C
250
300
350
400
10
9
8
7
6
5
4
3

Figure 4-21

Activation energies computed from the Arrhenius equation:

$$E_a = \frac{k \ln [(\rho/T)_2/(\rho/T)_1]}{\frac{1}{T_2} - \frac{1}{T_1}}$$

with k the Boltzmann constant equal to 1.9871×10^{-3} kcal/mole-K, were found to be as follows:

	Activation Energy, E_a, kcal/mole-K	
	CAB1104407LM9U	CAB1104415LM9U
250 to 312°C	6.04	6.00
312 to 400°C	4.98	4.80

These values are typical of fine-grained β"-alumina. (Both of these electrolytes were of microstructure Grade "A" according to Ceramatec.)[1] The observed radial resistivities corrected for cell metal component resistance compared as follows with Ceramatec's reported axial resistivities:

Electrolyte No.	Resistivity, ohm-cm at 300°C		
	Radial	Axial	Radial/Axial
CAB1104407LM9U	5.538	4.0	1.386
CAB1104415LM9U	5.385	4.0	1.346

The ratio of radial-to-axial resistivity of about 1.4 is typical of β"-alumina.

At a nominal operating temperature of 350°C the in-situ electrolytes had measured resistances of 3.62 and 3.89 milliohms, respectively. These values can be compared to Na/S cell values of 8.5 to 9.0 milliohms. Allowing 1.0 milliohm for the cathode current collector, the sulfur-electrode resistance would be in the range of 3.8 to 4.3 milliohms with a chromium-plated current collector.

4.3.4 OTHER DEVELOPMENTAL TESTING

Special tests conducted were related primarily to battery systems issues. These included: 1) direct comparison of cell performance in horizontal versus vertical orientation; 2) assessment of long-term storage effects; 3) determination of freeze-thaw capability for both load-leveling and electric-vehicle cells; and 4) documentation of failed-cell resistances. Also, documentation of cell open-circuit voltage as a function of depth of discharge resulted in data significantly different than that previously published.

4.3.4.1 Horizontal vs. Vertical Orientation. In January, 1984 testing of five EVEM-1 cells was begun to compare vertical and horizontal operation at 350°C. After 48 cycles in a vertical orientation, the cells were turned horizontally to obtain reference performance data, and returned to the vertical orientation. Data for the two orientations are compared in Table 4-12.

TABLE 4-12. COMPARISON OF DATA FOR VERTICAL AND HORIZONTAL OPERATION

Cell No.	Vertical Cycle-Averaged Resistance, milliohms	Vertical DOD* End of Discharge	Vertical Cycle* Capacity	Horizontal Cycle-Averaged Resistance, milliohms	Horizontal DOD* End of Discharge	Horizontal Cycle Capacity*
VA810	11.3	77.6	86.9	9.7	80.5	88.6
VA811	10.9	72.6	88.0	9.7	73.4	88.5
VA812	10.8	78.2	86.8	10.0	79.0	87.2
VA813	10.4	79.3	87.6	9.8	78.3	87.2
VA814	10.8	80.3	87.9	9.8	80.9	88.4
Mean Value	10.8	77.6	87.4	9.8	78.4	88.0
RSD, %	3.0	3.8	0.7	1.3	3.8	0.8

*Percent of theoretical

The cells used in this test were of the EVEM-1 type (designed to be operated horizontally). The apparent effect of operating the cells vertically with the same voltage cutoff conditions (1.7/2.3 V) was a 10 percent increase in cell resistance, but only a 1 percent decrease in capacity. Temperature effects could account for some of the performance variation, since average cell temperature was slightly lower in the vertical orientation. These cells were discharged at 100 mA/cm^2 and charged at 67 mA/cm^2 in both orientations.

The above listed cells were used for discharge pulse tests in early life after about 300 cycles. Four of the cells were on test at the end of Phase VB, having accumulated 1037 cycles with good performance. The fifth cell failed after 967 cycles when a leak developed near the welded end cap causing a sudden drop in capacity.

4.3.4.2 Long-Term Storage Effects. Special storage tests of Mark-II cells were concluded in 1984. The initial test matrix included seven cells which were stored at room temperature for one year after their construction. When heated and tested in 1982 following the year of storage, the performance was equivalent to that of cells tested soon after fabrication. Four cells were kept in the single-phase (discharged) region and three were in the two-phase (charged) region. Two were at 300°C, and five were at 350°C. Three were cycled monthly to check for performance trends, and four were cycled at the beginning of the test and at the end of 1982 and 1983. Two cells failed late in 1983 (after 20 and 22 months). These were discharged cells, one at 300°C and one at 350°C. The cell at 300°C had been cycled for brief periods at the end of each year, with 19 cycles having been accumulated. The cell at 350°C was cycled monthly and had accumulated 113 cycles. The failure rate for cells in this experiment was similar to the failure rate observed for cells in the 100-kWh battery. Testing of the remaining five was concluded early in 1984, with the remaining cells still exhibiting good performance. Post-test analysis showed less corrosion in these cells than in similar cells operating under normal cycles as described in Section 4.3.1.1.

4.3.4.3 Freeze-Thaw Capability. A freeze-thaw test was conducted on nine Mark-II cells taken from the 100-kWh battery after 675 cycles and more than 2.5 years operation. These cells were subjected to repetitive freeze-thaw cycles interspersed with electrical cycles. After more than 15 successful freeze-thaw cycles, the cells were changed to a horizontal position. Oriented horizontally, four of the nine failed within the next three freeze-thaw cycles and three others failed after completing 7, 13, and 27 horizontal cycles, respectively. The two remaining cells were returned to a vertical orientation and successfully withstood a total of 53 and 55 freeze-thaw cycles, respectively, before normal electrical cycling was resumed. These cells were tested for more than 200 additional electrical cycles before testing was voluntarily discontinued.

An experiment involving 15 special EVEM-1 size cells was performed to address freeze-thaw cycle behavior. Three conditions were represented by five cells each: 1) sodium only; 2) cathode composition approximately 10 percent sodium pentasulfide (Na_2S_5), (no sodium); and 3) discharged to a composition approximating sodium trisulfide (Na_2S_3), (no sodium). One early failure in each cell group was thought attributable to electrolyte or cell anomalies. The remaining 12 cells were demonstrated to be very rugged through freeze-thaw cycles at cooling and heating rates as high as 100°C/h, both horizontally and vertically. One horizontal "discharged" cell failed after 27 cycles, adding evidence that horizontal operation and low state-of-charge represent the most severe freeze-thaw conditions. Testing of the other 11 cells was discontinued after 29 to 35 freeze-thaw cycles. Visual post-test examination of these cells showed no container bulging or leakage, and X-ray examination did not indicate any electrolyte damage.

Through the fabrication and testing of exploratory cells, a new flexible safety-tube design was qualified and incorporated in ETX exploratory and prototype cells. Five of these cells successfully completed 40 freeze-thaw cycles while vertically oriented in a charged state. Subsequent freeze-thaw tests on ETX cells were conducted at three different states of charge. The tests were incomplete by the end of Phase VB, but it was clear that the fully discharged state represents a more severe condition for cells undergoing freeze-thaw cycles than does the charged state.

4.3.4.4 Post-Failure Resistance. The high and variable resistance of failed EVEM-1 cells was identified in the EVEM-1 bench test as an area for improvement. Early in 1984 a group of cells was assembled to evaluate internal design changes for post-failure resistance. Following safety tests in which the electrolytes were intentionally caused to fracture, the resistances of three cells were monitored while simulating charge and discharge cycles which the cells could experience in a battery. Later, two EVEM-1 cells which failed in normal testing were added to the group being monitored. The three-cell group was tested the longest with 40 electrical cycles before and 585 cycles after safety testing. The average resistances which are shown in Table 4-13 were measured for cycles at 14 A over a 4-h discharge and 10 A over a 5-h charge.

TABLE 4-13. RESISTANCE OF FAILED CELLS

As Failed		No. VDK02		No. VDK04		No. VDK05	
Days	Cycles	Dischg	Chg	Disch	Chg	Dischg	Chg
2	5	20	19	30	21	20	18
19	50	51	44	147	140	140	40
38	100	39	61	163	100	167	135
79	200	38	107	34	34	29	30
113	300	47	124	35	37	38	40
151	400	40	121	40	40	47	47
189	500	36	142	35	33	43	43
220	585	43	116	32	31	62	62

Temperature was maintained nominally between 350 and 360°C for these tests.

As can be seen from Table 4-13, results of the test were somewhat variable. Two cells (No. VDK04 and No. VDK05) had low resistance early in the test, only to increase to unacceptably high resistances between Cycle No. 30 and Cycle No. 130. Following Cycle No. 130, these cells had acceptably low resistance. The third cell (No. VDK02) developed a high resistance in the charging direction by about Cycle No. 110 which persisted throughout the remainder of the test.

The standard EVEM-1 cells that failed in normal testing had resistances above 100 milliohms (usually about 200 milliohms) for the first 200 cycles. The resistance of one continued to be high while the other dropped to about 40 milliohms after 200 cycles. It was concluded that while the design changes tested in the VDK-series cells offered potential for improvement under some conditions, they did not guarantee acceptable post-failure cell resistance. Development of an external (semiautomatic) shunt appears necessary.

4.3.4.5 Open-Circuit Voltage Documentation. Four load-leveling cells with chromium-plated cathode containers and theoretical capacities of 192 Ah were used to document open-circuit voltage (OCV) as a function of cathode composition. Further confirmation of the revised OCV curve fit was obtained with a 575-Ah theoretical capacity high-energy cell. All cells were new to minimize any reactant loss effects due to cathode container corrosion. Data were taken in both "charge" and "discharge" directions to quantify hysteresis effects. The cells were operated from 50 to 110 percent of theoretical capacity (Na_2S_3) at 300, 350 and 400°C. Increments of 2.5 Ah in capacity were used, each followed by a 3.5-h idle period to insure equilibrium conditions.

The data were fitted with three discrete straight line segments between the upper plateau of two liquid phases and the lower plateau of solid and liquid phases. The curve fits and derived equations are shown in Figure 4-22 where V is the OCV, T is the temperature in °C, and f is the depth-of-discharge (decimal equivalent of percent of theoretical; 0 = sulfur; 1.0 = Na_2S_3). Discrete slope changes in the data were noted at f values of about 0.64, 0.85, and 0.93. The data fit straight lines between these break points. For simplicity, and with little error, the latter break point was ignored, and a single line fit from f equal to 0.85 to the solid-liquid phase intersections. The Phase VB OCV data are considered more realistic of actual sodium-sulfur cells at or near equilibrium conditions than are the previously published data of Gupta and Tischer.

FIGURE 4-22. SODIUM-SULFUR CELL OPEN-CIRCUIT VOLTAGE

TABLE 4-14. COMPARISON OF OPEN-CIRCUIT VOLTAGE*

Depth-of-Discharge % of Theoretical	Open Circuit Voltage Phase VB Data**	Estimated Difference of Phase VB Data from Gupta-Tischer Data, V
60	2.062	+0.009
65	2.031	+0.017
70	1.988	+0.010
75	1.944	0.000
80	1.901	-0.012
85	1.858	-0.025
90	1.824	-0.026
95	1.790	-0.021
100	1.757	-0.014

*At 350°
**For cell with chromium-plated cathode container

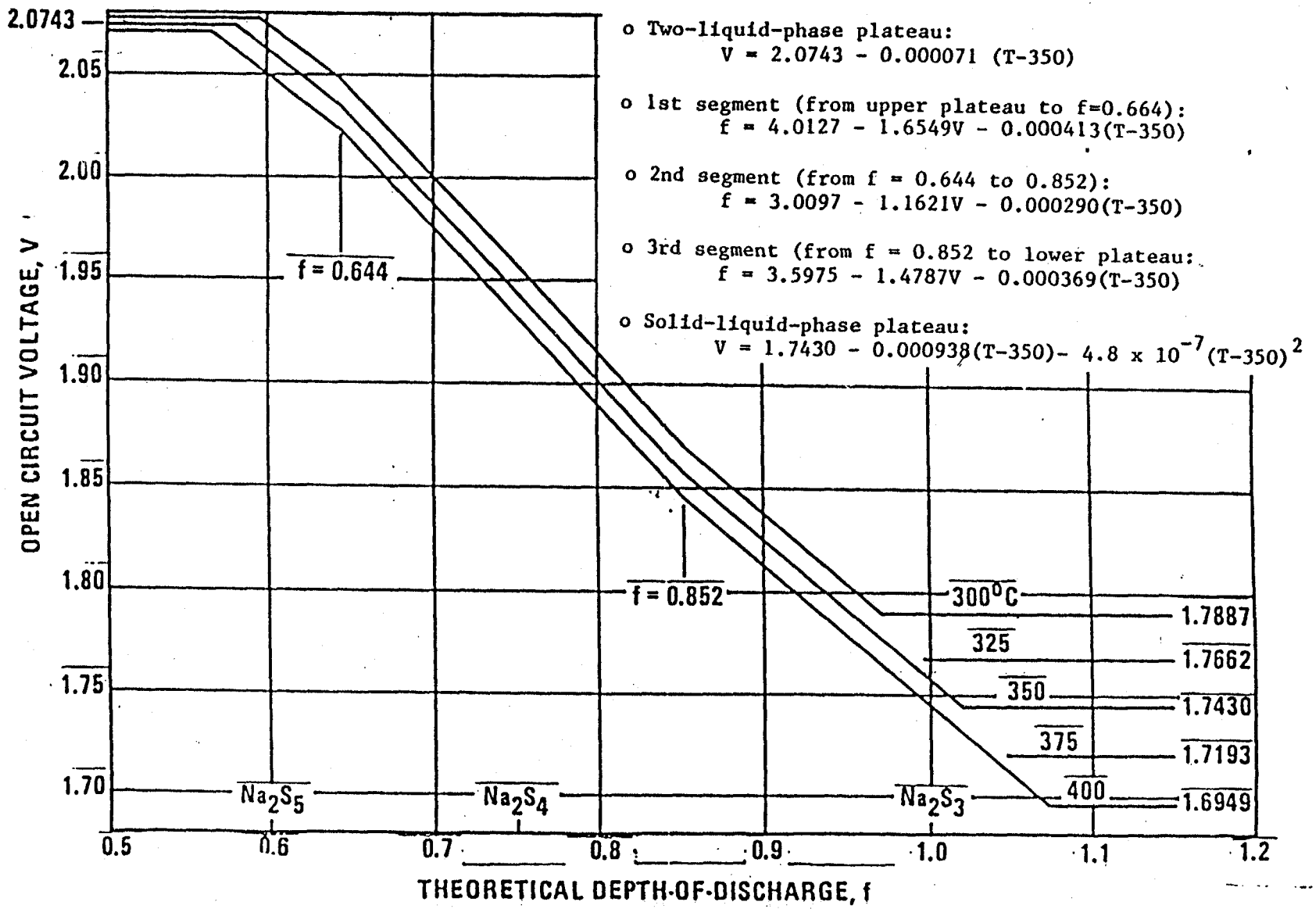
o Two-liquid-phase plateau:
V = 2.0743 - 0.000071 (T-350)
o 1st segment (from upper plateau to f=0.664):
f = 4.0127 - 1.6549V - 0.000413(T-350)
o 2nd segment (from f = 0.644 to 0.852):
f = 3.0097 - 1.1621V - 0.000290(T-350)
o 3rd segment (from f = 0.852 to lower plateau:
f = 3.5975 - 1.4787V - 0.000369(T-350)
o Solid-liquid-phase plateau:
V = 1.7430 - 0.000938(T-350)- 4.8 x 10^-7 (T-350)^2
OPEN CIRCUIT VOLTAGE, V
2.0743
2.05
2.00
1.95
1.90
1.85
1.80
1.75
1.70
f = 0.644
f = 0.852
300°C
1.7887
325
1.7662
350
1.7430
375
1.7193
400
1.6949
Na2S5
Na2S4
Na2S3
0.5
0.6
0.7
0.8
0.9
1.0
1.1
1.2
THEORETICAL DEPTH-OF-DISCHARGE, f

Figure 4-22

SECTION 5

ELECTROLYTE DEVELOPMENT AND PRODUCTION

Development and production of β"-alumina electrolytes were accomplished by Ceramatec, Inc., under subcontract to Ford Aerospace. Ceramatec's R&D efforts addressed goals of: 1) improved reliability; 2) improved nondestructive evaluation (NDE); and 3) reduced cost. Section 5.1 summarizes progress toward both improved reliability and the development of an improved NDE technique, and Section 5.2 addresses development toward cost reduction. Electrolyte production and the relocation of the β"-alumina pilot plant are discussed in Section 5.3.

5.1 ELECTROLYTE RELIABILITY

Previous efforts have identified factors considered to be important in electrolyte reliability. These include: 1) fracture toughness and strength of the electrolyte; 2) electrolyte size, surface area and wall thickness; 3) impurities in liquid sodium; 4) purity of the alumina raw material; 5) wetting characteristics of beta"-alumina surfaces by liquid sodium; and 6) stress corrosion (subcritical crack growth) of beta"-alumina in liquid sodium. The issue of an optimum grain size for maximum reliability still remains unresolved, other than to note that extensive cell lifetimes (over 2000 cycles) have been achieved in cells constructed with beta"-alumina electrolytes which do not have fine grained, uniform microstructures. On the issues of sodium purity and electrolyte size factors, preliminary sodium-sodium test data taken late in Phase IV and early in Phase V indicated that electrolyte lifetime is significantly enhanced when the purity of the sodium is increased and when the surface area and wall thickness of the electrolyte tube are reduced. Optimum conditions related to sodium purity and electrolyte size are yet to be determined.

The electrolyte, being a brittle component, is prone to failure under various conditions. Failure of the electrolyte, either under electrolytic conditions or by purely mechanical means, occurs when the stress intensity at the most severe flaw exceeds the fracture toughness. Improvements made in mechanical properties without sacrificing electrical performance are expected to enhance the ability of the electrolyte to withstand greater abuse. Processes which enhance fracture toughness, e.g., transformation toughening by the addition of a zirconia second phase, have been shown in other programs to improve the resistance to the formation and growth of sodium dendrites. It is anticipated that the electrolytes with improved toughness will exhibit improved reliability in operating sodium-sulfur cells. Mechanical property improvements, in particular the fracture strength, can be effected by controlling microstructural factors such as porosity (void content and void size) and grain size in processing. Extensive fracture testing of electrolyte tubes via a suitable burst test followed by microstructure evaluation is essential to establish a statistical base for reliability assurance procedures such as proof testing.

Ceramatec's recent work in developing a suitable burst/proof test for electrolyte tubing is summarized below as are other efforts related to electrolyte reliability including evaluation of: 1) residual stresses and strains; 2) static fatigue (subcritical crack growth) in liquid sodium; and 3) wetting of

beta"-alumina surfaces by liquid sodium. Also, the results of an extensive characterization study on standard zeta process tubing are summarized.

5.1.1 BURST AND NONDESTRUCTIVE PROOF TESTING OF ELECTROLYTES

The objective of a proof test is to ensure that a given part is guaranteed not to fail when subjected to a service stress which is lower than the proof stress, barring extensive subcritical crack growth during the service life. The objective of a burst test (in the case of a tubular geometry) is to determine the fracture strength and, more importantly, the origin of fracture or the type and size of the critical flaw or defect causing the failure. Once the type and the size of the strength limiting flaws are determined, appropriate measures can be taken to minimize the number and size of these flaws by suitable process modification. Another objective of burst testing many similar electrolyte tubes is to develop a Weibull probability for a given plot. This plot serves as the basis for selecting a proof stress level and for the construction of a proof stress diagram if subcritical crack growth occurs during service.

The electrolyte is expected to experience little or no stress during service at operating temperature as it is not a structural component. However, some service stresses may arise from: 1) tolerance buildup in cell design and/or assembly; 2) nonuniform heating, cooling, or solidification of cell reactants during freeze-thaw cycling; 3) residual stresses in the electrolyte due to sealing or processing; 4) stresses during the charging cycle due to the electrodeposition of sodium in surface cracks at the sodium electrode; and 5) mechanical stresses from the operating environment of the battery, i.e., mobile applications. Thus, it is essential to minimize the probability of failure during service by eliminating the weak electrolytes via proof testing, so that defective tubes are not assembled into cells.

In prior phases of the program, burst testing was conducted using pressurized air. The principal disadvantage of this method lies in the fact that the very large amount of energy stored in the tube (due to the high compressibility of the pressurizing gas) causes the tube to fragment catastrophically upon failure. The assembly must therefore be enclosed in a steel vessel for safety purposes. Furthermore, the extensive fragmentation on failure precludes locating the origin of failure and the nature of the flaw causing the failure. Thus, the use of air as a pressure transmitting fluid is unsatisfactory for burst testing. In a proof test, the objective is not to cause fracture but to load the tubes to a predetermined stress at which only the weak parts will fail. For these lower pressure tests, air as a pressure-transmitting fluid may be acceptable.

During Phase VB, experiments were carried out with hydraulic oil as the pressure transmitting fluid. A combination burst/proof tester for electrolyte tubes sealed to alumina headers was designed, constructed and placed into operation. The current version of the apparatus is operated manually. However, only small modifications will be required to adapt the proof tester for use in a quality control procedure on an assembly line.

To determine the origin of failure, it is necessary to examine the characteristic crack pattern in the tube after it has failed in burst testing. To facilitate this objective, all electrolyte assemblies to be burst tested were

covered with a cellophane tape to ensure that the fragments forming on fracture did not fall apart and were preserved for analysis of the crack pattern and scanning electron microscope (SEM) fractography to determine the exact origin of failure and the type and the size of the flaw responsible for failure. Identification and characterization of these flaws provided an indication of types of defects to be avoided in electrolyte fabrication.

Numerous EVEM-1-size electrolyte assemblies were burst tested. The geometry of burst testing, involving the arrangement of the electrolyte assembly over a mandrel covered by a rubber bag, clamping of the header, and pressurizing from inside the tube, effectively creates a biaxial state of stress in the tube wall, a hoop stress and an axial stress. The geometry is such that the hoop stress is twice the axial stress. Consequently, it was anticipated and confirmed experimentally that flaws located with their crack planes orthogonal to the hoop stress would lead to failure.

Electrolyte assemblies of the following types were burst tested: 1) standard zeta-process tubes; 2) standard zeta process tubes that were subsequently hot isostatically pressed (HIPed) at 1335°C in an attempt to increase the mass density and eliminate the large voids; 3) tubes fabricated from seeded slurry-solution spray dried (S^4D) powders; and 4) standard zeta process electrolyte tubes which had been exposed to humid air (59 percent relative humidity) for eleven days at room temperature. In Figure 5-1 the Weibull plots for the standard, standard and HIPed, and S^4D electrolytes are shown wherein $\ln[-\ln(1-F)]$ is plotted versus ln stress, where F is the cumulative failure probability and the stress is the hoop failure stress.

As seen in Figure 5-1, the standard electrolytes exhibited average strength values in excess of 15,500 psi with a Weibull modulus greater than 7. The Weibull plot was bimodal with a very low value of the modulus at low values of stress. The break occurred at about 14,000 psi. The implication is that if these electrolytes were proof tested at a hoop stress of about 14,000 psi (corresponding to fluid pressure of 2000 psi for an EVEM-1 tube), the weak electrolytes exhibiting a low Weibull modulus (about 13 percent) would be eliminated from the population.

The HIPed electrolytes also exhibited a bimodal Weibull plot, with an average burst strength in excess of 18,800 psi, although at the upper end, the Weibull plots for both the standard and standard-HIPed conditions seems to suggest that the flaws responsible for the tail of the distribution were formed during standard zeta processing, and were not eliminated during the subsequent HIPing operation.

The S^4D electrolytes exhibited average strengths in excess of 17,700 psi with a Weibull modulus of approximately 6.5. These preliminary results indicated that the Weibull plot is not bimodal and that the strength of the electrolytes prepared from S^4D powders is significantly higher than the strength of standard zeta process electrolytes. Although more data are required to confirm these conclusions, these preliminary results indicated that the large defects responsible for the bimodal Weibull distributions in the standard and standard-HIPed electrolytes are absent in tubes fabricated by the S^4D process. This result is extremely encouraging since it offers substantial credibility

to spray drying as not only a viable economic fabrication process, but also as a process capable of producing electrolytes of high reliability.

FIGURE 5-1. WEIBULL PLOTS FOR ELECTROLYTE BURST TESTS

Using SEM fractography, it was observed that large defects (approximately 50 to 150 μm) were responsible for failure in every case. These defects almost always were processing-related. It is encouraging that despite the presence of large processing-related defects, the electrolyte tubes exhibited high strengths. This is a strong indication that the intrinsic strength of beta"-alumina is very high. Thus, if appropriate process modifications can be made to eliminate the large defects, a substantial increase in electrolyte strength can be reasonably anticipated.

Typical defects observed were of the following three types: 1) large voids associated with large grains; 2) large voids; and 3) large grains. Using a

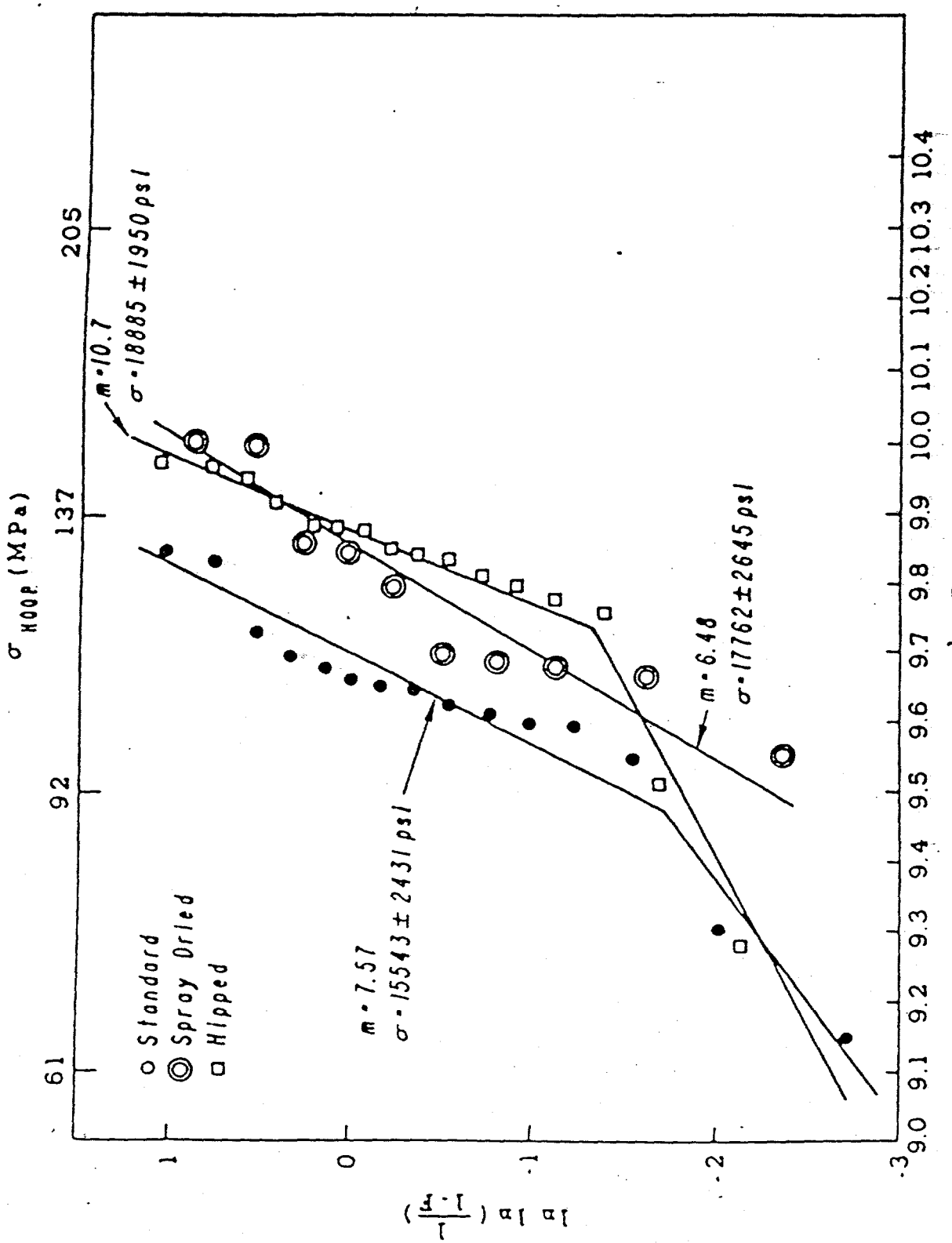
σ HOOP (MPa)
205
137
92
61
ln σ HOOP
10.4
10.3
10.2
10.1
10.0
9.9
9.8
9.7
9.6
9.5
9.4
9.3
9.2
9.1
9.0
ln ln (1/1-F)
1
0
-.1
-.2
-.3
m=10.7
σ=18885±1950 psi
m=7.57
σ=15543±2431 psi
m=6.48
σ=17762±2645 psi
Standard
Spray Dried
Hipped

Figure 5-1

value of the fracture toughness of beta"-alumina equal to 1.8 $MPa(m)^{1/2}$, flaw-size calculations were made. Calculated flaw sizes were in the range of 100 to 200 μm and consistent with the diameter of the regions consisting of the voids in the center of large grains. Large defects including pores were responsible for failure of the HIPed electrolytes. While HIPing improved the macroscopic density, presumably through the removal of small pores, large voids were not eliminated. The only way to ensure the absence of large voids is to prevent their formation during green forming.

Burst testing coupled with fracture analysis on numerous electrolytes of three varieties (standard, HIPed, and S^4D) showed that failure origins contained either voids alone or voids associated with large grains. Preliminary chemical analysis indicated that impurities may also play a role, but further work is needed for confirmation. These results, nonetheless, consistently point towards the need for improving the process to prevent the formation of large voids and/or large grains during green forming and sintering.

It is anticipated that electrolytes will be exposed to humid air in cell assembly. Since beta"-alumina has been known to be sensitive to moisture, the effects of limited exposure to moisture on the burst strength of standard electrolyte tubing were explored. A number of electrolytes were exposed to humid (59 percent relative humidity) air at room temperature for eleven days. The exposure to moisture increased the average burst strength by about 10 percent. This increase in strength has been verified on ring specimens broken in the diametral geometry as well. While deliberate exposure to moisture is not recommended for a number of reasons, these results clearly indicated that short-term exposure to moderate levels of humidity does not adversely affect the mechanical integrity of the electrolytes. Effects, if any, on sodium-sulfur cell performance remain to be identified.

In summary, a practical burst/proof test procedure was developed and used to test EVEM-1-size tubes made by various processes. EVEM-1-size assemblies exhibited burst pressures in excess of 2000 psi. The defects which caused mechanical failure were commonly large voids and/or grains introduced during processing. The intrinsic strength of beta"-alumina was found to be high, indicating that processing modifications which minimize the formation of these large failure-inducing defects will pay significant dividends in increasing the mechanical integrity and hence the reliability of the electrolyte. Moderate exposure to moisture had no adverse effect on the mechanical strength of electrolyte tubing. Proof testing has promise of providing an acceptable technique to assure electrolyte reliability.

5.1.2 RESIDUAL STRESSES (STRAINS) IN ELECTROLYTE TUBING

The objective of this effort was to determine residual stresses in the β"-alumina due to processing of the electrolytes and sealing them to α-alumina headers.

When an electrolyte is cooled to room temperature after the sintering or annealing operation, stresses can arise if a temperature differential exists between the inner wall and the outer wall of the tube (the outer wall being at a lower temperature). As the electrolyte is cooled through a temperature range

where thermally activated creep deformation can occur, the temperature gradient can create stresses (tensile in the outer region and compressive in the inner region of the tube) at high temperature. These stresses can be relieved at the higher temperatures by creep deformation. However, as the tube is cooled further, compressive stesses are expected to form in the relatively rigid outer regions of the tube which cooled first. These are, of course, balanced by tensile stresses in the inner regions (inner surface of the tube). These temperature differences lead to differential creep. Since sodium is in contact with the inner surface of the tube, the presence of significant tensile stresses is expected to enhance the propensity to degradation. The residual stresses arising from sealing of the electrolyte tubes to the α-alumina headers (caused by the mismatch in coefficients of thermal expansion) are expected to be small. The technique of strain gauging was chosen, since this technique is known to be very reliable and easy to use. Four strain gauges were mounted on an EVEM-1-size electrolyte sealed to an α-alumina header (two near the seal and two half way along the length of the tube). The strain gauges were mounted in two orientations on the tube (two axially and two circumferentially). After mounting the gauges, the electrolyte assembly was pressurized to 900 psi (6.2 MPa) in the proof-testing apparatus. Far away from the seal, the state of stress was biaxial with the circumferential value being twice the axial value. The ratio of the axial strain to the circumferential strain was found experimentally to be 0.24 which corresponds to a Poisson's ratio of 0.29, a reasonable value for the ceramic electrolyte. In this manner, the reliability of the strain measurement technique was confirmed.

To determine residual strains developed by thermal expansion mismatch between the α-alumina header and the β"-alumina electrolyte, strain gauges were mounted on the electrolyte tubes near the seal. The change in strain was recorded after the alumina headers were cut off. The residual strain developed during the sealing operation was found to be negligible.

To determine residual strains developed in the electrolyte due to processing factors, strain gauges were mounted on electrolyte tubes in the circumferential orientation. Subsequently, a longitudinal cut was made, and the change in strain recorded. In the majority of the experiments, the change in strain was found to be positive and indicative of compressive stresses on the outer surface and balancing tensile stresses on the inner surface, as would be expected due to differential creep (thermal tempering). The magnitude of the residual stresses in standard zeta process tubing was on the order of 600 to 800 psi. Under certain conditions related to rapid cooling and exposure to moisture, residual stress values up to 3000 psi were encountered. A value of stress on the order of 600 to 800 psi is too low to be of any real concern. However, a stress level on the order of 3,000 psi could influence electrolyte performance.

To determine if the cooling rate from a high temperature influences the magnitude of residual stress, two tubular segments from the same electrolyte tube were heated to 1460°C and held at this temperature for five hours to relieve any residual stresses that may have been present. One of the tubes was cooled very slowly (over several hours), while the other was cooled at the same rate as the standard EVEM-1 tubes are cooled in pilot production. The electrolyte tube which was cooled very slowly exhibited no detectable strain while the other tube had a strain on the order of 30 μin./in. (residual stress under

1000 psi). In the standard production of zeta-process electrolyte tubing, the electrolytes are not cooled rapidly (typically a period of several minutes from the annealing temperature to a temperature below which the creep deformation rate is insignificant). These results imply that any future process including rapid firing and cooling will have to also include thermal annealing followed by slow cooling.

Electrolyte tubes exposed to moisture for several days exhibited greater amounts of residual stress. When exposed to moisture (via humid air), the magnitude of the compressive stress in the electrolyte increased consistent with the hypothesis that moisture enters the crystal structure of β"-alumina. Since access of moisture to the inner surface of the tube is restricted, it is anticipated that more moisture enters in the outer regions than in the inner regions leading to greater expansion of the lattice on the outside, and the resultant increase in compressive stress. To verify this hypothesis, the relative humidity was controlled at 59 percent on the inside of several tubes while the outside was exposed to a desiccating environment for several days. After storage in the desiccator, a strain gauge was mounted on the electrolyte, and a longitudinal slit was made in the tube. The observed strain on the outside surface was tensile, confirming the hypothesis for preferential water penetration into the outside surface in the standard situation.

The following conclusions were drawn: 1) residual stresses on the order of 600 to 800 psi are present in standard tubing, compressive on the outside surface and tensile on the inside; 2) the rate of cooling from the annealing temperature affects the magnitude of residual stress (higher cooling rates can significantly increase the state of residual stress); 3) insignificant residual stresses are introduced during sealing of the electrolyte to the alumina header; 4) exposure to moisture enhances the magnitude of residual stress in the electrolyte (preferential penetration of water leads to compressive stresses on the outside surface of the electrolyte tube); and 5) low residual stresses (under ~1,000 psi) should have a minimal effect on electrolyte life and reliability.

5.1.3 STATIC FATIGUE

Numerous glasses and ceramics are known to exhibit time dependent failure caused by stress corrosion. This static fatigue phenomenon is a manifestation of subcritical crack growth which is generally dependent upon the environment and the temperature. One potential mechanism of electrolyte failure is the occurrence of subcritical crack growth in the presence of liquid sodium or sodium polysulfides under the action of externally applied stresses (e.g., arising from cell misalignment) or internal residual stresses present in the electrolyte. To assess the propensity to failure by subcritical crack growth in liquid sodium, static fatigue experiments were conducted.

An apparatus for applying a dead load on a β"-alumina ring specimen in diametral compression immersed in liquid sodium was designed and constructed. Several experiments were conducted in liquid sodium at 350°C wherein the time required for mechanical failure at a given load was recorded. A few samples broke over a period of time under dead load conditions at relatively high stress levels (over 20,000 psi). Because of statistical variability, a large

number of experiments are necessary before the subcritical crack growth parameter can be ascertained with any degree of accuracy. The most important conclusions based on this preliminary work are: 1) β"-alumina exhibits some tendency toward subcritical crack growth in liquid sodium at relatively high stress levels; and 2) residual or external stresses acting on the electrolyte should be kept low. (Stresses significantly below approximately 5 to 10 percent of the rapid fracture strength should not be a serious problem.)

5.1.4 WETTING OF β"-ALUMINA BY LIQUID SODIUM

The quality of the interface between liquid sodium and β"-alumina influences the operation of the sodium-sulfur cell. If the charge transfer resistance is large, the overall cell resistance will be high and the propensity for electrolytic degradation will be increased. To minimize the charge transfer resistance, it is necessary that physical wetting of the electrolyte by liquid sodium be optimized. The parameters which affect wetting were identified in the study described below.

The wetting of sodium was studied on β"-alumina tube sections which had been subjected to various post-sintering treatments. The samples included as-sintered standard zeta-process material, standard electrolyte tube sections which had been HIPed, and specimens chemically polished in hot phosphoric acid. Prior to the wetting experiments, all specimens were heated in air at 1200°C for 30 min. Some specimens were introduced into the glove box for testing immediately after the bake-out treatment, some were stored in a desiccator for five days; and some were left in the glove box for ninety days before testing. During the ninety-day storage, the glove box atmosphere contained 10 to 100 ppm of oxygen.

The wetting experiments were conducted in the glove box on a hot plate. To ensure a good and uniform thermal coupling between the hot plate and the specimen, copper coupling blocks were used. In the sodium-core design of the cell, the inside surface of the electrolyte contacts liquid sodium; hence, the sodium wetting characteristics were studied on the inner surfaces of the electrolyte tubes. All the samples were heated to 350°C in the apparatus and then cooled to 180°C before the drop of electrorefined sodium was introduced on the surface. The temperature was measured by introducing the tip of a thermocouple into the drop. Sessile drop photographs were taken as the temperature was increased to approximately 350°C. (Temperatures were stabilized for about 20 min.) Contact angles were measured on the developed and printed photographs.

As the temperature was increased, the contact angles in all cases decreased, and beyond 360°C, they were all less than 25°. Due to the concave nature of the surface, it was difficult to measure angles smaller than 25° accurately.

The results indicated that post-sintering treatments such as HIPing and chemical polishing have a positive effect on wetting. Except at 180°C when the contact angles were the same, liquid sodium seemed to wet HIPed β"-alumina better than it wet the standard material. Apart from increasing the density by ~2 percent, the HIPing operation may also modify the surface characteristics. The chemically polished material was more easily wet than either the HIPed or the standard β"-alumina. The polished electrolytes had a glossy, smooth surface, and were wet better by sodium even at the lowest temperature (180°C).

At higher temperatures, although not as apparent, the wetting characteristics were also better for the chemically polished electrolytes.

Among the storage conditions examined, long-term storage in the desiccator was the least favorable as far as wetting. The specimens tested immediately after the bakeout had the best wetting characteristics.

It was concluded that: 1) as the temperature is increased, the wetting of β"-alumina by liquid sodium is improved significantly; 2) chemically polished electrolytes have the best wetting characteristics; and 3) long-term storage of electrolytes can adversely affect the wetting characteristics, particularly when moisture is present.

5.1.5 ELECTROLYTE CHARACTERIZATION

Extensive characterization work was done on standard electrolyte tubing to determine microstructural (grain size and porosity) characteristics, crystallographic orientation or texture, and chemical uniformity, particularly near the surface.

The microstructure of standard electrolytes is known to be duplex. During the current work, the grain size of the fine-grained fraction was determined using the microscopic intercept method. The average grain size was ∿5 μm in the middle and inner surface regions of the wall while it was about 3 μm in the outside surface regions. Porosity levels were determined by the microscopic systematic point count technique. Porosity levels were ∿1 to 2 percent in the middle regions of the walls and ∿0.75 percent in the near-surface regions. At the closed end of the tubes, porosity levels were somewhat higher along with a significantly higher grain size (∿8 μm).

Inverse pole figure techniques using copper X-ray radiation indicated some preferred orientation of the β"-alumina grains in the near-surface regions, i.e., the c axis of the grains tends to be oriented orthogonal to the surface. Texture coefficients as high as about 1.5 were measured, indicating a moderate degree of texture in standard β"-alumina tubing.

5.1.6 SURFACE CHARACTERIZATION

The character of the surface of β"-alumina can influence the performance of the electrolytes in sodium-sulfur cells. Chemical inhomogenity in the near-surface region could affect the wetting of the β"-alumina by the cell reactants. Lack of wetting or the formation of insulating layers of nonstoichiometric composition could cause highly localized current densities during cell start-up. Segregation of impurities at the surface could also cause similar effects, and affect cell chemistry at the interface. Although much is known about the composition and impurities in bulk samples of β"-alumina, little work had been done previously on determining the composition of the near-surface (1000 Å to 10 μm) region.

Dr. Walter L. Roth, under subcontract to Ceramatec, studied the near-surface chemistry of β"-alumina electrolyte material using the Dynamitron Linear Accelerator located at the State University of New York at Albany. The analytical

techniques employed to determine concentration profiles were particle backscattering and Rutherford backscattering. A hot stage was constructed within the accelerator vacuum so that hydrogen concentrations at the surface could be measured at temperatures up to 400°C.

Rutherford backscattering spectra (RBS) were measured using 2-MeV alpha particles. In contrast to particle backscattering which is specific for a specific element, RBS measures the number and energies of the alpha particles scattered backward from all atoms with an atomic number of 8 (oxygen) or greater in a surface layer. The depth of penetration of RBS is less than 0.1 μm whereas particle backscattering is effective for determining concentrations of lithium and sodium to a depth of about 6 μm in β"-alumina.

Whole EVEM-1 electrolytes were delivered to Dr. Roth representing the following conditions: 1) as-sintered from various kiln locations; 2) prior to assembly in a sodium-sulfur cell by Ford Aerospace; 3) HIPed; and 4) HIPed and heat treated at 1200°C.

The investigation of the standard zeta-processed electrolytes indicated no significant variation of sodium or lithium concentrations in the near-surface region, 0.5 to 6.0 μm. Samples removed from top, bottom and middle, and examined on both the inner and outer surfaces of all standard electrolytes were practically identical in composition.

All standard zeta-processed electrolytes exhibited a very thin surface layer (0.1 μm) that was rich in sodium, oxygen and hydrogen. This surface skin was probably the result of reaction of sodium oxide with atmospheric water vapor and carbon dioxide and would be expected. No other elements, within the capabilities of the analytical equipment, were found to have any increased concentrations at the surface.

The HIPed electrolytes exhibited an unusually high sodium concentration to a depth of about 0.5 μm. Upon heating these electrolytes to 1200°C for 30 minutes, both the sodium-rich zone and the sodium-depleted zone disappeared and the concentration profile appeared to be the same as that of standard electrolytes, indicating the reaction causing the depletion and enrichment is reversible.

An <u>in-situ</u> hydrogen (presumed to indicate H_3O^+ concentration) desorption experiment was carried out by measuring the hydrogen density at a depth of 0.1 μm at temperatures up to 400°C in the accelerator vacuum of 10^{-5} torr. The hydrogen started to desorb rapidly at 200°C and continued up to 400°C where almost all of the hydrogen was removed after one hour at this temperature. Upon cooling, the sample started to absorb hydrogen from the vacuum chamber at about 120°C.

In summary, the zeta-processed β"-alumina appeared to be very uniform in composition without any impurity concentration at the surface. The reactions that cause the formation of a sodium- and water-rich surface skin during normal handling operations appeared to be totally reversible.

5.1.7 PROCESS SENSITIVITY

A critical examination was made of the fabrication operations associated with the standard zeta process. Beginning with the raw materials and continuing through quality acceptance and shipping, each step (approximately 25) in the operation was evaluated thoroughly for content, documentation, and quality of the product at that stage of the process. Particular emphasis was placed on evaluating the purity of the product at various stages in the manufacturing process. The salient features of the study are summarized below.

Electrolyte tubes produced by the zeta process are of high quality and possess physical properties which are fairly consistent from lot to lot. Inconsistencies resulting in rejects were found to be due primarily to problems in the pressing operation, gross impurities and dimensional control. The major problem with the zeta process appeared to be the number of operations (six) required in preparation of the powder, because each operation can introduce variability and contamination. Because of batch processing, minor fluctuations in each of the steps can result in considerable variation in the final product.

The operation found to be the most susceptible to contamination and variability was the method of binder addition. If continued use of the zeta process is foreseen (not a recommendation of Ceramatec), then substitution of slurry spray drying for pan drying is mandated. Slurry spray drying (i.e., the calcined and milled zeta precursor powder is suspended in an aqueous-based slurry), which was investigated in Phase III of this program, will have definite advantages including: 1) better control of impurities; 2) better distribution of the binder; 3) production of flowable and pressable powders; and 4) larger lot sizes. Changing the process over to slurry spray drying should eliminate many of the current reasons for rejection. However, problems associated with the production of crushable spray-dried agglomerates are more difficult in the slurry spray drying approach (in comparison to slurry-solution spray drying), and additional development is required.

In the area of isostatic pressing, incorporation of flowable spray-dried powders having a better distribution of binder should eliminate or minimize greenware rejects. A change to "near-spherical" closed-end geometry should aid in the elimination of rejects due to end-capping.

For the remaining operations of the production process, an upgrade in equipment to maintain cleanliness or to minimize technician error is recommended. Coating of certain processing equipment with ashless abrasion-resistant polyurethane should minimize contamination. In the green machining and grinding areas, replacement of the current manually operated equipment with semiautomatic machines should alleviate rejects due to breakage and out-of-specification dimensions, and also allow for greater reproducibility.

5.2 COST REDUCTION

Ceramatec's efforts toward reducing cost were focused on improvement of the slurry-solution spray drying process which has potential for ultimately reducing the cost of producing high-quality electrolytes. An overall plan for reducing production costs was also developed.

5.2.1 SLURRY-SOLUTION SPRAY DRYING (S^3D) PROCESS DEVELOPMENT

The technique of slurry-solution spray drying has several important advantages over conventional dry powder processing such as the zeta process.

- o It is essentially a single-step process prior to pressing and firing in that the labor- and energy-intensive operations of calcination and ball milling have been eliminated.
- o The alkalis are readily homogenized for reactive sintering.
- o The resulting powder, which is flowable and pressable, is suitable for automatic isostatic pressing.
- o The technique of seeding can be easily incorporated into the process.
- o The shrinkage on firing is very low (∿9 to 11 percent) compared to that of the dry powder zeta process (∿15 to 17 percent) leading to excellent dimensional control during sintering and annealing.

In the S^3D process, a low-viscosity and stable slurry is prepared by dispersing α-alumina particulates in an aqueous medium in which the alkalis (soluble salts of sodium and lithium) are present in solution. This slurry is then transformed into crushable soft agglomerates by spray drying.

During Phase VB, S^3D work concentrated on four areas: 1) development of optimized high-solids content slurries; 2) incorporation of seeding into the spray-drying process; 3) investigation of alternative atomization systems; and 4) testing of process modifications in sodium-sodium cells. The objective was to improve the processing efficiency and the resultant physical properties of β"-alumina ceramics produced from spray-dried powders.

5.2.1.1 Optimized High-Solids Content Slurries. High-solids content slurries are seen to be advantageous because of: 1) lower energy consumption during drying; 2) increased product throughput efficiency resulting from less product deposition on the dryer walls; and 3) potential improvement in the uniformity, size and homogeneity of the spray-dried granules.

In conventional spray-dried ceramics, solids contents generally range from 60 to 70 percent by weight. Spray drying of α-alumina is a typical example where the powder is added to a solution containing an organic dispersant, humectant, and plasticizer. The dispersant, a polar compound usually in the form of an ammonium or sodium salt of a modified carboxylic acid, is adsorbed onto the surface of the alumina. Dispersion occurs via the well-known "double-layer" theory.

In spray drying of β"-alumina, the presence of excessive amounts of hydroxyl and alkali ions in solution complicates and disrupts conventional dispersing action. Many dispersants have a low salt tolerance or work in a pH range below 10. Published dispersion literature for alumina suggests that two optimum pH ranges exist for low-viscosity suspensions--one at a pH of ∿4.7, the other around pH of 11.5. The β"-alumina slurry, containing dissolved LiOH and NaOH,

has a pH of ∿13. Consequently, the pH for this system is not optimum and common dispersants are rendered ineffective. Because of this problem, stable slurries had been prevously achieved only by dilution to approximately 40 percent solids content. To overcome these deficiencies, Ceramatec investigated three methods for development of high-solids content slurries: 1) nonconventional dispersants; 2) alternative alkali sources; and 3) emulsion-based slurries.

Nonconventional Dispersants. A survey was made of available dispersants for use in high pH systems. Manufacturers were consulted for help in determining conditions and quantities to be used. More than fifty different compounds were examined. A class of compounds composed of lignin derivatives was identified as providing superior dispersion capability. Sixty percent slurries prepared using these compounds were highly fluid, possessing viscosities of ∿100 centipoises. An optimum lignin compound and amount were selected, incorporated into a 60 percent solids slurry, and spray dried. The size distribution of agglomerates, retained moisture content, and total organic content were examined.

While low-viscosity, high-solids content slurries could be achieved, difficulty was encountered in sintering the pressed powders to high density. Several different sintering conditions were tried, but the best density values obtained were still only ∿97 percent of theoretical. Additional experiments conducted at 40 percent solids with this dispersant suggested that inhibition in densification was the result of the dispersant, and not the solids content, per se. Because of the problems encountered in achieving adequate densities, further work on these types of compounds was discontinued.

Alternative Alkali Sources. One method of attaining high-solids content slurries is a reduction in the pH of the system to a point where common dispersants are effective. Alkali salts of carboxylic acids had been used as raw materials in the past. However, these materials had generally not produced crack-free ware during subsequent bisquing and firing operations. One compound not previously investigated was sodium carbonate. Several bench-top slurries were prepared using this sodium oxide source. Sodium carbonate exhibits only moderate solubility in water, and under certain conditions, the dissolved carbonate ions react with soluble lithium ions to form insoluble lithium carbonate. This condition was avoided, and the use of sodium carbonate reduced the ionic strength of the slurries and pH to ∿10, allowing use of conventional dispersants. Consequently, several highly fluid 60 percent solids slurries were prepared and spray dried. Seeding was incorporated into these slurries to promote conversion to the β" phase and competitive grain growth during sintering and annealing. The throughput efficiency was very high (greater than 93 percent for small batches).

Sintering of powders derived from these high-solids content slurries was conducted at temperatures between 1560°C and 1575°C, followed by annealing at 1475°C for one hour. The achieved densities (ranging between 3.23 and 3.26 g/cm^3 were among the best achieved for a spray dried powder. The resistivity values (3.6 ohm-cm at 300°C) and four point modulus of rupture (245 MPa) were characteristic of materials prepared from seeded compositions.

Repeated attempts were made to isostatically press EVEM-1 electrolytes from this material. However, all of the compacts fractured during the pressing oper-

ation. Apparently, the carbonate system does not provide sufficient binding strength to enable crack-free material to be prepared. Further development is needed to optimize this material with respect to forming.

Emulsion-Based Slurries. A third method of overcoming the detrimental effects of high pH systems is through emulsion systems. Water-insoluble oils can be easily suspended and dispersed using selected emulsifying agents. By coating the ceramic raw material particulates with an insoluble oil, and selecting compatible emulsifiers, dispersion and viscosity control can be achieved in slurries. In effect, the process alters the apparent surface characteristics of the alumina particulates. A classification system has been developed for determining the hydrophilic or lipophilic nature (HLB System) of various oils. Based on this system, emulsifiers can be selected which match the oil. During Phase VB, oils with a range of high and low HLB values were examined. An appropriate system was developed which utilized a low-HLB oil and appropriate emulsifiers. The system was highly tolerant of the presence of sodium and lithium hydroxides. Fluid 60 percent solids content slurries were prepared, spray dried and sintered. Limited data were acquired on the properties of these electrolytes before the end of the program. Densities ranged from 3.17 to 3.23 g/cm^3 with resistivities ranging between 4.7 and 5.9 ohm-cm (300°C). Preparation of electrolyte tubes from these materials also proved to be difficult. Cracking of the ware during the pressing operation was the dominant problem. Several tubes were prepared crack-free, but they did not meet other visual inspection criteria. Time and budgetary constraints at the end of the program limited efforts in pursuing an effective solution to this problem.

Overall, development and incorporation of high solids content slurries proved to be more difficult than anticipated. Either adequate densification was not acheived, or granule compaction difficulties prevented the forming of crack-free greenware. However, with moderate additional research, it is probable that these limitations can be overcome.

5.2.1.2 Seeded Slurry-Solution Spray Drying. Previously, incorporation of fine seed crystals (<10 μm) of 100 percent β"-alumina into unconverted precursor powders had been shown to catalyze conversion to the β"-alumina phase. The seeds act as nucleation sites for growth of β"-alumina grains, and the number of nucleation sites determines the average grain size. For nonspray-dried materials, an optimum seed content of ∿2 percent and seed size of <10 μm was determined.

Work on the development of this process for spray drying was performed in Phase VB. Following the recipe developed for nonspray-dried powders, electrolytes were fabricated and characterized. It was found that conversion to the β"-alumina phase was rapid for spray-dried powders, but that control over exaggerated grain growth was difficult. Therefore, additional work was performed to characterize seeded spray-dried powders. In particular, the effects of seed size, seed quantity and annealing conditions on physical, mechanical and endurance characteristics were evaluated extensively.

Fully converted seeds were prepared by sintering of zeta-process powders and subsequent dry milling. The seeds were classified into two size ranges using a conventional air classifier. Both fractions were unimodal with mean

sizes of 3 and 15 μm, respectively. Four lots of powder were prepared from these two batches of seeds. The seed content was varied from 2 to 5 percent for each size fraction. The spray-dried powders, prepared from Reynolds RCHPSDBM alumina and hydroxides as the alkali sources in slurries containing 40 percent solids, were characterized and sintered over a range of conditions.

In general, excellent densities were achieved (i.e., >3.21 g/cm^3) for most sintering conditions. In all cases, the density values achieved through the use of the fine seed fraction were higher than those involving the use of coarse seeds. In some cases, increasing the seed content from 2 to 5 percent resulted in a slight reduction in density (∿0.01 g/cm^3). Annealing tended to improve the density of all materials, especially at the lower firing temperatures.

Electrolytes prepared under optimized conditions had the following average properties: 1) mass density of 3.23 g/cm^3; 2) ionic resistivity at 300°C of 3.6 ohm-cm; 3) four point modulus of rupture of 234 MPa (∿34,000 psi); 4) hoop stress (on EVEM-1 electrolyte tubes at failure) of 123 MPa (∿18,000 psi); 5) microstructure classification of Grade B[1]; and 6) shrinkage on firing of 9.9 percent. The burst-test data for these electrolytes (shown in Figure 1) demonstrate that electrolytes fabricated from S[4]D powders have strength characteristics superior to those of the zeta-process electrolytes.

The process of seeding appears to have clear advantages over the prior methods used for enhancing the conversion to the β" phase and controlling the microstructure during sintering. In order to achieve low resistivity values in unseeded S[3]D powders, an extensive firing schedule (annealing before and after sintering) was required. The S[4]D process eliminates the need to perform the preannealing operation and makes the current firing schedule comparable to the standard zeta process. (Additionally, through selection of appropriate sintering schedules, elimination of annealing altogether should be possible.) In addition, seeding produces a uniform microstructure and the lowest resistivity achieved to date for a Bayer process alumina raw material (RCHPSDBM). Seeding desensitizes the process to sintering temperature, and reduces the actual firing times. The latter effect will minimize compositional changes through soda loss and reduce cost.

5.2.1.3 Alternative Atomization Systems. A key factor in obtaining a low-cost spray-drying process is the selection of drying equipment which results in high product efficiency (total solids product output divided by the solids product input). Product loss results due to: 1) adherence of semidried granules to the drying chamber wall during the evaporation process (instead of falling into the collection area); and 2) inability of product collection equipment to trap the very fine aggomerates and particulates (minor loss).

Prior work with the Bowen dryer resulted in product throughput efficiencies ranging from 28 to 67 percent. The major loss was the result of product build-up on the chamber wall. In some instances, the entire wall became uniformly coated to a depth in excess of 2 cm. In contrast to this, standard spray-drying runs of pure α-alumina resulted in product efficiencies in excess of 90 percent. The major reason for this difference is the presence of soluble alkali salts. The colligative properties of slurries containing dissolved alkalis dramatically depresses the evaporation rate of individual droplets. As a result, some of the droplets do not have sufficient time to dry prior to contacting the chamber walls. This problem can be corrected by: 1) increasing the dryer diameter to allow longer residence times for individual droplets; or 2) decreasing the average droplet size.

The currently used Bowen spray dryer has a fairly narrow chamber, and utilizes two-fluid nozzle-type atomization. In addition to this DOE-owned dryer, Ceramatec owns a NIRO spray dryer with a significantly larger diameter chamber and rotary atomization. Both of these dryers are laboratory scale. Survey experiments were performed with both dryers to determine if product efficiency might be improved by changes in atomization methods or dryer types.

For the Bowen dryer, pressure nozzle equipment and ultrasonic atomizers were investigated. The former was eliminated from consideration because these types of atomizers generally produce fairly coarse sprays and are not compatible with the current drying equipment. An ultrasonic-type atomizer installed in the Bowen dryer was found to produce an acceptable spray size and pattern. The atomizer produced agglomerates predominately less than 43 μm. A 93 percent product efficiency was achieved in a large pilot run (30 kilograms) making it one of the highest to date of any slurry-solution spray drying batch. However, because the atomizer uses sonic velocity air, considerable distortion of individual agglomerates as well as satellite-type agglomerates were observed. This powder was therefore less flowable than the standard β"-alumina spray dried powders.

In the NIRO dryer, an experiment was conducted using rotary atomization. This process uses centrifugal force to atomize the slurry in the radial direction inside the dryer. Changes in agglomerate size are related to changes in the speed of the atomizer wheel. Using wheel atomization, an 87 percent efficiency was achieved. Considerable build-up of product was noted in the atomizer area of the dryer. The average agglomerate size for this powder was smaller than typical, and flowability was poor. However, other properties of the powder and sintered material were acceptable and characteristic of seeded powders.

This preliminary work suggested that the critical equipment for spray drying is the atomizer. High efficiencies were achieved via the use of an atomizer which produces small droplets. However, these small agglomerates reduced the flowability of the powder. To correct this problem, low velocity atomizers are needed and should be developed for this application involving moderately viscous slurries.

5.2.1.4 Sodium-Sodium Cell Testing. One lot of seeded slurry-solution spray dried powders was prepared using ultrasonic atomization. Approximately 20 EVEM-1-size electolyte tubes were fabricated from this material and character-

ized. Reynolds RCHPSDBM was used as the source of α-alumina in slurries with 40 weight percent solids. These tubes had an average mass density of 3.23 g/cm^3 and an ionic resistivity of 3.5 ohm-cm at 300°C. Eleven of these parts were glass-sealed to α-alumina headers and burst tested. (These results were shown in Figure 5-1 and discussed earlier.) Also, five parts were sealed and placed in sodium-sodium cells for endurance testing. These tubes performed acceptably with little asymmetry in resistance. The S^{4}D electrolytes operated with an average cell resistance of 4.6 ohm-cm at 326°C compared to 5.6 ohm-cm at 390°C for control zeta-process electrolytes also on test. More than 200 Ah/cm^2 (total for both directions) had been passed at a current density of 0.65 A/cm^2, by the end of Phase VB.

5.2.2 ELECTROLYTE COST-REDUCTION PLAN

In 1984 a program was outlined by Ceramatec to lower the cost of β"-alumina electrolytes and insulating seals. Results of Ceramatec's study are highlighted below.

To put the issue of electrolyte cost in perspective, the breakdown of the current and projected direct costs (excluding overhead costs) for the fabrication of Mark-II electrolytes was compared. This comparison is given in Table 5-1.

Table 5-1. Breakdown of Current and Projected Electrolyte Fabrication Costs

Cost Item	Current Costs (%)	Projected Costs (%)
Raw Materials	6	44
Variable	11	7
Manufacturing Labor	36	10
Energy	31	30
QC Labor	16	9

In the current standard zeta process, the very expensive (~$15/lb in relatively small quantities) and high-purity Baikowski α-alumina is used. Yet this cost item represents only 6 percent of the direct costs, indicating that most of the direct costs in current pilot-scale operations are related to labor and energy. The projected cost breakdown is based on the assumption that the alumina raw material cost is $0.50/lb. Even at this low cost, the raw material represents approximately 44 percent of the direct costs. It is clear that in addition to reducing raw materials cost, it is imperative that cost-effective and energy-efficient continuous processing methods (e.g., spray drying, near net-shape forming of electrolytes and headers, continuous bisquing and sintering, automated QC and proof testing, etc.) be an integral part of the manufacturing process. Also, it is desirable that the properties and performance of the electrolytes be densitized to impurities in the raw materials and variabilities in the fabrication procedures. Attention should also be given to cell designs which permit greater flexibility in the specification of dimen-

sional tolerances for the electrolyte assembly, leading to improved manufacturability and lower cost.

When introducing cost-reduction practices into an electrolyte manufacturing development program, three interlocking objectives should always be present: 1) lower cost; 2) higher reliability; and 3) better performance. At this stage of development, attention has been almost exclusively directed toward performance and reliability issues with relatively little attention directed to cost-rediction matters. As the focus on cost reduction becomes more intense, it will be important to guard against an inadvertant drop in reliability and performance. Ceramatec believes that all three objectives can be realized, and that the S^4D process, when fully optimized and integrated into automated and continuous production, will meet all of the criteria related to cost, performance, and reliability.

Table 5-2 summarizes Ceramatec's recommended approach to cost-effective manufacturing development of electrolyte assemblies.

Table 5-2. Development of Cost-Effective Electrolyte Manufacturing

Item	Current Status	Next Step
Raw Materials	Baikowski CR-30 Reynolds RCPHSDBM	Lower Cost Materials A-16SG and Others
Powder Preparation	Calcine/Dry Ball Mill	-
	Slurry-Solution Spray Drying	Scale up, Optimize Seeding, Incorporate Zirconia Toughening(?)
Forming	Wet Bag Isostatic	Dry Bag Isostatic
Configuration	25 to 50 mm OD 200 to 600 mm L 1 to 3 mm Wall	Optimize L/D & Wall for Dry Bag Forming
Bisquing	24 to 48 h Batch Cycle	Continuous Process Optimize for Thickest Cross Section
Sintering and Annealing	Batch; 2 h to 1575°C 1 h at 1475°C Pt-Lined Carriers	Continuous Firing Refractory Development
Finish Grinding	Manual	Automatic
Headers	Isostatic Press	Uniaxial Press
	Green Machine	-
	Sinter	Sinter
	Diamond Grind All Surfaces	Size Critical Dimensions Only
Glass Seal	Manual Application	Automate
	Batch Fire	Continuous Fire
Inspection	Dimension, Dye Check Proof Test	Automate

The need for cost reduction is a two- and, perhaps, a three-stage requirement: 1) lowering the cost to an intermediate level (factor of ten reduction) while maintaining present levels of electrolyte assembly quality and performance; 2) lowering the cost to a level (perhaps a factor of 50 reduction) commensurate with adequate quality for commercial sales of energy storage and electric vehicle batteries to selected and relatively small volume market segments which will develop prior to 1990; and 3) lowering the cost even further (factor of 100 reduction) by extensive automation to produce a cost-effective product for very large volume utility load-leveling and private passenger car applications. It is emphasized that, for successful cost reduction, the volumes of electrolytes which are manufactured annually must increase accordingly (e.g., ~1000 per year to ~10,000 per year to more than 1,000,000 per year for the three steps, respectively).

5.3 PILOT-PLANT PRODUCTION

The current DOE Pilot Plant is a 6,000-ft^2 facility in which β"-alumina electrolyte tubes over a range of sizes can be manufactured both by the standard dry powder zeta process and by wet processing techniques such as slurry and slurry-solution spray drying. The plant also has the capability for manufacturing high-quality alumina seal headers and glass-sealing these parts to the electrolyte tubes. The facility, which was relocated during 1983, is capable of producing up to 20,000 EV assemblies per year.

5.3.1 ELECTROLYTE PRODUCTION

During Phase VB, over 1500 electrolyte assemblies, sized primarily for EV batteries, were produced and delivered to Ford Aerospace. These electrolytes (produced by the dry powder zeta process) were of excellent quality in terms of high mass density (3.26 g/cm^3), low sodium ion resistivity (4.3 ohm-cm @ 300°C) and high diametral fracture strength (247 MPa). In addition, these electrolytes were very round (i.e., Max/Min OD = 1.004) with less than 0.4 percent variation in the diameter (24.7 mm) and less than 3 percent variation in the wall thickness (1.5 mm) and very straight since they were sintered by a vertical hang-firing technique developed during Phase VB.

Although production was accomplished by a labor-intensive batch process, overall powder efficiencies were good and improved through the course of the program. Production records for ETX electrolytes (produced in 1984) showed a yield of 68 percent compared to a 52 percent value for earlier EVEM-1 assemblies. Most of the losses occurred in pressing/green machining (~10 percent) and sintering (~18 percent).

In addition to the deliverables, 165 standard zeta-process electrolytes of the EVEM-1 size were produced for HIPing and proof-testing evaluation.

HIPing was used as a means to provide electrolytes with mass densities near theoretical values for property evaluation. HIPing is not envisioned to be a viable manufacturing process, other than for specialty products. Conventional zeta-processed electrolytes already have very high densities (3.26 g/cm^3), and with S^4D process optimization and additional production experience, it is expected that the densities of these electrolytes will approach those achieved

by the zeta process. Approximately 65 zeta-process tubes were fabricated for HIPing using Baikowski CR-30 alumina. HIPing increased the mass density of these parts from 3.25 g/cm^3 to 3.28 g/cm^3. This increase was reflected by a significant improvement in the translucent nature of the tubes and a slight reduction in overall dimensions. Ionic resistivities remained essentially equivalent to values prior to HIPing. The diametral fracture strength of the HIPed tubes was approximately 20 percent lower than commonly observed values and was probably due to a small increase in the average grain size. (The microstructure classification changed from Grade A to Grade B level during the HIPing operation.)

Of the 65 HIPed EVEM-1 tubes, approximately 50 were judged acceptable for sealing to α-alumina headers and additional testing. Twelve of these sealed assemblies were delivered to Ford Aerospace, and the remaining assemblies were subjected to various characterization tests at Ceramatec, especially burst testing which was described in Section 5.1.1.

Approximately 100 EVEM-1 electrolytes were fabricated by the standard zeta process using Baikowski CR-30 alumina for proof and burst testing. These tubes were prepared from one powder lot and sintered in approximately 10 batch firing runs. The average mass density of these tubes was 3.25 g/cm^3, the ionic resistivity was 4.6 ohm-cm at 300°C, and the microstructure classification was Grade A. After sealing to α-alumina headers, these assemblies were subjected to various environmental conditions and burst tested as reported in Section 5.1.1. Twelve of these electrolytes were proof tested at 9.7 MPa (1400 psi) and forwarded in January 1985 to Ford Aerospace for evaluation in sodium-sulfur cells.

5.3.2 RELOCATION, RECONSTRUCTION AND REQUALIFICATION OF PILOT PLANT

Expiration of the lease on the Arapeen Drive, Salt Lake City, pilot-plant location on December 31, 1982, necessitated that all usable equipment be removed from that facility and relocated. Equipment was stored in Ceramatec's facilities adjacent to the selected new site pending DOE's authorization to proceed with the design and reconstruction of the Pilot Plant which was received in March 1983. The facility was functionally operational by the end of September and fully qualified in both the standard zeta process and the slurry-solution spray drying process by the end of October 1983. In the interim, Ceramatec supplied program requirements for electrolytes using its own facilities.

The reconstructed pilot plant utilized all available equipment from the former location that was in good operating condition. Improvements were made in environmental control to reduce sources of contamination, control of dust emissions, physical layout of the equipment, and power distribution. The calciner was replaced with a commercial unit with improved temperature control and uniformity.

After reconstruction was completed, each piece of processing equipment was operated and certified upon production of acceptable quality product. Electrolytes were manufactured, inspected for dimensional conformance, and destructively tested to insure that the acceptance criteria were achieved. The electrolytes produced in the reconstructed facility were equal to or better than the electrolytes produced in the former facility in all respects.

SECTION 6

BATTERY DEVELOPMENT

The Phase VB battery development task objectives were: 1) design, fabrication and testing of a 36-kWh Electric Vehicle Engineering Model (EVEM-1) battery; and 2) test and evaluation of a 100-kWh Stationary Energy Storage (SES) experimental battery constructed during Phase IV of the program. An iterative systems approach was used in these efforts, such that results from battery development fed back into cell, electrolyte, and supporting research activities. Despite difficulties encountered in the development of battery systems, valuable lessons were learned regarding the needs and appropriate directions for future component and cell development.

The electric vehicle (EV) and SES battery development efforts are presented in the following sections.

6.1 EV BATTERY DEVELOPMENT

The principal effort in EV battery development was the design, development test, fabrication, assembly and bench test of the EVEM-1 battery. This effort is described in Section 6.1.1. Other EV battery work involved: 1) refurbishment of the EVEM-1 modules for installation into a Ford-funded battery (CARBAT-1) to be evaluated in an LN7 test-bed vehicle; 2) post-test analysis of CARBAT-1 following an instrumentation-caused electrical fault; 3) reconfiguration and retest of the EVEM-1 modules (CARBAT-1A); 4) operation and maintenance of a sodium-sulfur battery-powered utility vehicle; and 5) preliminary analysis and supporting tests to determine the effects of battery circuit design and electrical control strategy on battery reliability. These latter efforts are presented in Sections 6.1.2 through 6.1.6, respectively.

6.1.1 EVEM-1 BATTERY

The design, development testing, fabrication and bench test results of the EVEM-1 battery are presented below.

6.1.1.1 EVEM-1 Design. Design goals for the EVEM-1 battery which were established in cooperation with Ford Motor Company engineers are shown in Table 6-1. These goals were considered challenging, but achievable. Detailed cell design and performance parameters were described in Section 4.1.1. As noted, the EVEM-1 cell design was primarily driven by the peak pulse power requirements in combination with the test-bed vehicle packaging constraints specified for the subsequent CARBAT-1 assembly. Preliminary selection of the battery electrical circuit, packaging concept, and thermal management approach was done iteratively and simultaneously with the cell design.

The battery circuit--consisting of eight modules in series with four 15-cell series strings connected in parallel per module--was selected to minimize adverse effects of cell failure on battery performance and reliability. The key tradeoff variable was the number of cells in series per string. As string length is increased, load-sharing improves among parallel strings with unbalanced numbers of failed cells. On the other hand, worst-case cell

TABLE 6-1. ELECTRIC VEHICLE ENGINEERING MODEL-1 (EVEM-1) DESIGN GOALS

Nominal Voltage:	240 VDC
Rated Capacity:	166 Ah at C/3
Delivered Energy:	36 kWh at C/3
Electrical Efficiency:	89% at C/3 Discharge C/6 Charge
Peak Power (30 sec. pulse):	54 kW at 0-50% DOD 44 kW at 80% DOD
Continuous Power:	16 kW to 80% DOD
Weight:	884 lb (402 kg)
Volume:	10 ft^3 (283 l)
Thermal Loss:	300 W at 350°C
Life:	200 Cycles; 1 Year

voltage extremes at end-of-discharge and end-of-charge worsen with increased string length. A 15-cell string length was chosen primarily to limit the end-of-charge voltage on any cell to <6 VDC. At the same time, battery capacity was projected to be nearly unaffected by a single cell failure in any one 15-cell string, assuming a post-failure cell resistance of less than about five times the nominal cell resistance.

A modular cell packaging concept was selected, as shown in Figure 6-1. The 60 cells were arranged horizontally in a hexagonal pattern with the four strings stacked vertically. Each cell was electrically isolated from its neighbors by a braided fiberglass sleeve. Added isolation was provided by glass-coated aluminum separators between each vertical layer of cells. A glass-coated stainless steel module casing held the cells in position. Cell orientation was alternated in the strings so that only short aluminum interconnections were required between cells. The module bus bars were constructed of aluminum and served two functions--string current collection and cell thermal control. Cooling-air passages and electrical heaters were incorporated into the bus bars for the latter function. Ceramic spacers and braided fiberglass sleeving were used to isolate the bus bars from the cell ends and the module casing.

The battery thermal management approach included use of: 1) a vacuum-insulated thermal enclosure (CARBAT-1) to limit the heat-loss rate to about 300 W_{th}; 2) dispersed electrical heaters in multiple circuits for both heatup and loss compensation; and 3) forced ambient-air cooling for removal of up to 4.2 kW_{th} during high-rate (~16 kW_e continuous or rms-equivalent dynamic load) discharge. For the EVEM-1 bench test the modules were partially isolated and insulated by conventional mineral board material. The module heaters were derated by ~90 percent for normal battery operation. Three independent control circuits--center, peripheral and top--were used to minimize internal

FIGURE 6-1. EVEM-1 MODULE DESIGN CONCEPT

temperature differences. A single air supply blower (rated at 75 SCFM) with on/off control was used with a top-mounted manifold for distribution to the modules.

6.1.1.2 EVEM-1 Development Testing. In addition to previously noted EVEM-1 cell tests, the performance of a representative 15-cell string was evaluated and a 60-cell prototype module was tested to verify performance, thermal control, safety and ruggedness. The 15-cell string tests included discharge at C/3 and C/2 and recharge at C/3. As shown in Figure 6-2, the load sharing among the cells was excellent. Only at the end-of-charge did significant differences in cell voltage occur.

Performance tests of the prototype module also showed excellent cell and string load-sharing in the absence of failed cells. However, one cell became effectively open-circuited on discharge, limiting module capacity to about 70 percent of the rated value. Pulse power capability was also excellent, exceeding the peak power ratings by about 20 percent after discharging 70 percent of rated capacity. Thermal control was marginal in these tests, due primarily to poor penetration of the cooling air to the bottom string. This led to an improved bus-bar configuration for the EVEM-1 bench test.

A total of eight cells were intentionally failed by severe overcharging to demonstrate the safety of the prototype module. No propagation of these cell failures was observed. Following this safety test the module was subjected to 1.5 g's random vibration, transverse to the cells' axes, for one hour. Although no new cell failures occurred, other minor shortcomings of the module design were noted and eliminated in the final EVEM-1 modules. In particular, the aluminum string fuses proved susceptible to fatigue failure and were replaced by aluminum/steel bi-metal shunts for monitoring string currents.

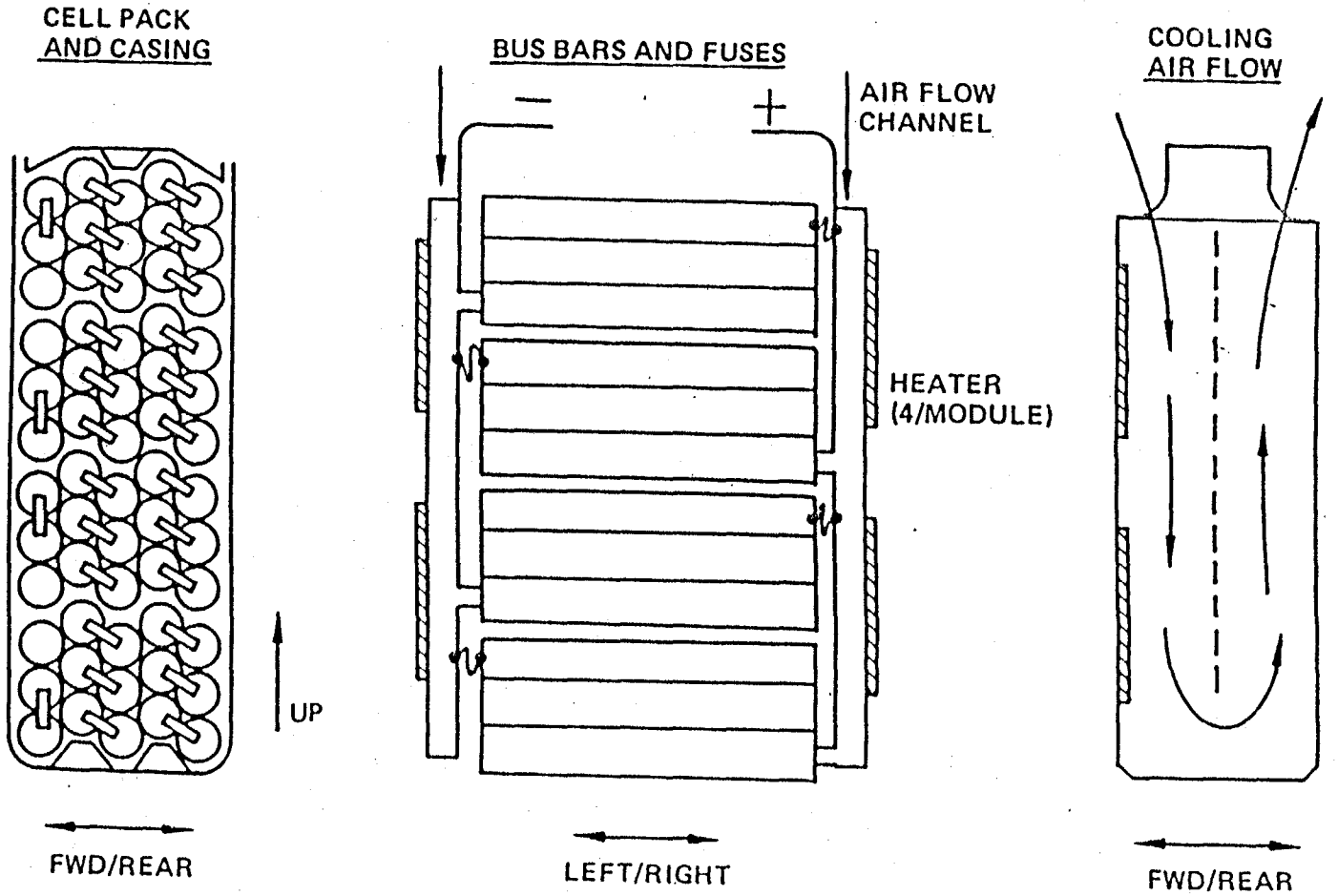
CELL PACK
AND CASING
UP
FWD/REAR
BUS BARS AND FUSES
AIR FLOW
CHANNEL
HEATER
(4/MODULE)
LEFT/RIGHT
COOLING
AIR FLOW
FWD/REAR

Figure 6-1

6.1.1.3 EVEM-1 Fabrication. Approximately 800 EVEM-1 cells were fabricated in a single production run. All materials, components, and subassemblies were completely documented as to source, lot numbers, inspection data, and processing parameters so that complete traceability and correlation with performance was maintained. Fabrication was conducted in accordance with detailed manufacturing operations sheets which contained specific fabrication instructions and critical inspection steps throughout the sequence. Upon completion, individual cells were assembled into 15-cell series strings and heated to the battery operating temperature of 350°C for verification of capacity and performance of each cell. After cooling, those cells that did not achieve rated performance were removed from the string and replaced with individual cells that previously had been operated and met design performance.

Strings then were assembled into the finished module with appropriate temperature and instrumentation leads to allow monitoring of the performance of each string during battery operation. The eight modules (Figure 6-3) then were connected in series and enclosed within approximately 6 in. of standard mineral board insulation (Figure 6-4). An air distribution system was attached to the top of the assembly for temperature control during the test, as shown in Figure 6-5.

FIGURE 6-2. 15-CELL STRING TEST--VOLTAGE DISPERSION

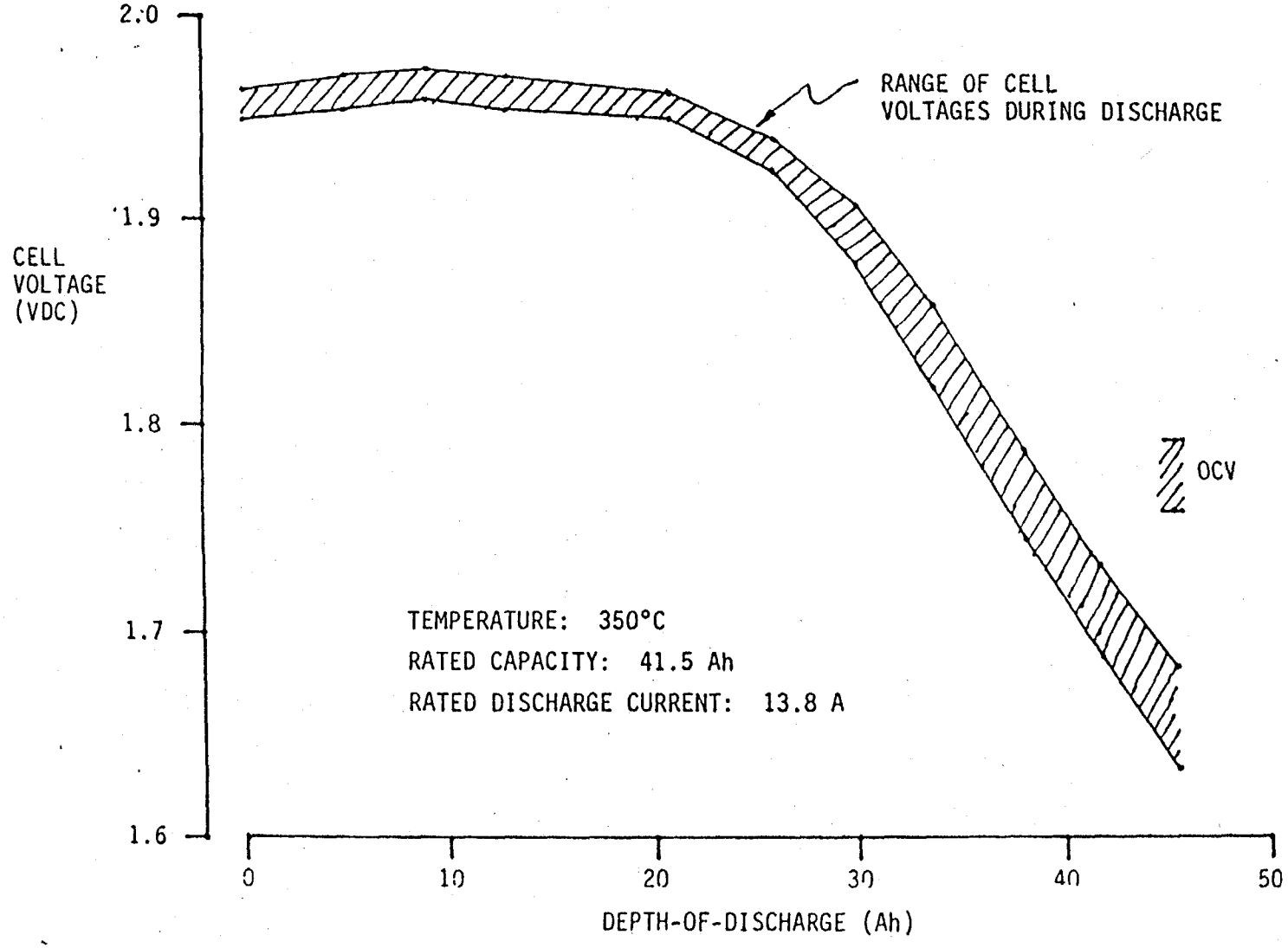
2.0
1.9
1.8
1.7
1.6
CELL VOLTAGE (VDC)
RANGE OF CELL VOLTAGES DURING DISCHARGE
OCV
TEMPERATURE: 350°C
RATED CAPACITY: 41.5 Ah
RATED DISCHARGE CURRENT: 13.8 A
0
10
20
30
40
50
DEPTH-OF-DISCHARGE (Ah)

Figure 6-2

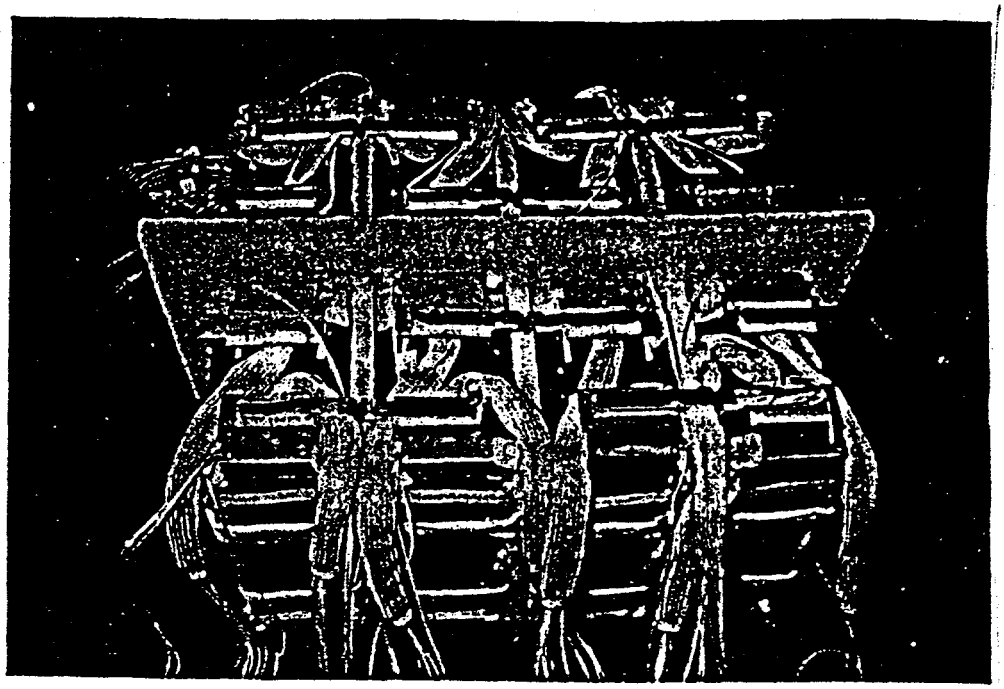

FIGURE 6-3. EVEM-1 BENCH TEST SUBASSEMBLY

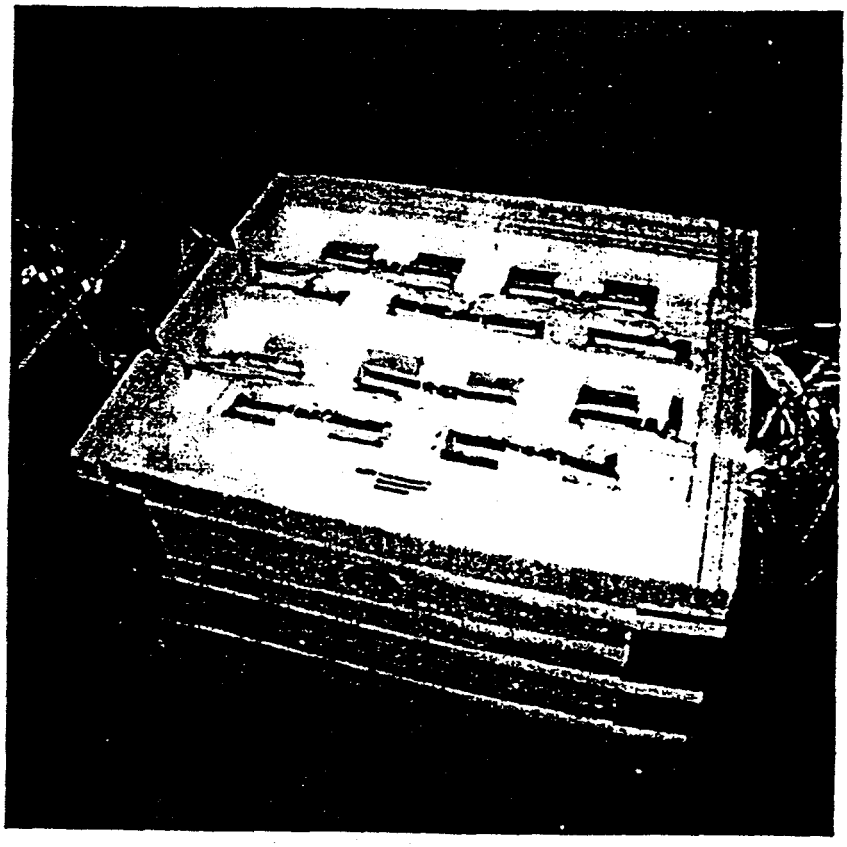

FIGURE 6-4. INSULATED EVEM-1 BENCH TEST ASSEMBLY

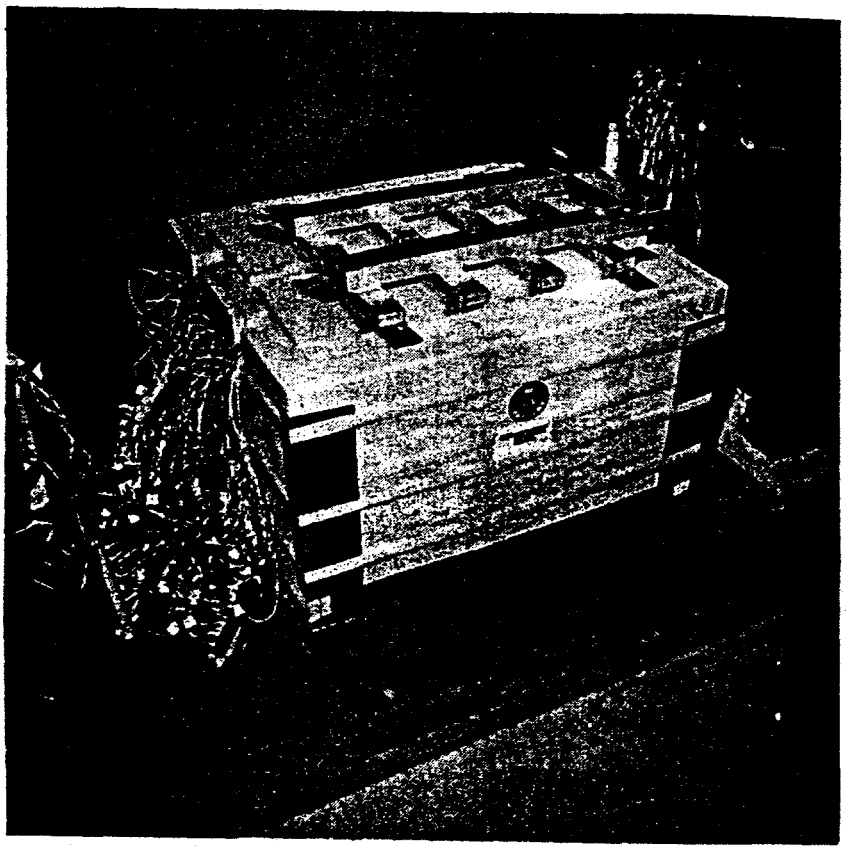

FIGURE 6-5. FINAL EVEM-1 BENCH TEST ASSEMBLY

6.1.1.4 EVEM-1 Bench Test. After assembly and checkout, the EVEM-1 battery tests were conducted as summarized in Table 6-2. Approximately fifteen cells failed within the first two test cycles, most probably due to stresses associated with heatup of the modules. Another seven cells failed in the course of testing, possibly due to test equipment problems related to regenerative pulse testing. The cell failures occurred in six of the eight modules, and in two modules the combination of high post-failure cell resistance and unbalanced failure distributions among the four strings limited the battery's capacity to about 75 percent of rated. For Cycle Nos. 10-12 these two capacity-limiting modules were electrically bypassed, allowing demonstration of full capacity in the remaining six modules. These six modules had an estimated nine cell failures, distributed such that no string had more than one failure. Two modules had no failed cells. In this condition the battery readily sustained the power and regenerative pulses typical of the operation of an electric vehicle.

The results of the EVEM-1 bench test, although not wholly successful, did verify pretest predictions of performance in both constant-current (Figure 6-6) and 30-s pulse (Figure 6-7) discharges.

Upon completion of the bench test sequence, approximately 22 cells were noted to be inoperative. These cells failed or became inoperative in a completely benign manner, reproducing the failure characteristics established during single-cell and prototype module tests.

TABLE 6-2. EVEM-1 BENCH TEST CYCLE SUMMARY

Cycle No.	Date	No. of Modules	Discharge Conditions	% Rated Capacity	kWh Delivered	
1	6/9	8	28 A constant current (C/6)	59	23	
2	6/13	8	28 A constant current	81	30	
3	6/15	8	56 A constant current (C/3)	75	27	
4	6/17	8	56 A constant current	87	31	
5	6/20	8	28 A background/∿200 A pulses	80	30	
6	6/22	8	28 A background/ 200 A pulses /∿70 A regenerative pulses	65	24	
7	6/23	8	56 A constant current	72	25	
8	6/28	8	56 A constant current	64	23	
9	6/30	8	56 A constant current	76	27	
10	7/5	6	56 A background/∿200 A pulses /∿70 A regenerative pulses	84	22	(30)*
11	7/7	6	28 A background/∿200 A pulses /∿70 A regenerative pulses	101	28	(37)*
12	7/8	6	84 A constant current (C/2) to 80% DOD/28 A constant current to 100%	101	26	(34)*

NOTE: Recharge conditions included 28-A and 14-A constant current plus voltage-limited taper charge and module equalization

*Numbers in parentheses indicate energy that would have been delivered from eight modules.

FIGURE 6-6. EVEM-1 PERFORMANCE - 28 A AND 56 A DISCHARGES

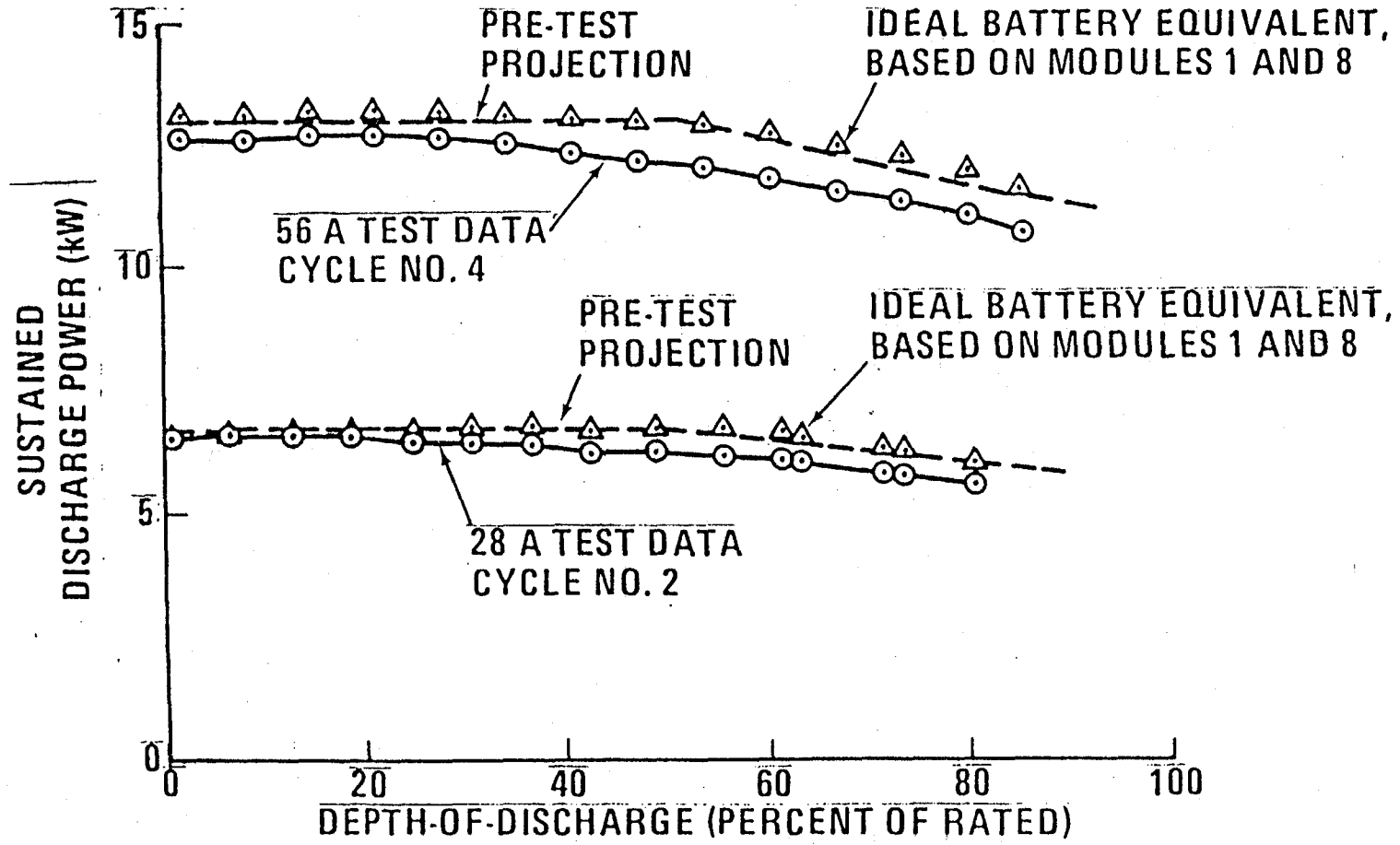
15
10
5
0
SUSTAINED DISCHARGE POWER (kW)
PRE-TEST PROJECTION
IDEAL BATTERY EQUIVALENT, BASED ON MODULES 1 AND 8
56 A TEST DATA CYCLE NO. 4
PRE-TEST PROJECTION
IDEAL BATTERY EQUIVALENT, BASED ON MODULES 1 AND 8
28 A TEST DATA CYCLE NO. 2
0
20
40
60
80
100
DEPTH-OF-DISCHARGE (PERCENT OF RATED)

Figure 6-6

FIGURE 6-7. PROJECTED BATTERY PULSE POWER

After cooling the EVEM-1 modules to ambient temperature, one module with no failed cells was reheated to operating temperature to gain confidence in the freeze-thaw capability of the battery cells and modules. No cells failed on heatup, and a low-rate discharge/charge cycle (Figure 6-8) was successfully completed. The module was then cooled to ambient temperature.

FIGURE 6-8. EVEM-1 BENCH TEST, MODULE NO. 1 RETEST

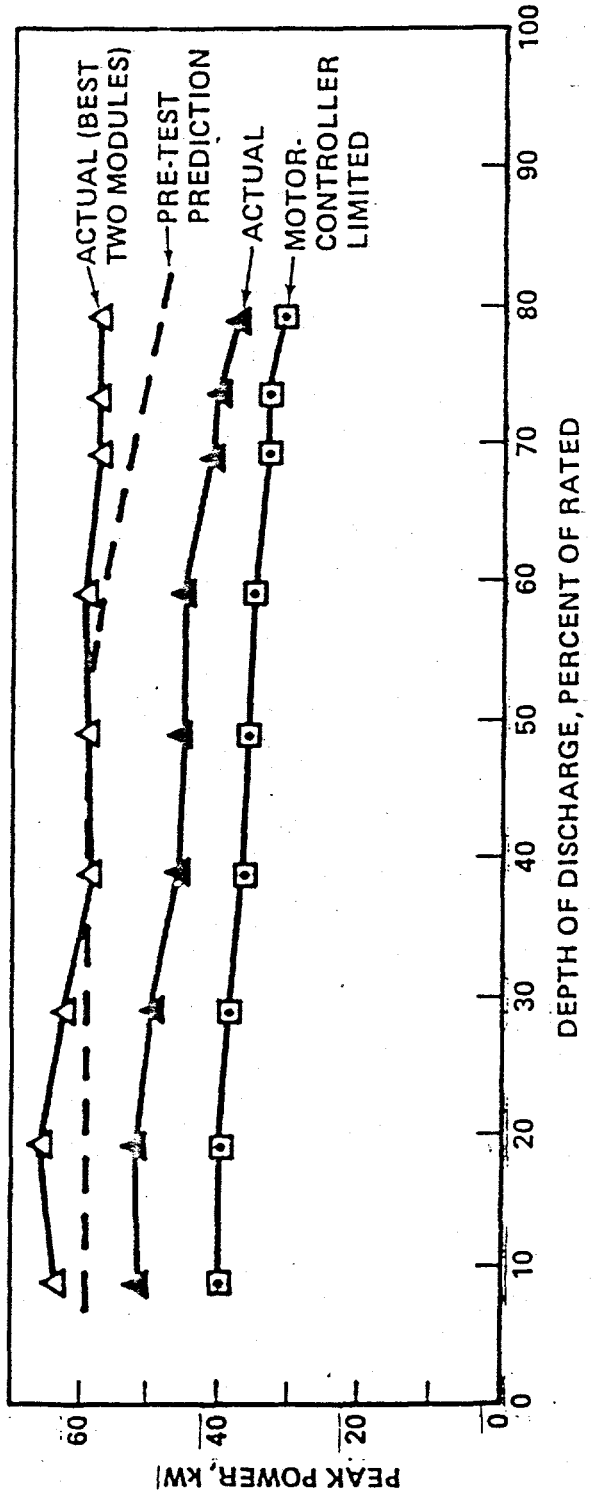
ACTUAL (BEST TWO MODULES)
PRE-TEST PREDICTION
ACTUAL
MOTOR-CONTROLLER LIMITED
PEAK POWER, kW
0
20
40
60
0
10
20
30
40
50
60
70
80
90
100
DEPTH OF DISCHARGE, PERCENT OF RATED

Figure 6-7

RATED CAPACITY: 166 Ah
DISCHARGE CURRENT: 28 A
DISCHARGE ENERGY: 4780 Wh
CHARGE ENERGY: 5045 Wh
ROUND-TRIP EFFICIENCY: 94.7%

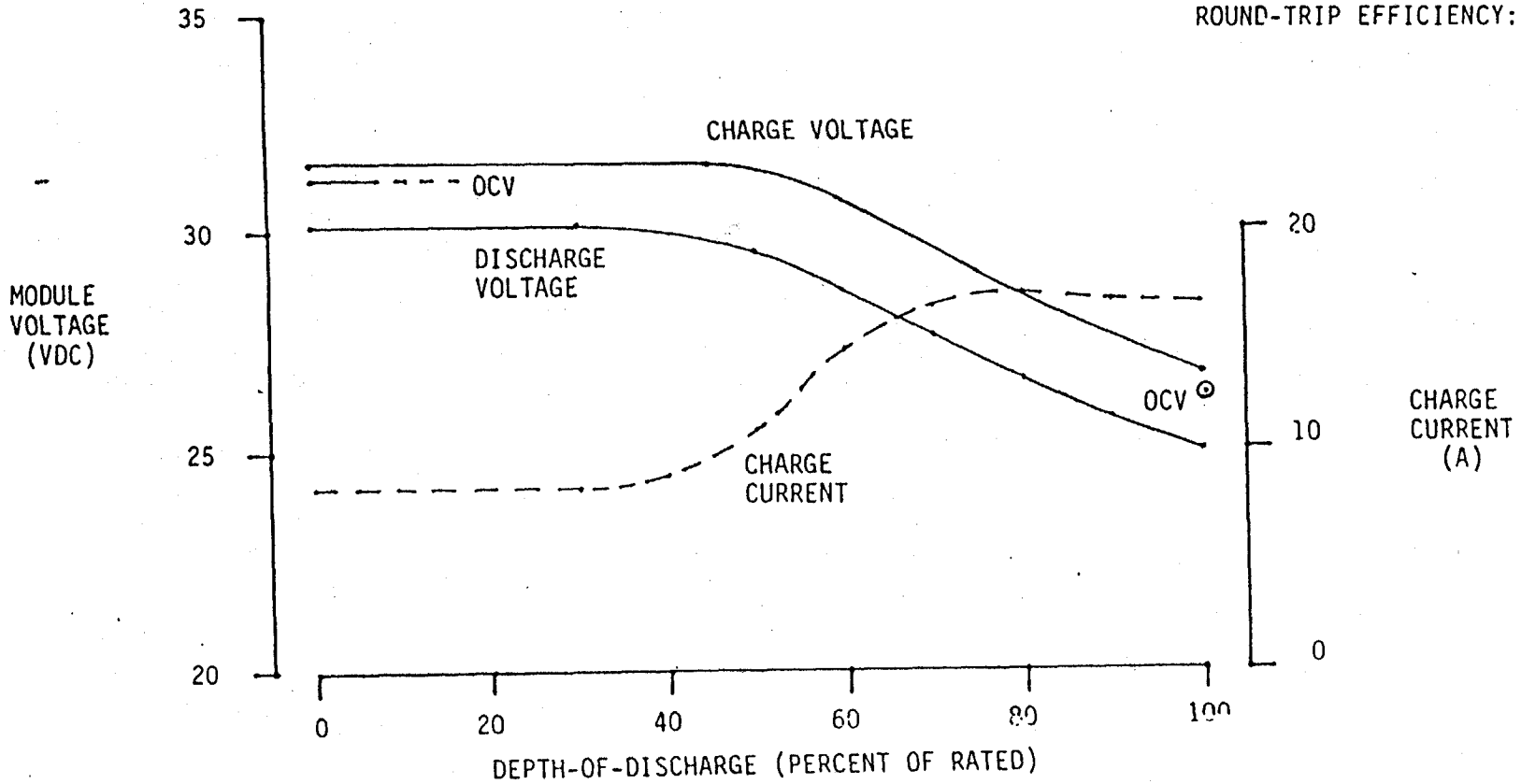

Figure 6-8

The key areas identified as requiring improvement for the battery over the long range are cell reliability, recharge strategy and thermal control for sustained power. Even so, battery bench-test performance was deemed adequate to proceed to dynamometer and in-vehicle testing. The battery was refurbished by replacement of failed or questionable cells. Integration of the battery into an LN7 vehicle and transportation to Dearborn for further evaluation was undertaken with Ford funds.

6.1.2 CARBAT-1 TEST AND POST-TEST ANALYSIS

The objectives of the CARBAT-1 effort were to: 1) evaluate a full-scale sodium-sulfur battery in a test bed vehicle with representative dynamic electrical load profiles; 2) validate the battery performance model used in the Ford EV simulation computer programs; and 3) provide experimental battery data for use in the on-going ETX program, a DOE/EHV-funded effort at Ford Research.

The eight EVEM-1 modules were refurbished by replacing all failed or suspect cells with pretested spare cells. The modules were then installed in a double-walled vacuum thermal enclosure (obtained from the Linde Division of Union Carbide Corporation under Ford Research sponsorship) as shown in Figure 6-9. Note the routing of approximately 400 instrumentation leads from the modules to terminal strips on the front of the enclosure.

FIGURE 6-9. CARBAT-1 ASSEMBLY

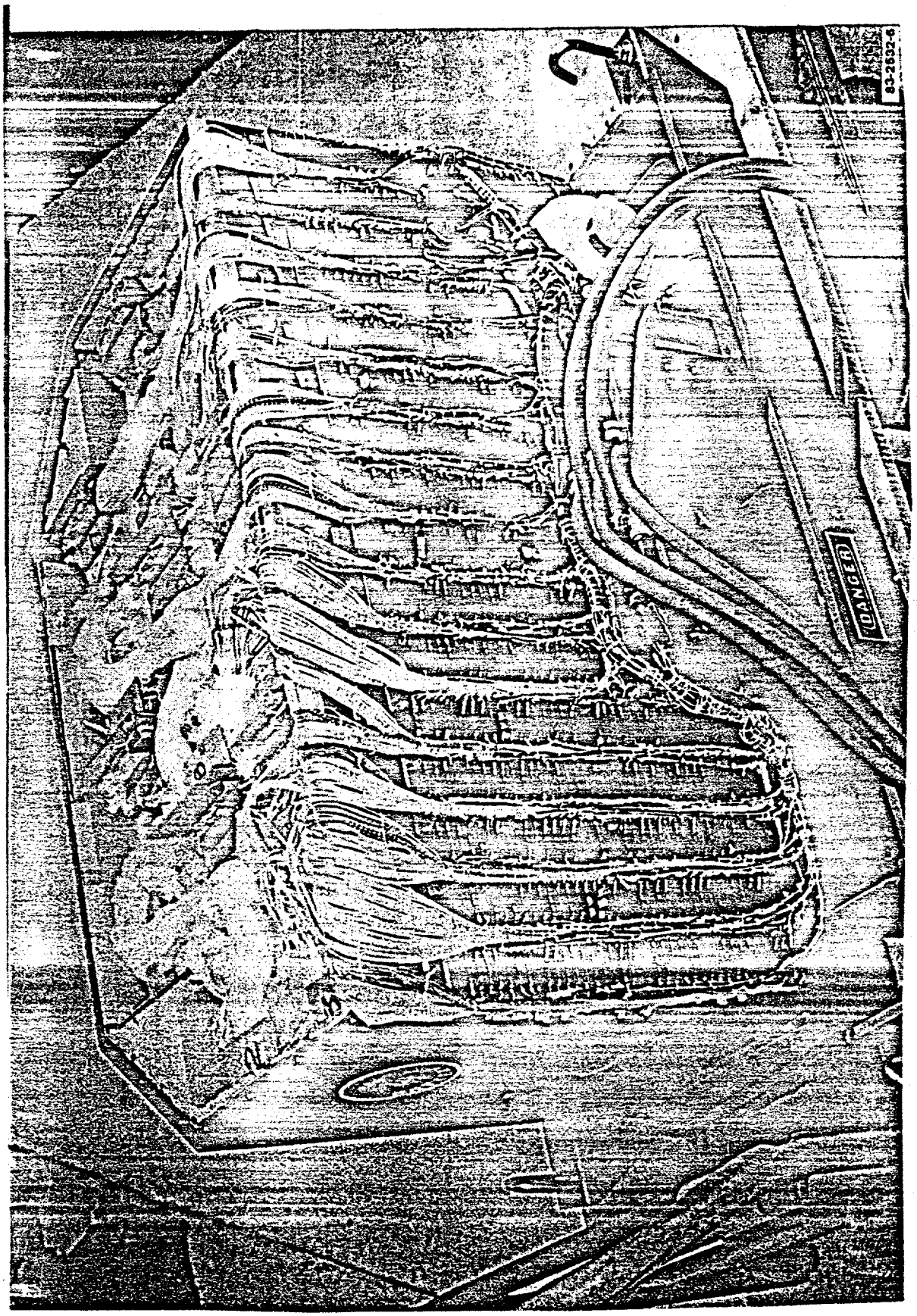

Figure 6-9

The CARBAT-1 assembly was successfully installed within the battery compartment of the LN7 test-bed vehicle, and was shipped in that vehicle from Newport Beach, California to Dearborn, Michigan.

After heatup of the battery at Dearborn, diagnostic tests indicated approximately 13 cell failures scattered among 11 of the 32 strings in the battery. At that point, the battery's power capability would have been acceptable, although rated capacity might not have been achieved. During the period following the diagnostic tests, modifications in the external heater control circuitry were implemented, along with adjustments in the heater supply voltage and three setpoint temperatures, to obtain good temperature uniformity among the strings.

After a weekend idle period and just prior to starting the planned battery testing, a severe electrical fault occurred within the battery. Several anomalous instrumentation readings were observed, along with significant venting of smoke from within the battery enclosure. Shortly thereafter the battery was cooled to ambient, returned to Newport Beach, and inspected to determine the cause of the fault.

Battery disassembly and post-test analysis were accomplished with the participation of Dr. James E. Battles of Argonne National Laboratory. The main objective of these activities was to establish the cause of the incident at Dearborn. Highlights of the examination procedure included: examination of all lead wires for damage; removal, weighing and inspection of modules; removal and inspection of bus bars and standoffs; measurement of all cell voltages and checking for short circuits to casings; physical inspection and X-ray of all cells in groups of five; and conduction of supporting analyses and tests. Obseration were well documented photographically.

It was confirmed that the incident had been the result of the shorting of two externally parallel thermocouples to their respective bus bars. This thermocouple circuit was intended to indicate average bus-bar temperature of all eight modules during the in-vehicle test, and was not being monitored during the heatup phase. The short circuit led to discharge of two modules with the current carried by the thermocouple wires, resulting in burning off of the insulation and extensive damage to adjacent lead wires.

Despite this generally disappointing result for the CARBAT-1 effort, it was shown that the cell failures occurring on heatup neither contributed to the instrumentation fault, nor led to propogation of additional cell failures within the high energy density battery core. The large majority, about 340, of the cells were available for further testing in a battery.

6.1.3 CARBAT-1A RECONFIGURATION AND TESTING

Since more than 340 cells were available from CARBAT-1, it was planned with DOE/SNL concurrence, that a reconfigured battery, designated as CARBAT-1A, be assembled and tested. CARBAT-1A consisted of six reconfigured EVEM-1 modules, each containing 60 cells series-connected into a single string. Aluminum rods were added between cells such that any failed cell could be bypassed using a welded connector without cooling the module to ambient temperature. The six modules were installed, along with six independent thermal-control subassemblies,

into the CARBAT-1 enclosure (Figure 6-10). Each module's power leads were passed through the top insulation to permit flexible interconnection of the modules into various battery circuits. Battery instrumentation included only nine internal temperatures and each module's voltage and current.

Based on the modules' open-circuit voltages, approximately eight cells failed during the heatup of CARBAT-1A. Initial diagnostic cycles of the battery at six- and three-hour discharge rates showed that half of the modules had high and erratic resistance as a result of cell failures. The other three modules were discharged in parallel to as much as 74 percent of rated capacity. Recharge of the modules required individual taper charging.

Both hot and cold maintenance operations were performed on the CARBAT-1A modules to bypass failed and blocking cells, and to replace failed cells with spares. These efforts were successful to the extent that three modules were finally cycled individually to 75 percent of rated capacity in a stable, repeatable manner. The remaining modules experienced too many cell failures (12 to 15 each) to provide useful data as part of a battery. The three stabilized modules were subsequently tested in parallel. Two modules, with an imbalance of three active cells, performed as expected. However, the third module apparently experienced an additional cell failure just prior to this test and became blocked early in the discharge of the three-string parallel circuit. In the following cycle a cell failure in one of the active modules blocked that module's discharge. It was evident that the cells' inability to fail short would continue to create blockage of the strings, and no further tests were attempted.

FIGURE 6-10. CARBAT-1A ASSEMBLY

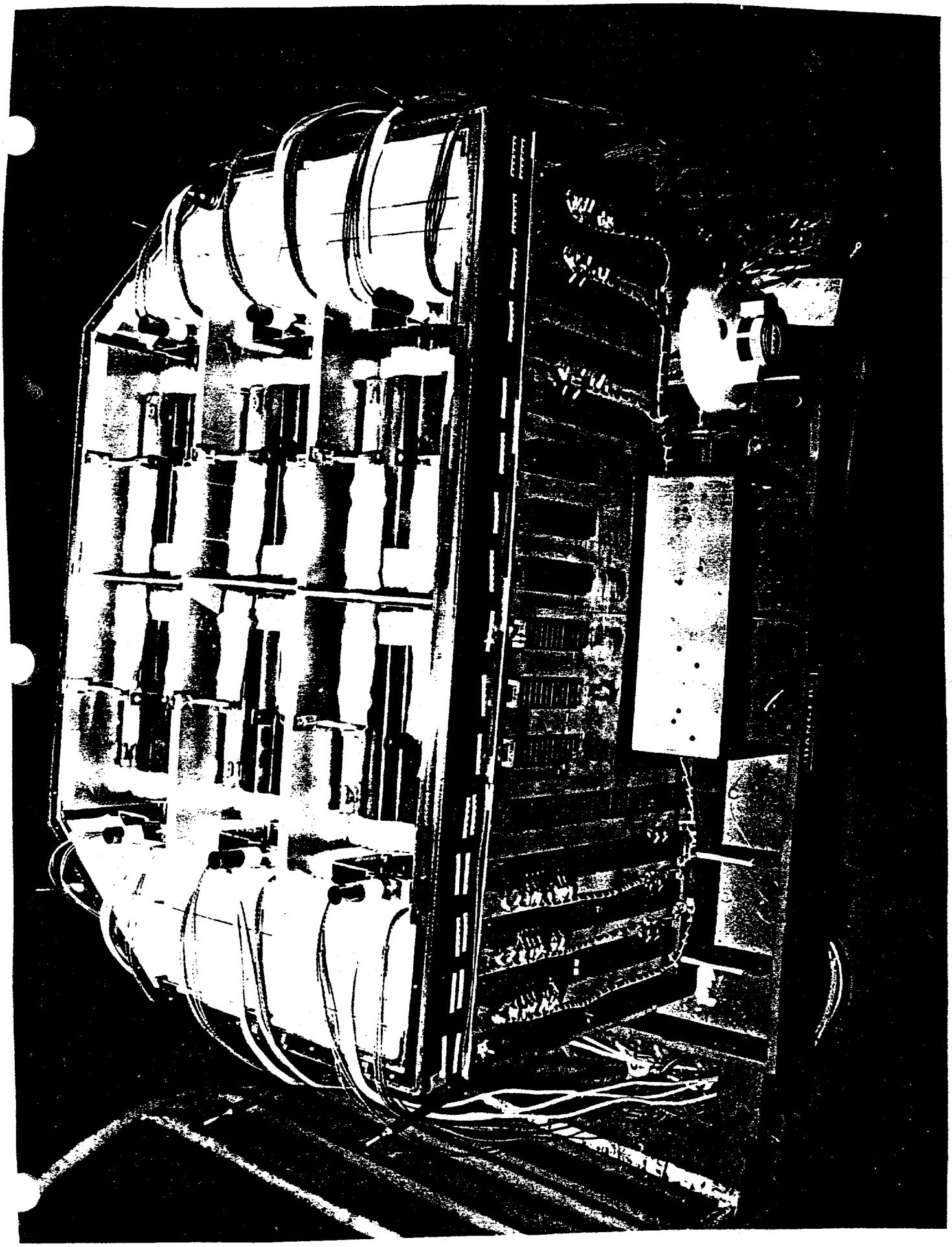

Figure 6-10

Post-test analysis of failed cells from the EVEM-1, CARBAT-1, and CARBAT-1A assemblies was inconclusive with regard to dominant electrolyte failure modes and any correlation of cell failures with manufacturing process variables. However, it was established that internal devices for assuring low post-failure cell resistance would probably not be sufficiently reliable. This conclusion is based on the wide variety of electrolyte fracture modes observed, the inability of proposed devices to assure electronic bridging across the failed electrolyte, and the highly corrosive post-failure environment to which a system of metallic conductors would be exposed for long durations at high current densities.

The lessons learned from these EV battery development efforts include the following. First, battery reliability--defined broadly as the ability of the battery to maintain adequate performance in spite of random cell failures--is critically dependent upon achieving high cell reliability. The most important cell requirements are high freeze-thaw reliability and positive assurance of low post-failure resistance. These requirements are not strongly affected by the selection of a battery circuit, but longer strings of series-connected cells (60 to 120, for example) can provide battery load-sharing and thermal management benefits. Since internal devices for providing low post-failure cell resistance do not appear feasible, it is mandatory that the battery design allow for easy bypass of failed cells without cool-down of the battery. Alternatively, an external, automatic failed-cell bypass device should be developed.

A second general conclusion is that battery chargeability can be improved by: 1) more flexible control of the charging power supply; 2) providing for isolation of strings as they become fully charged; and 3) maintaining good temperature uniformity among the parallel-connected strings.

Finally, battery thermal control during relatively high-power discharge operation must be improved. This will occur naturally in conjunction with improved cell reliability and with the use of fewer, longer strings of cells in series. It may be necessary, however, to provide independent heating/cooling controls for each parallel-connected string to positively assure the desired temperature uniformity.

6.1.4 ELECTRIC-POWERED UTILITY CART

A 38-month demonstration of a Na/S battery's ability to power an electric vehicle began in 1981, when the lead-acid battery of an electric-powered utility cart was replaced with a Na/S battery of 52 Mark-IID cells. Tests confirmed the anticipated five-fold increase in range over that obtained with the lead-acid battery.[1]

The cart was used to transport cell components and raw material between the cell assembly building and other Ford Aerospace buildings. When the demonstration ended in 1984, the cart had been operated 122.6 hours (517 miles), powered by its Na/S battery. During the 38-month demonstration, about one-fourth of the original cells were replaced, generally by cells taken from other tests. The battery was serviced hot; i.e., a replacement cell was preheated to 300°C, then inserted into the battery in place of the old cell, which also was removed hot. The battery was encased in a box-like structure

with a removable lid to facilitate servicing. The cells were aligned vertically; i.e., the sodium reservoirs were above the sulfur containers.

The demonstration was terminated primarily because the supply of replacement cells was exhausted. In addition, the copper wire used to interconnect the cells had corroded excessively.

6.1.5 EV RELIABILITY STUDY

An experimental effort was undertaken to characterize long string operation and evaluate its reliability under various control methods. Forty cells previously fabricated and evaluated in a two-year internally funded 96-cell reliability test were reconnected in series to create a string with a nominal rating of 80 V and 55 Ah. Individual cell instrumentation permitted voltage distributions to be measured at 30-s intervals. The string was heated in a large oven and operated for 52 electrical cycles under increasingly stressful control conditions determined by overall string voltage.

The results are summarized in Table 6-3. During the first two periods (Cycle Nos. 1-7 and 8-12), restrictive voltage limits constrained the capacity to 57 percent and 67 percent of the rated value, respectively. Following bypass of a defective cell, the capacity increased to 78 percent (Cycle No.s 14-27), then to 96 percent of rating (Cycle Nos. 28-45) with the controls set for 1.60 volts per cell (average) on discharge and 2.35 volts per cell (average) on charge. During this period, the capacity was stable with an average of 53.1 Ah with a small relative standard deviation (S/X) of 0.014. During the last 7 cycles, more extreme control settings (to 1.50 and 2.50 volts per cell) caused failure of 9 cells.

Table 6-3. String Performance

Cycle Number	Control Settings, V	No. of Cells	Discharge Capacity Ah Range		Statistics	
			Highest	Lowest	Average	RSD*
1-7	1.80/2.25	40	37.7	27.1	31.4	0.100
8-12	1.70/2.30	40	41.5	32.3	36.9	0.108
14-27	1.70/2.30	39[1]	43.7	40.6	42.83	0.019
28-45	1.60/2.35	39	54.3	51.8	53.08	0.014
46-49	1.50/2.50	39[2]	63.2	35.8	-	-
51-52	1.60/2.35	30	49.7	49.5	-	-

*RSD = $S/\bar{X}$ = relative standard deviation

[1]Bypassed Cell No. 28

[2]Caused 9 cell failures

The cell voltages were very well balanced throughout the cycling, with two exceptions: 1) near the end of charge for each cycle; and 2) during intervals when one or more cells were in the process of failing. Determination of the precise voltage distribution, especially near the end of the charge cycle, was thwarted by the algorithms used for data acquisition and control. As a consequence, the most severe voltage experienced by a cell just before shutdown was often not recorded on tape. The maximum recorded voltage level impressed on any cell at end of charge increased rapidly as control limits were widened. The results are summarized in Table 6-4.

Table 6-4. Voltage Abuse

Control Limits, Average Volts/Cell		Recorded Cell Voltages, V		Comments
Chg	Dis	Max	Min	
2.25	1.80	2.35	1.65	
2.30	1.70	5.1	-2.15	Cell No. 28 bypassed
		6.4	1.65	Cycle No. 22
		≤5	1.65	All other cycles
2.35	1.60	9.9	1.54	Cycle No. 39
		7.8	1.55	Cycle No. 31
		≤5	1.55	All other cycles
2.50	1.50	>10	-8.2	Induced 9 cell failures

In summary, long strings were shown to yield stable performance and high capacity. It was demonstrated that cells can withstand momentary charging voltage stresses approaching 10 V. Moderately complex charging algorithms and controls appeared necessary to manage the voltage stresses in high-voltage strings to avoid premature cell failures. An algorithm based on implied string resistance was subsequently developed and used in the CARBAT-1A tests described in Section 6.1.3. Analyses indicated an optimum system of this type will provide high battery reliability essentially independent of voltage.

6.2 STATIONARY ENERGY STORAGE (SES) BATTERY DEVELOPMENT

The development of batteries for SES applications emphasized the construction and electrical testing of small sections of the large batteries projected for load leveling (LL). In Paper No. 809105 presented at the Intersociety Energy Conversion Engineering Conference in August 1980, the proposed sodium-sulfur battery system was described.[2] The battery comprises over 500,000 cells subdivided into series-connected modules, the smallest repairable units. Each module, in turn, consists of series-connected submodules (groups of cells interconnected in parallel). The total number of submodules in series sets the battery's total voltage: the total current depends on the number of cells connected in parallel in each submodule.

In early 1981 Ford Aerospace completed construction of a 100-kWh battery system comprising four modules in individually heated compartments of a large enclosure and necessary control and test hardware. The system provided a means of gaining hands-on experience in battery startup, operation and servicing. It also enabled the evaluation of fuse links, bus interconnections and control systems for thermal management and electrical cycling. Construction and early tests of the battery have been described elsewhere.[1] Section 6.2.1 discusses the results from 2.5-years of testing of the battery.

In 1984, two reconfigured modules were assembled from cells taken from the 100-kWh battery. These modules are discussed in Section 6.2.2.

6.2.1 100-kWh BATTERY TESTING

The 100-kWh battery utilized 512 Mark-IID cells of the type discussed in Section 4.2.1. It represented a full-current (but low-voltage) segment of future utility batteries. Each of its eight submodules comprised 64 cells interconnected in parallel. Two submodules connected in series formed a module, and each of the four modules was contained in a separate compartment of the test enclosure.

During the first year's operation, control-system faults necessitated repairs to two modules, which required freezing and thawing of those cells. These repairs were partially successful, one module being unaffected. The other module, however, still performed unsatisfactorily after its initial repair; and after two further unsuccessful attempts to correct its deficiencies, the battery was operated without it. Paper No. 829097 presented at the Intersociety Energy Conversion Engineering Conference in August 1982 discusses these repairs and other events occurring in the first year's operation.

After the removal of the damaged module, the remaining battery continued to operate for over two years, discharging 5 hours daily unless the system was temporarily unavailable (generally due to test equipment malfunction). Figure 6-11 summarizes battery availability. Initially faulty charge-control equipment was the greatest cause of downtime. Toward the end of the second year, the control microprocessor frequently over-heated and caused the system to stop; and once the battery was idled for 65 days to utilize the microprocessor for another test.

Electrolyte fracture results in a "shorted" cell, i.e., an internal short circuit and self-discharge of the cell. Since the cells within a submodule were in parallel, a shorted cell led to self-discharge of the submodule until the fuse associated with the failed cell blew and removed it from the circuit. Often the resistance of a shorted Mark-IID cell in the 100-kWh battery was not low enough at first to draw sufficient current to blow its fuse. It often persisted as an internal short for days, sometimes for several months, leading to charge imbalance among the submodules and loss of capacity in the battery.

FIGURE 6-11. AVAILABILITY OF 100-kWh BATTERY

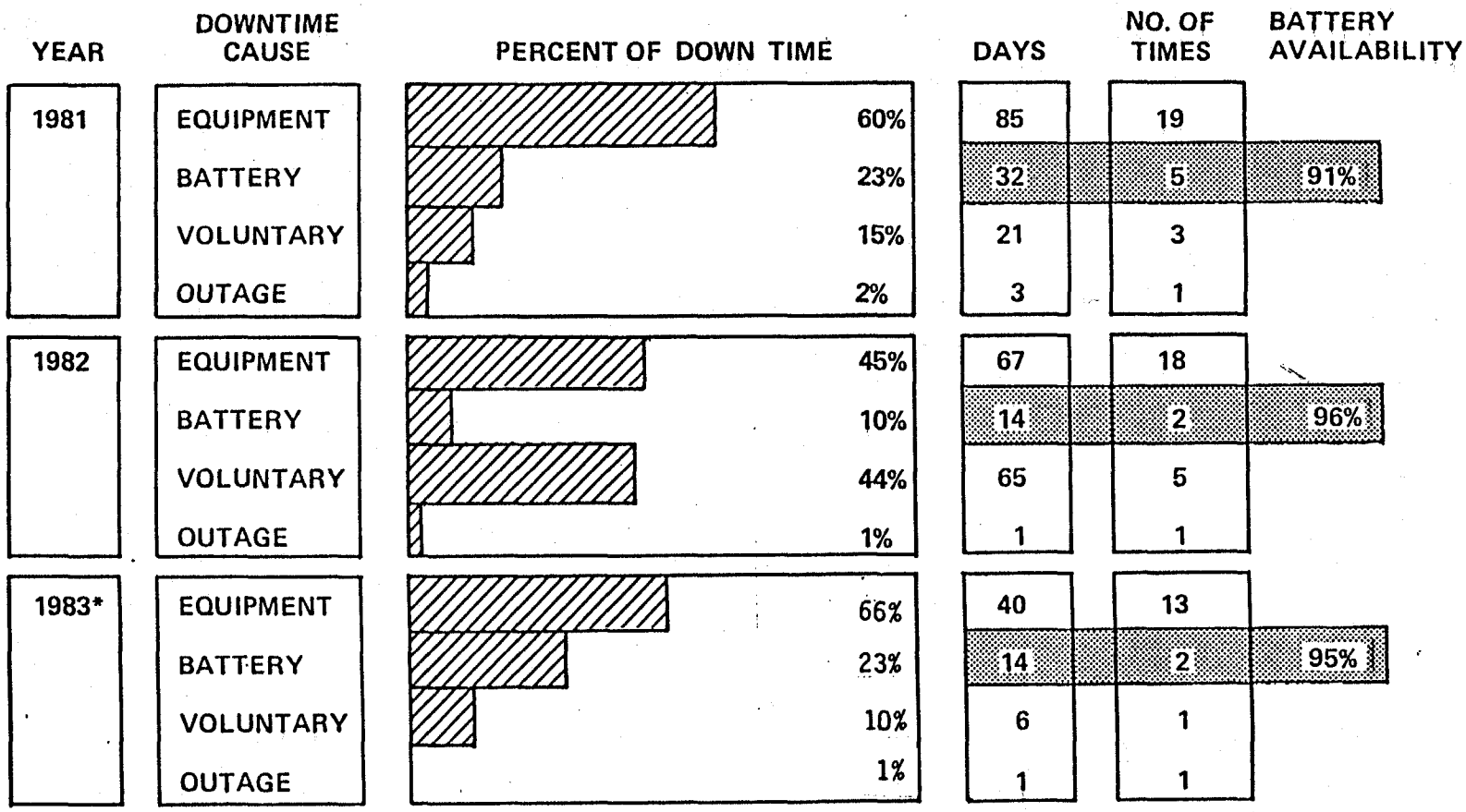

* 284 DAYS (TEST TERMINATED OCTOBER 11, 1983)

Figure 6-11

Table 6-5 summarizes the battery's status at the end of the test. Its initial 100 percent coulombic efficiency decreased rapidly during the first six months to approximately 80 percent and remained essentially constant thereafter. The loss of efficiency occurred because a number of fuse links did not blow after an electrolyte fracture, but continued to draw current.

TABLE 6-5. STATUS OF 100-kWh BATTERY
(End of Test, October 1983)

Duration of Test:	675 cycles 32 months
Cumulative Output:	47 MWh
Efficiency:	
Coulombic	80 percent
Watt-Hour	60 percent
Cells:	
Operable	295 (77 percent)
Inoperable	89 (23 percent)

After 32 months of operation, 89 cells (of the 384 comprising the reduced-size battery) were inoperable, primarily because of electrolyte failures. Many of these existed for some time as shorted cells, but eventually the fuses blew on all but the most recently failed cells. At the end of the test, there were 18 shorted cells within the six submodules. Included in the 89 inoperable cells were 11 good cells in which the fuse links blew when an excessive current momentarily surged through the battery. This was caused by a charge-control system fault early in the test.

Figure 6-12 is a Weibull probability plot for cell failures due to electrolyte fracture. Two straight lines are shown in the plot. Those failures occurring before Cycle No. 300 fall along a line whose slope and intercept infer that they are caused by a mechanism which increases linearly with time and has a characteristic life of 860 cycles. Those failures after 300 cycles, on the other hand, fall along another line occurring at an essentially constant rate with a characteristic life of 2700 cycles. (The characteristic life (α) is the estimated point in time at which 63 percent of the cells will have failed.) The plot includes the four failures which have occurred in the reconfigured (2 x 48) module described in Section 6.2.2. These failures fall along the same trend line as the late failures in the original battery.

FIGURE 6-12. ELECTROLYTE FAILURE STATISTICS

6.2.2 MODULE RECONFIGURATION AND TESTING

In October 1983 testing of the 100-kWh battery discussed above was concluded after ~675 cycles in more than 2.5-years operation. Following cool-down of the last three modules, visual and X-ray examination as well as open-circuit voltage measurements indicated that 273 of the 384 cells were operable. Ten cells were selected for a test to establish survivability of repetitive freezing and thawing (discussed in Section 4.3.4.3). Two modules were reconfigured from the remainder as described below.

The alternate method of interconnecting cells in the reconfigured modules was selected because it effectively blocks leakage current from failed cells, a major problem in the 100-kWh battery in which failed cells persisted as shorts, leaking current and causing energy efficiency to deteriorate. In the new method, cells are connected in series to form short (two or three cell) strings, and 48 short strings are joined in parallel to form a module as shown in Figure 6-13. When a cell fails, the remaining (partner) cell(s) in the string block leakage current.

Testing of the first reconfigured module began in April 1984. By the end of February 1985, this module completed 207 cycles, discharging once daily for 5 hours at ~960 A. Performance is summarized in Figure 6-14. Typically, more than 80 percent of the discharge capacity was restored in the first 7

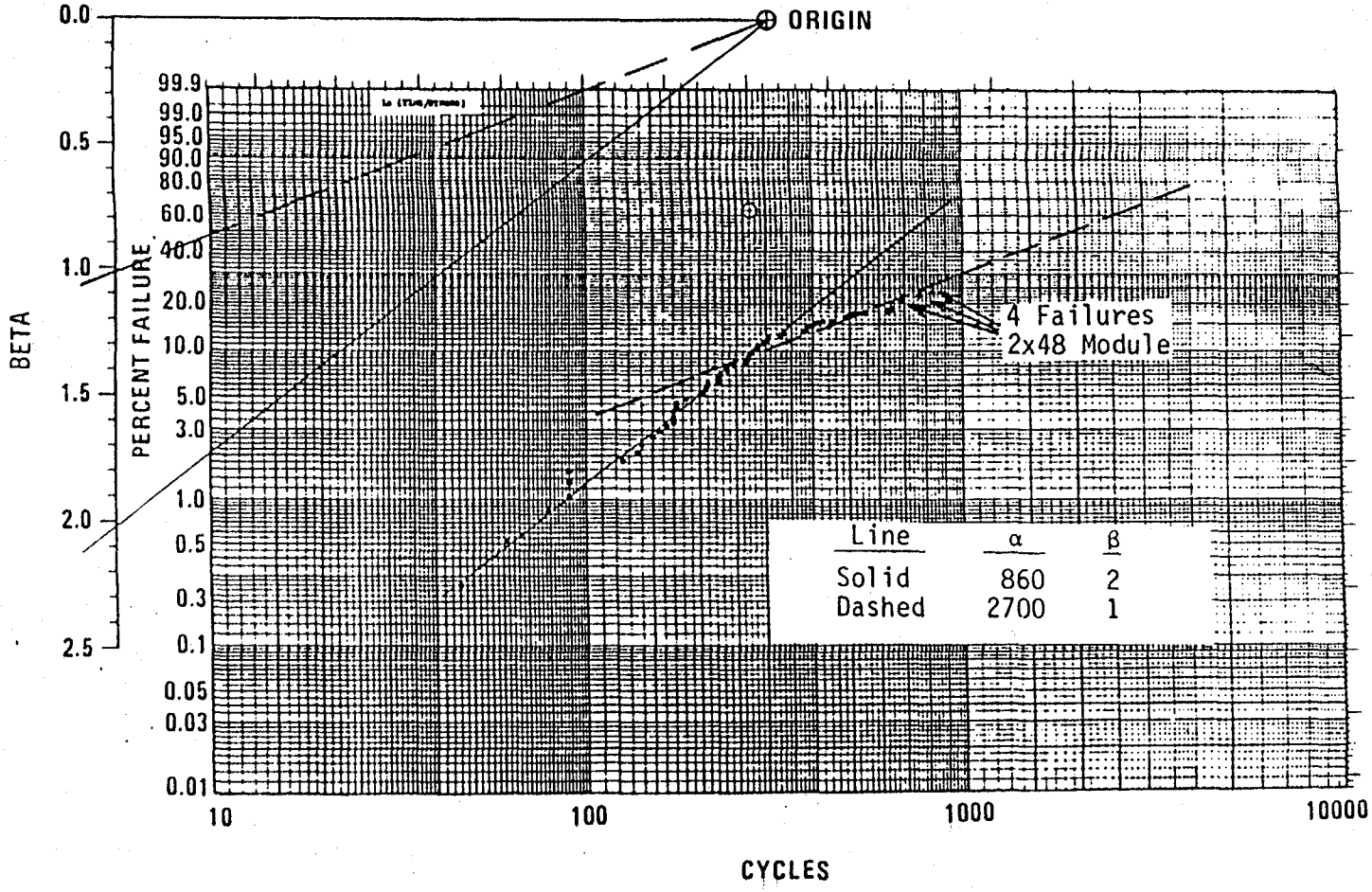

Figure 6-12

6-18a

hours of a 10-hour taper charge. The module remained at idle for two hours after discharging and at least 7 hours after charging, and despite the presence of failed cells, its coulombic efficiency remained 100 percent. The energy efficiency, consequently, remained constant at 75 percent.

When a failed cell's partner fails, the voltage across the string should be sufficient to blow the string's fuse. However, this remains to be demonstrated within the module since, so far, no failed cell's partner has failed. Eight failed cells exist, three of which have been exposed continuously to 3 to 5 V, twice the voltage across an operating cell, for more than 300 days.

A 3 x 48 module also was assembled in 1984. However, during its installation in an upper compartment of the battery enclosure, a major section of its upper bus contacted several rows of cells. This caused shorts to form leading to the failure of cells during heatup. The module was cooled and the remaining good cells were reconfigured into a second 2 x 48 module in December 1984 to provide additional data to validate the two-cell string concept which continues to appear promising in the first reconfigured module. A special charging procedure was used to equalize the states of charge among the cells in the second module, and tests of the two-module battery were initiated.

FIGURE 6-13. SHORT-STRING CONFIGURATIONS

- **STRING OF 2 CELLS IN SERIES**
- \+ YIELDS LEAST PENALTY IN LOST CELLS
- – 5 VOLTS ON SURVIVING CELL

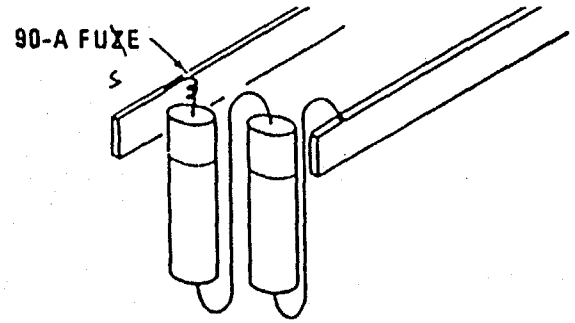

- **STRING OF 3 CELLS IN SERIES**
- \+ SHUNTS BALANCE OVERVOLTAGE CAUSED BY FAILED CELL
- – LOSE 2 GOOD CELLS PER FAILURE

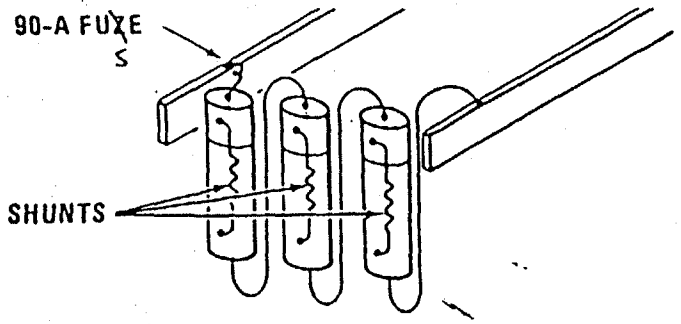

MODULES CONSIST OF 48 STRINGS

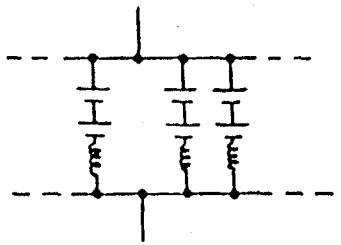

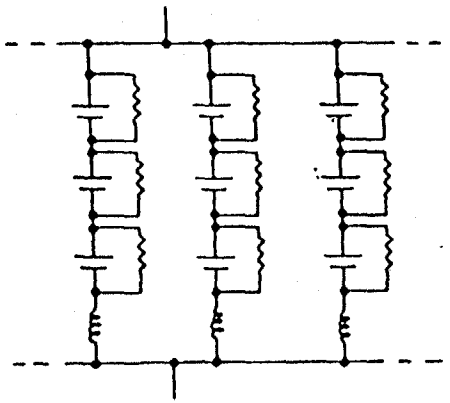

BENEFITS: REMAINING CELL BLOCKS LEAKAGE CURRENT
ELIMINATES CHARGE CONTROL SYSTEM.
PROVIDES SAME OUTPUT ENERGY PER CELL.

Figure 6-13

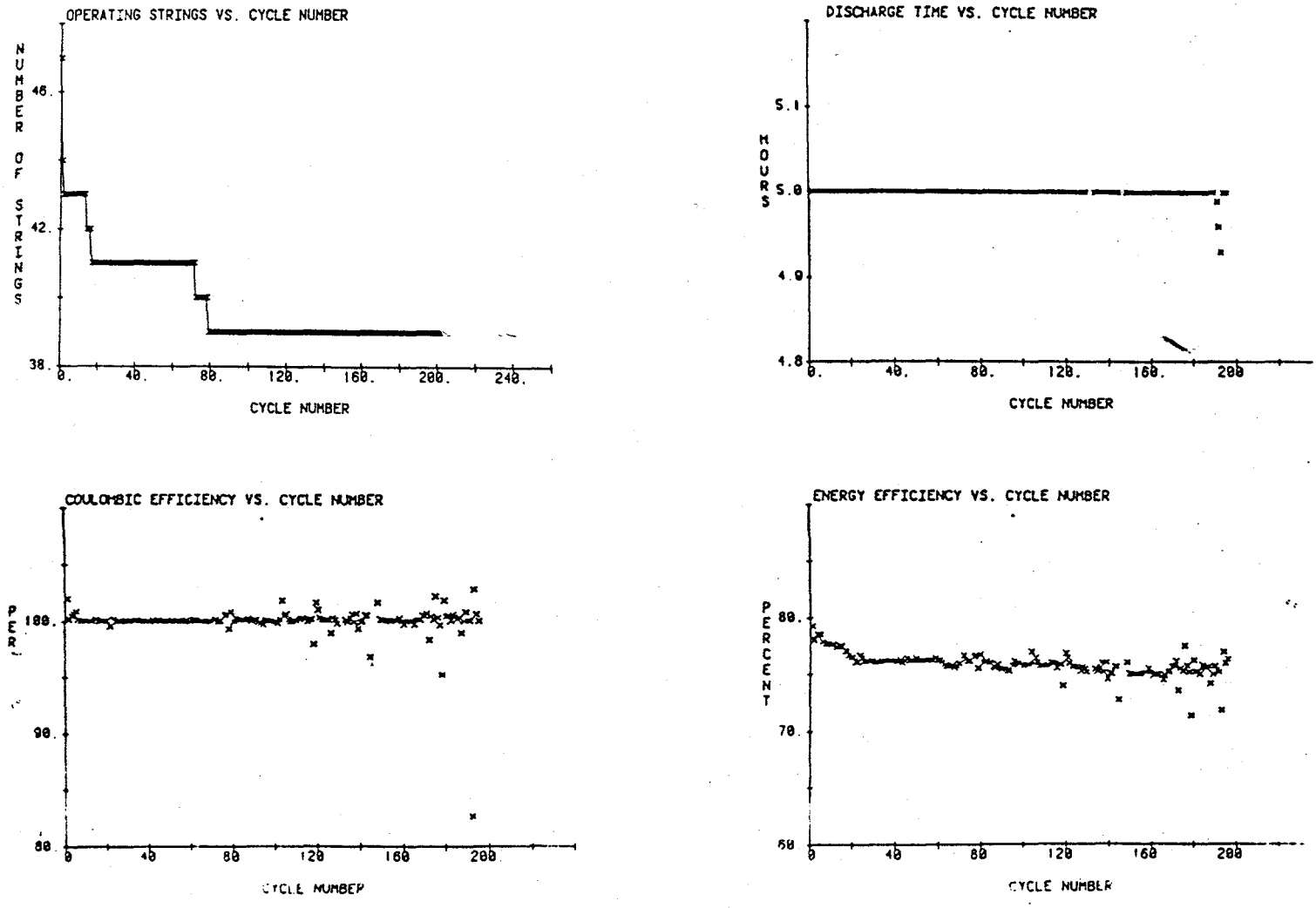

FIGURE 6-14. PERFORMANCE OF 2 X 48-CELL MODULE

REFERENCES

1. Sodium-Sulfur Battery Development, Interim Report for period 1 March 1980 through 30 September 1981, DOE Contract No. DE-AM04-79CH10012, in publication.

2. Haskins, H.J. and C.R. Halbach, "Sodium-Sulfur Load Leveling Battery System," Proceeding of the 15th Intersociety Energy Conversion Engineering Conference, Seattle, Washington, August 18-22, 1980, Paper No. 809105.

3. Bridges, D.W. and H.J. Haskins, "Operation of a 100-Kilowatt-Hour Sodium-Sulfur Battery," Proceedings of the 17th Intersociety Energy Conversion Engineering Conference, Los Angeles, California, August 8-12, 1982, Paper No. 829097.

4. Gupta, N.K. and R.P. Tischer, "Thermodynamic and Physical Properties of Molten Sodium Polysulfides from Open-Circuit Voltage Measurements," J. Electrochem. Soc., 119, 1033-1037, August 1972.

5. Sodium-Sulfur Battery Development Phase IV Interim Report for March 1, 1978 - February 29, 1980 under DOE Contract No. AM02-79CH10012, DOE Report No. DOE/CH/10012-T2, October 1980.

APPENDIX A

MATERIALS FOR THE SULFUR ELECTRODE CURRENT COLLECTOR

This appendix summarizes work performed by the Research Staff of Ford Motor Company under the tripartite contract No. DE-AM04-79CH10012.

A.1 OBJECTIVES AND REQUIREMENTS

The objectives of the program carried out at Ford Scientific Laboratory were to search for, prepare and test materials suitable for use as the surface of the positive current collector in contact with the polysulfide/sulfur (PS) melt. High operating temperature and corrosive properties of PS melts restrict severely the possible candidates.

Material requirements are very severe. Due to the thermodynamic instability of metals in PS melts the current collector must in most cases consist of a metal substrate protected by a coating. Its characteristics involve:

- Corrosion stability under conditions of exposure to electrochemical cycling.
- Sufficient conductivity, such that the resistance introduced by the coating is acceptable (<0.2 ohm cm^2) in comparison with that of the entire cell.
- Preferential wettability for sodium polysulfides rather than sulfur.
- Adherence to the substrate under conditions of electrochemical and thermal cycling.
- Impermeability, or compatibility with a self-healing (passivating) substrate.
- Cost viability.

A.2 MATERIALS AND TESTING METHODS

Materials tested are listed in Table A-1. Among metals only those which become covered with a protective sulfide layer were chosen for study: Cr, Mo and Al. As opposed to semiconducting sulfides formed on Cr and Mo, the passivating layer on aluminum is an insulator and the metal cannot be used without modifications imparting conductivity at the current collector/melt interface. The rationale for the choice of other materials studied is discussed in the following text.

Testing methods included: 1) corrosion tests performed in laboratory sealed glass cells (Figure A-1a); 2) chemical melt analyses; and 3) surface examinations using SEM with EDAX attachment, X-ray diffraction and electron microprobe before and after the corrosion tests. The corrosion tests consisted of polarizing the tested sample for times up to 13 months in various regimes, either to simulate conditions to which the material may (even

Table A-1. Materials Tested

Metals	Carbon	Ceramics	Composites
Chromium	Glassy Carbon	Cr_2O_3 (CP & HP) Doped with (0.1-2.0 w/o)	Al/SiC
Aluminum	Grafoil	NiO	6061/20% Acicular
Molybdenum	Graphite	Ta_2O_5	6061/34% Acicular
		Li_2O	1100/20% Acicular
		MgO	1100/20% Granular
		Perovskites $La_{(1-x)}Sr_xCrO_3$	Conductive Glass
		x = 0.01	
		x = 0.16	

locally) be exposed in practical cells, or to perform diagnostic experiments exploring the conditions for the materials' stability. A number of in situ measurements of chromium-plate corrosion rate were carried out using Cr^{51} labeled chromium. The cell was screened so that only radiation from Cr which passed into the melt could reach the detector (Figure A-1b).

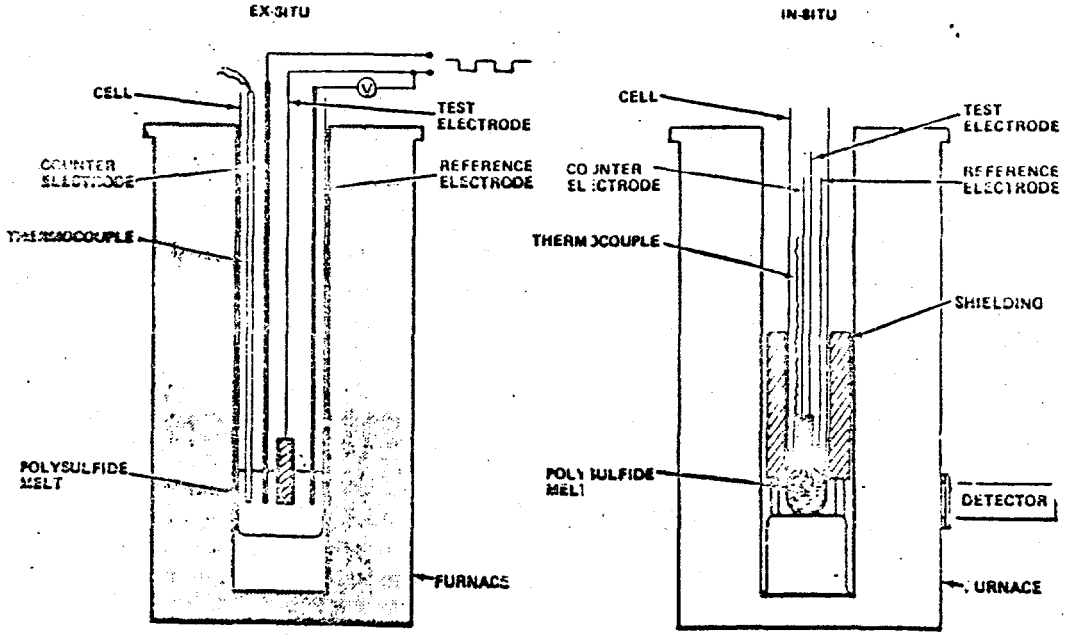

Figure A-1. Corrosion Test Cells
A - ex situ, B - in situ measurements

A.3 RESULTS

The following sections summarize results of the experimental effort.

A.3.1 CHROMIUM PLATE

The chromium plate used extensively as a container coating in Ford Aerospace's practical cells had behaved erratically in that the number of charge-discharge cycles varied drastically: some cells were capable of more than a thousand cycles, while others suffered loss of capacity and resistance increase already within the first hundred cycles. Both phenomena were ascribed to chromium corrosion products blocking the felt container interface, parts of the felt and/or solid electrolyte. Attempts to correlate the irreproducible chromium behavior with a number of controllable parameters have failed. The study, which aimed at the definition of factors responsible for this irreproducible behavior and at determination of conditions for chromium applicability in practical cells, gave the following results:

- A standard method of producing a reproducible duplex coating consisting of inner, crack-free and outer, stress-relaxed chromium layers was developed. Excellent adhesion to the stainless steel substrate and between the two chromium surface layers was achieved.

- Among parameters suspected of affecting the chromium corrosion rate, the presence of contaminants such as moisture and hydrogen ions was found to have little effect on the corrosion rate.

- Among plating conditions which were found to be of no or minor importance, are: plating current density within the 150 to 600 mA/cm^2 range, and counter electrode material (lead or platinum).

- Annealing temperature seems to affect the uniformity of pit formation in the surface sulfide layers. The latter are always produced upon exposure of Cr plate to sulfur (liquid or vapor) or PS melt. Their morphology depends on the cycling regime and affects the amount of the metal which passes into the melt. However, even under the worst conditions (discussed below) the maximum thickness of chromium lost in the form of sulfide never exceeded 1 μm in three months of dynamic testing and no pits were formed in the outer chromium sulfide layers which reached deeper than ∿3 μm.

- The morphology of chromium sulfide layers depends on the potential imposed on the surface: down to ∿-150 mV (sodium pentasulfide reference), large crystals (∿10 μm) similar to those formed in the presence of sulfur vapor are formed which have large voids between them. Cycling limited cathodically to this chromium potential does not produce a disruption of the smooth sulfide surface and very little chromium passes into the melt. At potentials below -150 mV, nucleation becomes easier and small (submicron size), closely packed crystals grow randomly all over the surface leaving little void space between them. Cycling with the cathodic chromium potential cut-off at ≤-200 mV results in blistering and disruption of the sulfide layers and passage of larger amounts

of chromium into the melt. Results of diagnostic experiments aiming at a clearer understanding of the corrosion mechanism and phenomenology behind the observed correlations remain to be evaluated.

In practice, it seems that the duplex chromium plate can be used as the positive current collector coating provided the precast felt electrode is uniformly distributed over the surface. This should preclude the current collector surface from becoming (even locally) the electrode at which faradaic reactions involving lower polysulfides (disulfide) occur and polarize this surface to the low cathodic potentials. Ford Aerospace's successful cycling (>600 cycles to date) of 12 practical cells with duplex chromium coatings on stainless steel and mild steel containers and filled with uniformly precast sulfur/felt electrodes seems to bear out this conclusion.

A.3.2 DOPED CHROMIUM OXIDES

Doped chromium oxides were expected to be suitable candidates on the basis of previous experience with chromium oxide which was found to be corrosion resistant in static corrosion tests. The high resistivity of chromium oxide required attempts to impart better semiconductive properties to this material. This was achieved by doping with lower valence metal oxides. The electrochemical behavior of these materials is exemplified in Figure A-2. As opposed to samples with higher valence dopants and NiO, the resistivity of lithia- and magnesia-doped materials stabilized during electrochemical cycling at sufficiently low values to satisfy thin coating requirements. Attempts to produce such coatings were unsuccessful to date. It seems that a chromium surface would have to be developed. Neither surface nor melt examination showed any discernible changes caused by up to 1000 cycles. The initial increase in resistivity was interpreted by means of diagnostic experiments, in terms of sample equilibration with the extremely low oxygen pressure in the cell environment. This leads to an increase of oxygen vacancies and a concurrent decrease of the number of hole carriers in these p-type semiconductors.

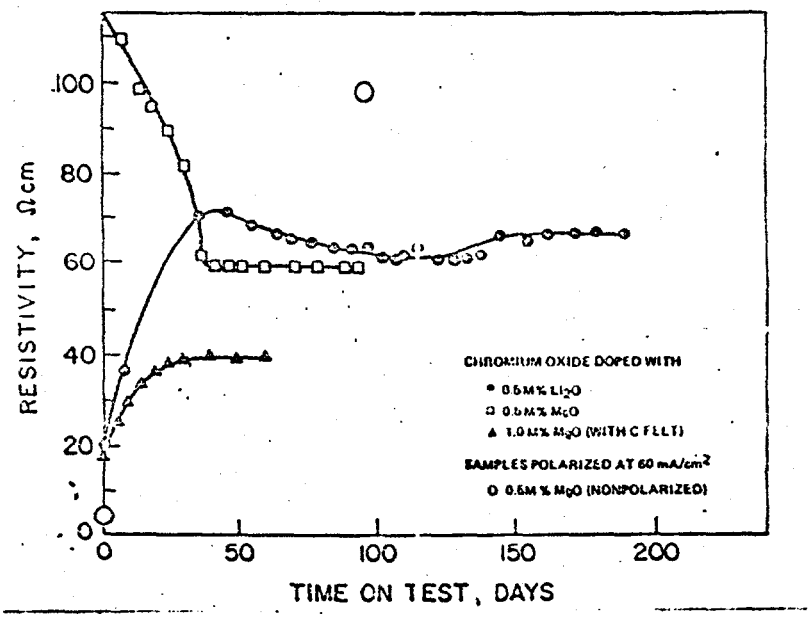

Figure A-2. Resistivity of Doped Chromium Oxides as a Function of Time

A.3.3 PEROVSKITES

Much higher conductivities were achieved with lanthanum chromite perovskites (Figure A-3). Although the initial resistivity seemed to increase linearly over ∿1000 cycles, the resistivity extrapolated to 10 years would be still below 40 ohm cm. Here, also, no corrosive attack was observed.

A few attempts to produce perovskite coatings by sputtering and plasma spraying produced nonadherent and/or structurally and compositionally altered materials.

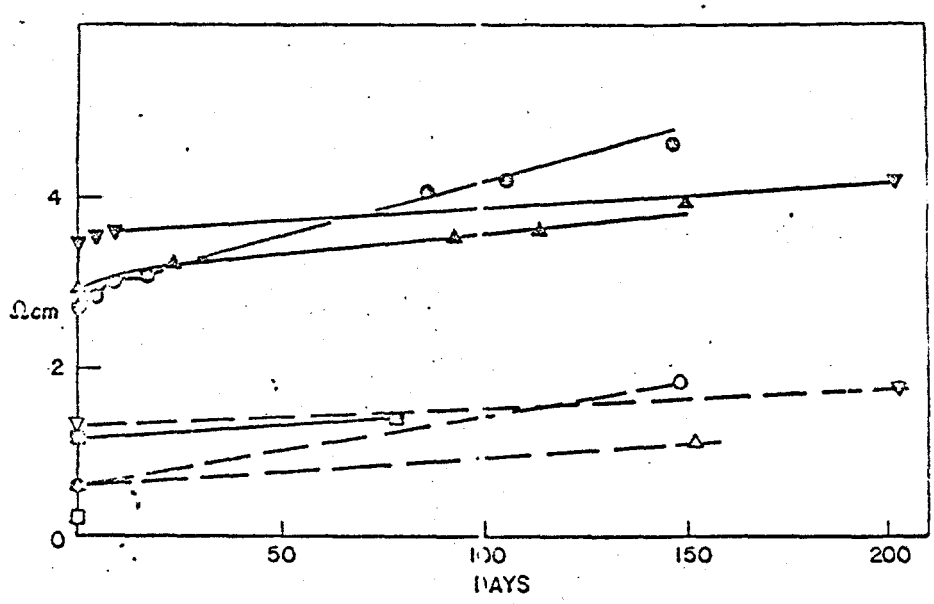

Figure A-3. Resistivity of Perovskites as a Function of Time. (Solid lines - in situ, interrupted lines - ex situ measurements; squares - $La_{0.84}Sr_{0.16}CrO_3$; circles & triangles--$La_{0.99}Sr_{0.01}CrO_3$)

A.3.4 ALUMINUM

Aluminum passivation behavior was tested since the metal can be used as a self-healing substrate for coatings or in conductive composites as the container material or a lining. It can be seen (Figure A-4) that aluminum is passive within a range of ∿-0.9 V to (at least) +1.5 V which vastly exceeds the potentials of the practical sulfur electrode. The residual currents increase somewhat with increasing content of alloying metals, not exceeding, however, 50 $\mu A/cm^2$. Thus aluminum can be used as a substrate or as a composite matrix.

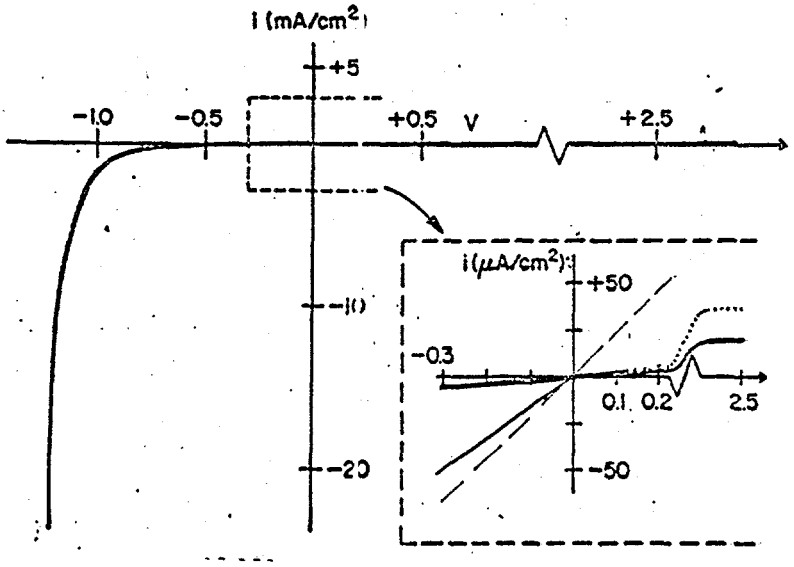

Figure A-4. Polarization Curves for Aluminum Alloys. (Solid line - 99.999 pure; Dotted line - 1100 alloy (99%); Interrupted line - 6061 alloy (95%)

A.3.5 ALUMINUM/SILICON CARBIDE (Al/SiC) COMPOSITES

Several types of Al/SiC composites were cycled for periods up to 13 months. All composites showed metallic conductivity. The variables were SiC particle shape and concentration, surface preparation and aluminum alloy composition. The latter factor was found to be immaterial for 6061 or 1100 alloys.

Polished surfaces were inferior to the etched ones. Composites containing 34 or 20 percent acicular SiC particles (Figures A-5 and A-6) behaved in a stable manner during cycling which was carried out for 8 to 13 months (up to ~1800 cycles). Materials with granular particles (Figure A-7) abruptly "passivated" within less than two months cycling, and aluminum accumulated within this time in the melt amounted to ~800 ppm.

Post-test SEM examination of (polished) samples with acicular particles showed no signs of corrosive attack. The melt after about one year of cycling, contained 400 to 900 ppm of Al in the case of samples containing 20 percent SiC but only 50 ppm in the case of 34 percent SiC concentration, confirming results shown in Figure A-4.

Samples with the higher concentration are also superior in terms of preferential wettability by polysulfides. The constant value of the anodic current (Figure A-8) indicates that the rate of sulfur desorption is sufficiently fast in the case of samples containing 34 percent SiC, whereas it inhibits the charging current (Figure A-9) in the case of 20 percent SiC content.

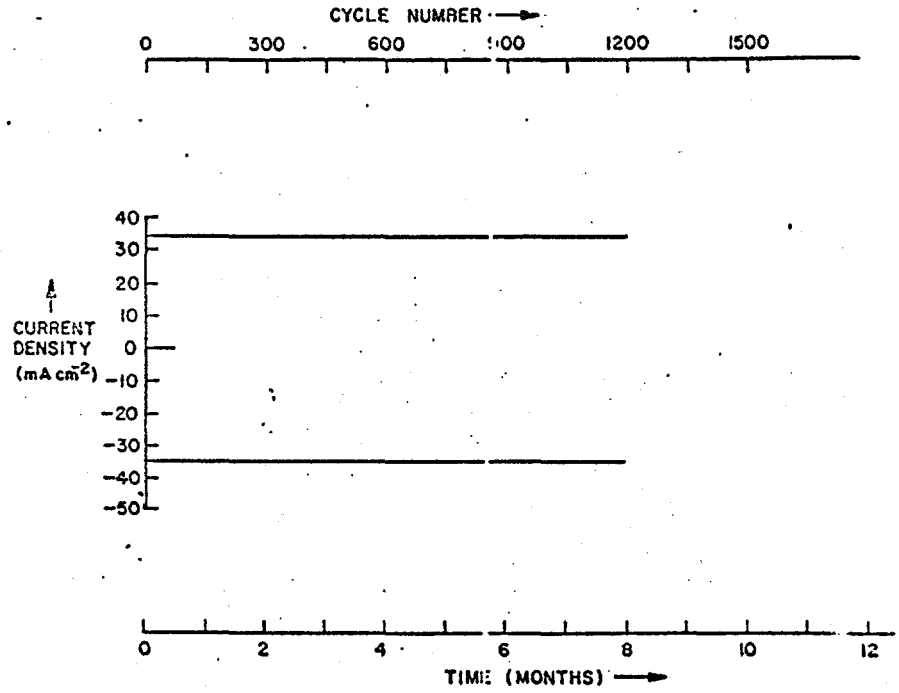

Figure A-5. Cathodic and Anodic Current Density During Cycling of Al/SiC (34 wt. percent) Acicular Material, as a Function of Time/Cycle Number

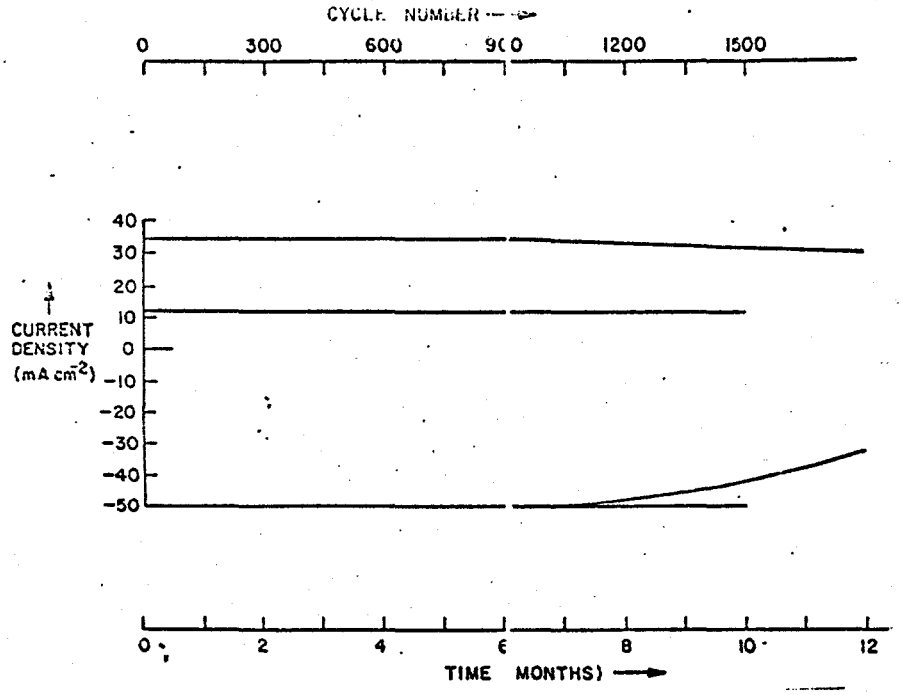

Figure A-6. Cathodic and Anodic Current Density During Cycling of Al/SiC (20 wt. percent) Acicular Material, as a Function of Time/Cycle Number

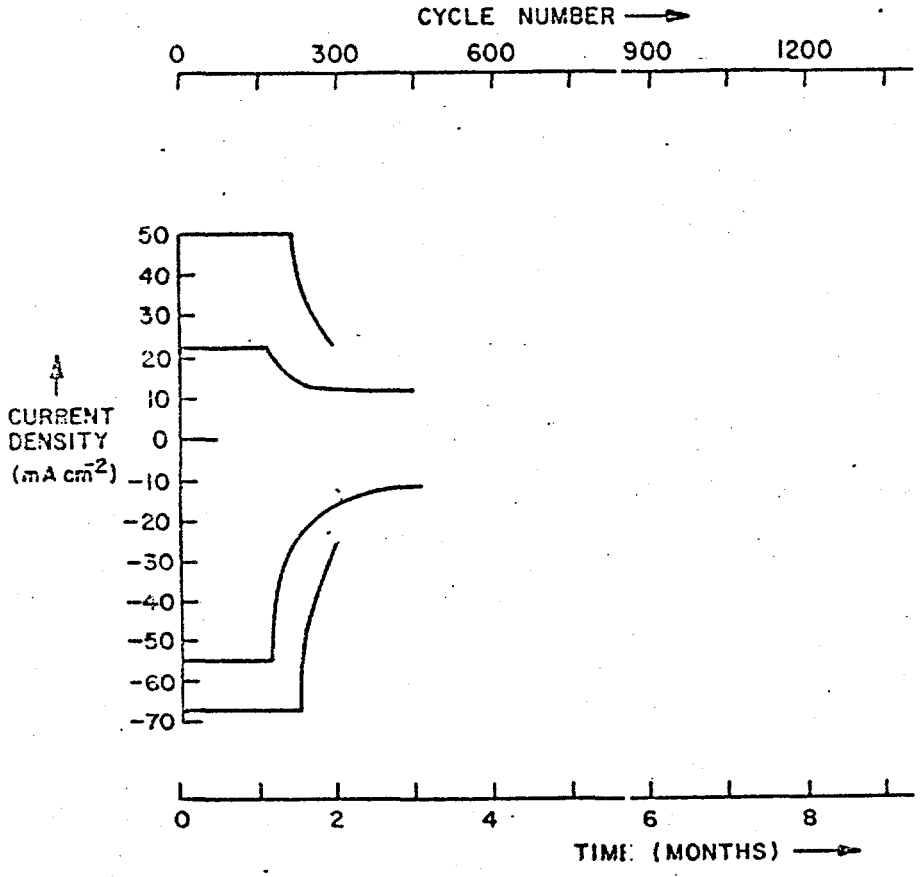

Figure A-7. Cathodic and Anodic Current Density During Cycling of Al/SiC Granular Material, as a Function of Time/Cycle Number.

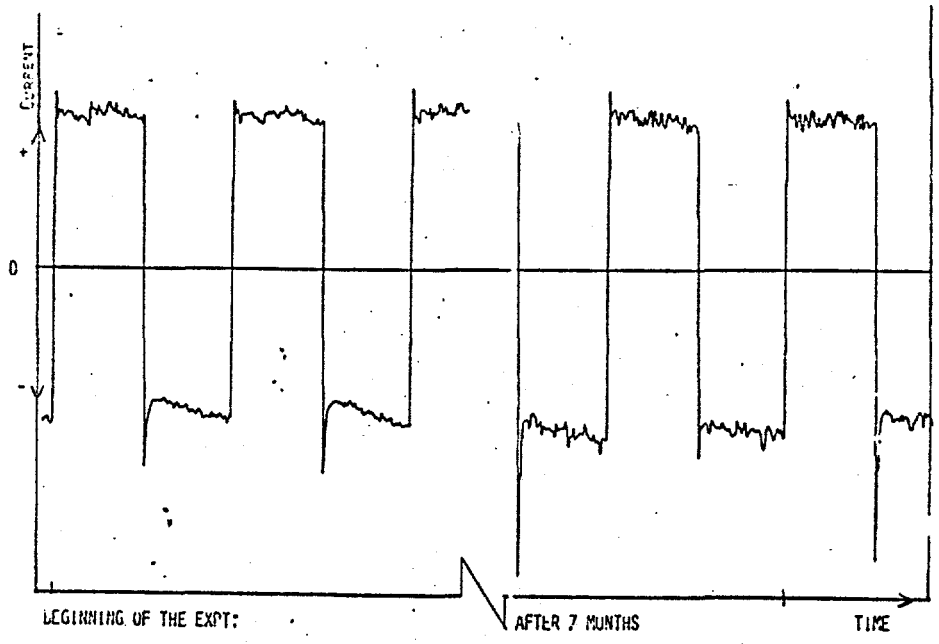

Figure A-8. Current as a Function of Time During Cycling of Al/SiC (34 wt. percent) Acicular Material

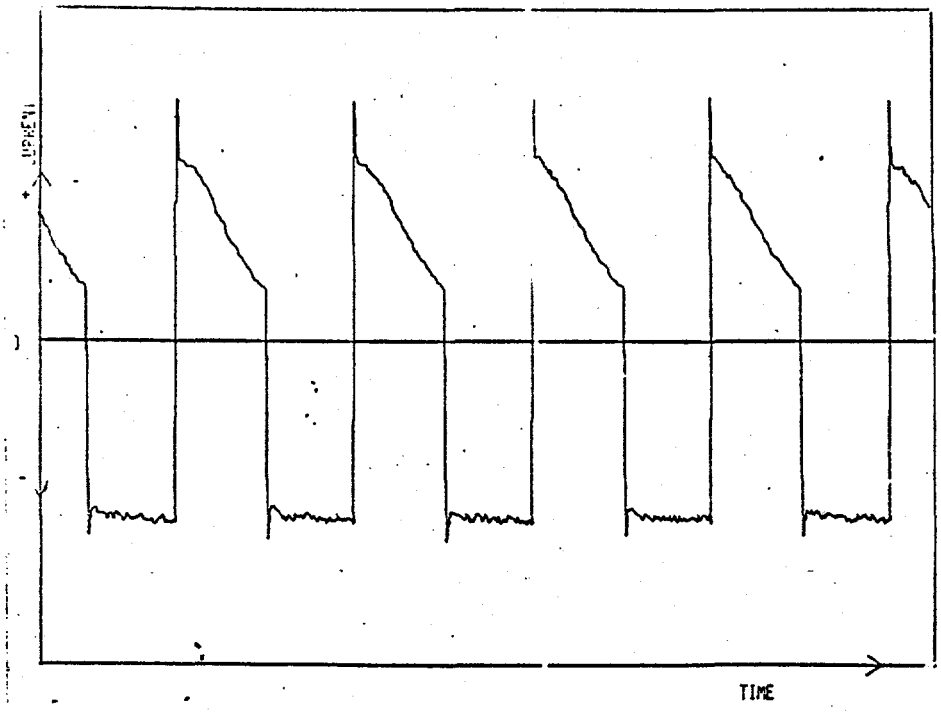

Figure A-9. Current as a Function of Time During Cycling of Al/SiC (20 wt. percent) Acicular Material

It was concluded that Al/SiC composites can be used as a lining, or container material of the Na/S cell.

A.3.6 CONDUCTIVE GLASSES

Conductive glasses were found to behave electrochemically in a stable manner over 1500 cycles (Figure A-10). However, some samples initially lost their current-carrying ability. The irreproducibility was ascribed to the fact that each sample was coated separately and, thus, perhaps not quite reproducibly by the vendor. A SEM study showed an initial loss of conductive material from the surface. This, however, did not cause an increase of ohmic resistance (Figure A-11), and did not affect the electrochemical stability (Figure A-10). Although analyses of the melts indicated some progressive leaching of the conductive material (in one case ∿300 ppm of the material were found after 10 months), the electrode performed with excellent stability over this time period.

The adsorbability of sulfur on the conductive glass surface is higher than in the case of aluminum composites: charging currents are limited to a greater extent by the slow rate of sulfur desorption from the surface.

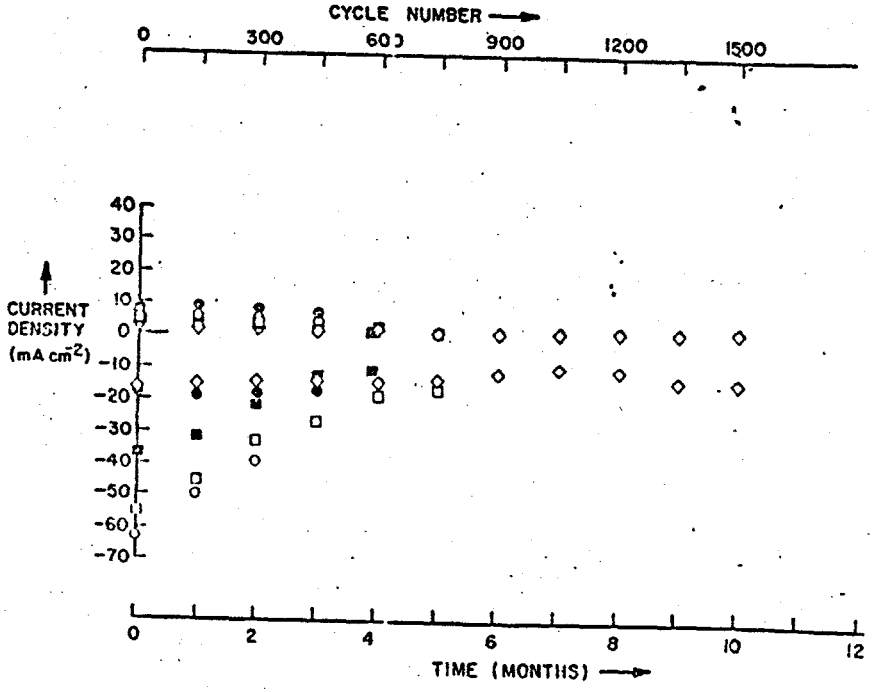

Figure 10. Cathodic and Anodic Current Density During Cycling of Conductive Glass-Coated Materials as a Function of Time/ Cycle Number.

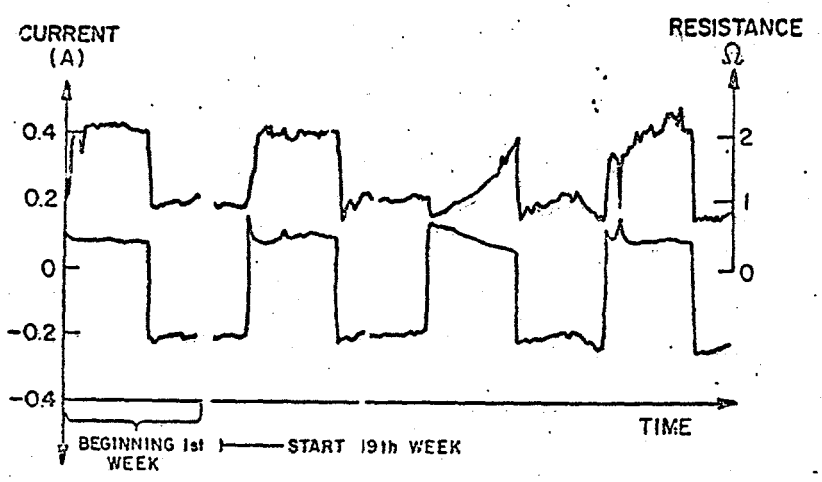

Figure A-11. Current (lower curve) and Resistance (upper curve) During Cycling of Conductive Glass-Coated Material as a Function of Time.

A.4. SUMMARY

Based on Phase VB materials research efforts, the following conclusions were reached:

- o Two types of coatings (duplex chromium plate and conductive glass) were found to be suitable for the current collector/polysulfide melt interface.
- o The working regime ensuring high stability of chromium plate was defined.
- o Aluminum/SiC composites were found to be suitable for material of the current collector or its lining.
- o Several single and mixed ceramic oxides were found to be corrosion stable in the environment of the operating sulfur electrode; however, their application requires development of thin coatings. Attempts to produce such coatings have as yet been unsuccessful.